Doctoral Dissertation

STRUCTURAL HEALTH MONITORING OF CABLES USING SMART SENSORS IN CABLE-STAYED BRIDGES

Seunghoo Jeong

Department of Urban and Environmental Engineering
(Urban Infrastructure Engineering)

Graduate School of UNIST

2020

STRUCTURAL HEALTH MONITORING OF CABLES USING SMART SENSORS IN CABLE-STAYED BRIDGES

Seunghoo Jeong

Department of Urban and Environmental Engineering
(Urban Infrastructure Engineering)

Graduate School of UNIST

Structural Health Monitoring of Cables using Smart Sensors in Cable-stayed Bridges

A dissertation
submitted to the Graduate School of UNIST
in partial fulfillment of the
requirements for the degree of
Doctor of Philosophy

Seunghoo Jeong

December 2, 2019
Approved by

Advisor
Young-Joo Lee

Co-advisor
Sung-Han Sim

Structural Health Monitoring of Cables using Smart Sensors in Cable-stayed Bridges

Seunghoo Jeong

This certifies that the dissertation of Seunghoo Jeong is approved.

December 2, 2019

(signature)

Committee Chair: Young-Joo Lee

(signature)

Committee Member: Sung-Han Sim

(signature)

Committee Member: Myoungsu Shin

(signature)

MARCO TORBOL

Committee Member: Marco Torbol

(signature)

Committee Member: Robin Eunju Kim

(signature)

Committee Member: Seung-Seop Jin

ABSTRACT

Structural Health Monitoring of Cables using Smart Sensors
in Cable-stayed Bridges

by

Seunghoo Jeong

Doctor of Philosophy in Engineering
Ulsan National Institute of Science and Technology

Cable-stayed bridge designs have been the preferred construction for long-span bridges since the first advent of the modern cable-stayed bridge (Stromsund Bridge, Sweden) in 1955. With an increasing number of cable-stayed bridges worldwide, the need for bridge maintenance has received significant attention to prolong the lifespan of bridges by ensuring serviceability and operability within a safe level. A stay-cable is one of the principal load-carrying components of cable-stayed bridges, which means that the cable condition influences the safety and integrity of the entire bridge. However, stay-cables are vulnerable to vibration stemming from wind, rain, and traffic, owing to their inherently insufficient capacity to reduce vibration. Excessive vibrations in stay-cables can potentially cause long-term fatigue accumulation and serviceability issues. Therefore, monitoring the health condition of a stay-cable is required to ensure the serviceability and operability of not only the stay-cables but also the entire bridge.

With this motivation, this study aimed to propose a structural health monitoring (SHM) system for stay-cables by using cost-effective smart sensors. To achieve this objective, four SHM systems were developed to deal with the SHM-related issues of stay-cables which include serviceability failure, vibration control, and structural condition assessment. First, an automated real-time serviceability assessment system using wireless smart sensors was developed based on bridge design specifications for serviceability assessment. When the displacement of the cable in the mid-span exceeds either the upper or the lower bound provided in most bridge design specifications, it is considered as a serviceability failure. The system developed in this study featured embedded onboard processing, including the measurement of acceleration, estimation of displacement from measured acceleration, serviceability assessment, and monitoring through wireless communication. A series of laboratory tests were carried out to verify the performance of the developed system. Subsequently, an automated cable

damping monitoring strategy was proposed. The presented method was used to automate damping estimation under external conditions, such as wind, rain, vehicle, and damper installation. For completeness, this study examined various damping estimation methods to determine the appropriate approach for damping automation. The selected method, satisfying conditions for automation in damping estimation tailored to the stay-cable, was applied to cable responses obtained from in-service bridges in the Republic of Korea to monitor the cable damping ratio under different wind conditions. Furthermore, a series of tests were conducted to verify the monitoring performance of the proposed automation approach. Third, this study proposed a serviceability assessment method considering vibration control to assess the level of serviceability of stay-cables. Cable serviceability failure was defined according to the range of acceptable cable responses provided in most bridge design specifications. The probability of serviceability failure was determined by means of the first-passage problem using VanMarcke's approximation. The proposed system effectively allows calculation of the failure probability depending on the properties of any installed vibration control method. To demonstrate the proposed method, the stay-cables of the Second Jindo Bridge in South Korea were evaluated, and the analysis results accurately reflected the cable behavior during a known wind event.

As aforementioned, implementing a control scheme is efficient to decrease the probability of serviceability failure. Accordingly, this study developed an Arduino-based integrated cable vibration control system implementing a semi-active control algorithm to enhance the serviceability level. The integrated vibration control system was built on the low-cost, low-power Arduino platform, embedding a semi-active control algorithm. A MEMS accelerometer was installed on the platform to conduct state feedback for the semi-active control. The Linear Quadratic Gaussian control technique was applied to estimate the cable state and obtain a control gain, and the clipped optimal algorithm was implemented to control the damping device. The magneto-rheological damper was selected as a semi-active damping device, controlled by the proposed control system. The developed integrated system was applied to a laboratory-size cable with a series of experimental studies for identifying the effect of the system on cable vibration reduction.

Lastly, an automated cable tension monitoring system that can measure tension forces using deep learning and wireless smart sensors was developed. The tension force is widely used as one of the physical quantities determining the behavior of cables. The automated system was designed by using the Raspberry Pi platform, one of the cost-effective single-board computers, with a MEMS accelerometer. A fully automated peak-picking algorithm tailored to the cable vibration was developed using the region-based convolution neural network to apply the vibration-based tension estimation method to automated cable tension monitoring. The developed system features embedded processing on wireless smart sensors, including data acquisition, power spectral density calculation, automated peak-picking, post-processing for peak-selection, and tension estimation. Laboratory and field tests were conducted on a cable to validate the performance of the proposed automated monitoring system.

TABLE OF CONTENTS

LIST OF FIGURES

LIST OF TABLES

1. INTRODUCTION

1.1. Motivation

With an increasing demand for long-span bridges, cable-stayed bridges have been widely applied to construction owing to their high structural stiffness and aesthetic appearance [1, 2]. Since the construction of the Stromsund bridge as the first modern cable-stayed bridge in Sweden (1955) [3], the maintenance of constructed bridges has received substantial attention to preserve their structural integrity and prolong their service life [4]. Among the various maintenance concerns of cable-stayed bridges, wind- and rain-induced vibration has been recognized as one of the primary problems threatening their structural operability and serviceability since its first observation at the Meiko-West Bridge in Japan reported in 1986 (Figure 1-1) [4, 5]. A stay-cable, which is one of the most significant load-carrying members of a cable-stayed bridge, is vulnerable to vibrations induced by external loads such as wind, rain, and traffic owing to its inherently low damping ratio and high flexibility [4, 6-9]. If the cable is continually exposed to vibrations, the lifespan of both the main cable and the cables between the main cable and the bridge deck is reduced owing to stresses and fatigue, threatening the bridge's safety and serviceability, as well as the level of safety for the public using the bridge [10-12]. Therefore, structural health monitoring (SHM) of a stay-cable is required to assure the serviceability and operability of not only the stay-cable but also the entire bridge, and this can be achieved by continual monitoring of cable conditions such as serviceability level with vibration control, cable tension force, and damping ratio.

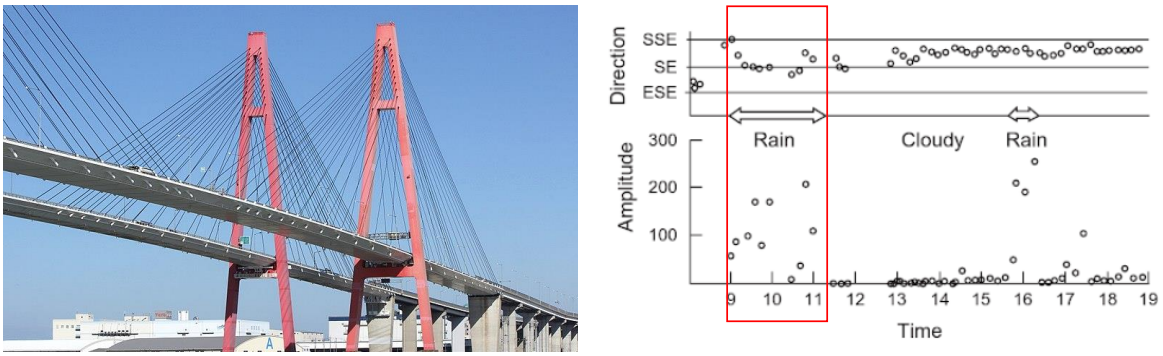

(a) Meiko-West Bridge in Japan (b) Rain-induced vibration [13] (unit: mm)

Figure 1-1. Example of rain-induced vibration on the Meiko-West Bridge (1986)

The structural integrity of any civil construction can be preserved by maintaining its serviceability and operability within acceptable levels [4, 14]. Of these two parameters, serviceability tends to be a

primary concern in terms of structural safety because users are likely to be sensitive to a serviceability issue far earlier than an operability issue [4, 15]. It is noted that serviceability determines the ability of a structure to be used, whereas operability is related to the ability of a system to continue functioning [4, 16]. Therefore, monitoring serviceability with respect to cable vibration should be emphasized as one of the critical maintenance efforts for cable-stayed bridges [4, 17-19].

However, thus far, little work has gone into developing a cable serviceability assessment system. The serviceability level can be assessed by monitoring the vibration amplitude and damping ratio. The vibration-based assessment has been performed in terms of assigning design codes and assessing serviceability levels accordingly. Serviceability levels are defined in the design codes that specify the allowable level of serviceability for bridge users from the developed countries [4]. Based on the design codes, a previous study evaluated the serviceability of footbridges under human-induced vibrations using long-term measurement data [20]. The serviceability of the bridge was considered a failure when the lateral and vertical accelerations of the structure exceeded the limits of comfortable acceleration provided by the guidelines. While this study demonstrates the assessment of serviceability based on vibration data, real-time monitoring of amplitude-based serviceability was not considered. As one of the factors affecting the serviceability level of long-span bridges, the damping ratio of a stay-cable has been identified by a system identification method [21-23]. However, little effort has been expended to automate damping estimation.

In addition, little work has been conducted to assess the effects of cable vibration control on cable serviceability. Instead, to keep the serviceability of the cables within an acceptable level, researchers have proposed vibration control methods. For example, passive control was introduced using viscous dampers attached transversely to stay-cables near the deck anchorages [6, 11, 24]. When well-tuned, such passive viscous dampers can provide supplemental damping to a cable without requiring external power [6]. As a result, this type of damper has been widely applied to many cable-stayed bridges worldwide, including the Brotonne Bridge in France (1983), the Sunshine Skyway Bridge in Florida (1988), and the Aratsu Bridge in Japan (1989) [11]. The semi-active damper has also received attention as a promising method for mitigating cable vibration, particularly for very long cables [11, 24, 25].

The magnetorheological (MR) damper, one of the more widely used types of semi-active dampers in civil engineering applications, has been applied to the Dongting Lake Bridge in China (2002), the Eiland Bridge in the Netherlands (2005), and the Shandong Binzhou Yellow River Highway Bridge in China (2007) [11, 24, 25]. However, many theoretical and experimental studies have used the MR damper in a passive mode without embedding a semi-active control algorithm [5, 12, 24, 26-28]. Without consideration of the state-feedback of the cable response, unique cable dynamics are neglected, and it is difficult to maximize the efficiency of the MR damper. Even though the MR damper is used with semi-active control, this control system cannot be easily applied in the real-world owing to

equipment requirements, including the data acquisition system, the damping device, several cables, and a power supply device. A previous study developed a structural vibration control system using the low-cost, low-power Arduino platform into which a semi-active control algorithm has been embedded [29]. However, this Arduino-based control system was applied to a three-story shear building, and few studies regarding the implementation of the Arduino-based control system on a stay-cable have been reported.

Both the serviceability level and the tension force of the stay-cable have been used as a useful physical quantity to assess the health condition of the cable as well as the soundness of the bridge [1, 2, 30-35]. For instance, cable tension is used to maintain the alignment of cables and ensure that the loading of the cable is within the safe range during the construction of cable-stayed bridges [1, 30]. When the bridge is in service, the tension force of the cable is an essential indicator to assess the structural safety and integrity of the entire bridge [1, 2, 9, 30-32]. The cable tension force varies in real-time due to the traffic loads and other environmental effects, and the variation of tension force can cause safety problems with the cable as well as the bridge [32-34, 36]. For example, a reduced tension force of a cable can make other cables become overloaded, subsequently affecting the structural soundness of the bridge [2]. The continual change of tension force can make the stay-cable have fatigue damage and corrosion in the connector [32-34]. In addition, small variations within 10 % of the designed tension force could cause significant variations of bending moments in the pylons of the cable-stayed bridge [36]. Therefore, cable tension needs to be monitored accurately and continually for the maintenance of cable-stayed bridges, not only during construction but also during the service life of the bridge [1, 2, 9, 30-34, 36]. To monitor the tension force of the cable, previous works have proposed a cable tension monitoring system implementing the vibration-based approach [9, 30, 31]. These studies have shown the possibility of monitoring cable tension force automatically by identifying natural frequencies through a peak-picking method.

Although previous studies have exhibited success in monitoring cable tension, tension monitoring automation still has limitations in that the proposed systems are only valid on specific applications. The threshold-based peak-picking method searches for peaks that are greater than a preselected value to remove less important peaks. However, the user-defined threshold is dependent on the types of civil structures and may fail to remove undesirable peaks due to noise [22, 37, 38]. The peak-picking method that identifies a local maximum around predefined natural frequencies may identify undesirable peaks under the change in modal properties of the cable due to structural damage and environmental effects [37]. Currently, deep learning has shown a potential of automated peak-picking from the frequency domain representation of structural response, making it possible to extract natural frequencies automatically [37]. However, this proposed peak-picking method may detect undesirable peaks when applied to the cable response because this method was tailored to responses from general structures such as beams, trusses, and cables. In addition, the mentioned technique required high computation

power to perform peak-picking, which can be a burden for embedded processing. Therefore, further study is necessary to develop an automated cable tension monitoring system that embeds a peak-picking method tailored to a stay-cable for robust modal identification.

1.2. Objectives

On the basis of the mentioned motivation, this study aims to propose a structural health monitoring (SHM) system for stay-cables in cable-stayed bridges by using cost-effective smart sensors. To achieve this objective, SHM systems were proposed to address SHM-related issues of stay-cables which include serviceability assessment and monitoring, vibration control, and tension force monitoring (Figure 1-2 and Table 1-1). Especially, an automated system was developed to monitor the level of serviceability and tension forces by embedding automation processing to smart sensor platforms. The smart sensors can perform embedded processing from data acquisition to analysis by itself, which can make automation be possible. A more detailed explanation regarding current problems and research objectives of each topic are shown below. It is noted that this dissertation is based on published and submitted articles by the author [4, 8, 39, 40].

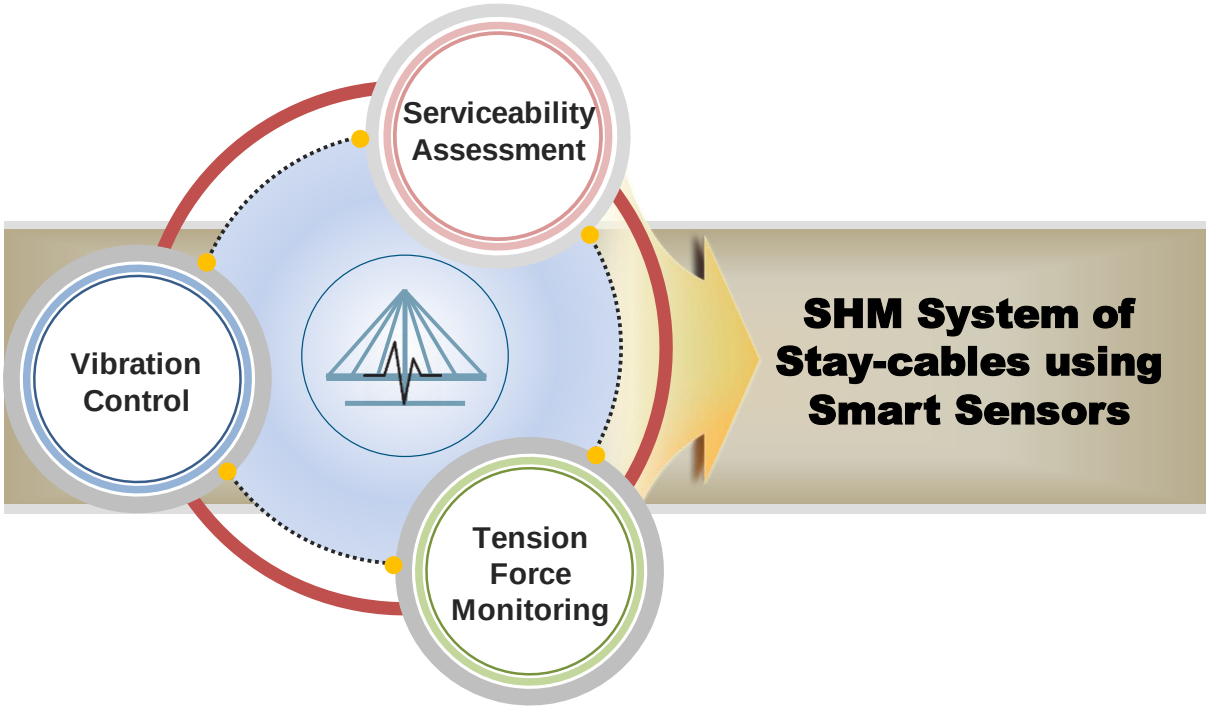

Figure 1-2. Outline of the structural health monitoring of stay-cables

Table 1-1. Objectives of four research topics

	Problems	**Research Objectives**
Serviceability Assessment and Monitoring	▪ Little prior research to develop an automated real-time serviceability assessment system ▪ Lack of research using smart sensor	▪ To develop an automated real-time serviceability assessment system using wireless smart sensors (for maintenance purpose)
	▪ Little prior research aimed at monitoring cable damping automatically	▪ To develop an automated cable damping monitoring method (for maintenance purpose)
	▪ Little prior research to assess the effects of vibration control on serviceability ▪ Prior studies have focused on vibration control	▪ To propose and evaluate a serviceability assessment method equipped with vibration control (for construction design)
Integrated Vibration Control System	▪ Little prior research to use of MR damper with an embedded semi-active control algorithm ▪ Lack of research using smart sensor	▪ To develop a cable vibration control system using MR damper with an embedded semi-active control algorithm
Automated Tension Force Monitoring using Deep Learning	▪ Imperfect demonstration for full automation considering different cable tensions ▪ Lack of research using smart sensor	▪ To develop the embedded sensor system for tension force monitoring, possible to measure the force under the different tension conditions

1.1.1. Topic 1: Serviceability Assessment and Monitoring [4, 39]

Cable serviceability is studied by assessing a serviceability level, monitoring damping, and evaluating a probability of serviceability failure considering control devices. First, an automated real-time system monitoring cable serviceability is developed using wireless smart sensors. Based on the design code from the United States [41], the serviceability failure of a stay-cable is defined as the case when the displacement of the cable in mid-span exceeds twice the diameter of the stay-cable with upper and lower bound. The serviceability assessment system for stay-cables proposed in this study was developed using the Raspberry Pi platform, which is an open-source single-board computer with low cost and low power consumption. The system features embedded on-board computation, including the acquisition of cable response using the MEMS accelerometer, estimation of displacement from the measured acceleration, serviceability assessment, and monitoring through wireless communication. Bridge inspectors can command the system through wireless communication, prompting it to send information back to the bridge inspectors related to the serviceability status of the stay-cable. A series of laboratory tests were conducted to verify the performance of the developed system.

As the stay-cables are vulnerable to vibration due to low inherent damping ratio, monitoring damping ratio continually is crucial to assess the level of serviceability. Accordingly, this study aims to present an automated cable damping monitoring strategy. For completeness, this study examined various damping estimation methods to determine the appropriate method for damping automation. The selected method, satisfying conditions for automation tailored to the stay-cable, was applied to cable responses under different wind conditions, obtained from in-service bridges in Korea. Proposed damping automation method was verified through monitoring data of cable responses in Hwatae Bridge, that results in different damping ratio depending on various wind speeds.

Lastly, this study proposes and evaluates a serviceability assessment method equipped with vibration control using the first-passage probability. A failure event, in terms of the cable serviceability, was defined as the case in which the subject cable response reached either the upper or lower bound of serviceability provided by the selected design code. The cable serviceability failure probability was then determined by means of the first-passage problem using VanMarcke's approximation. To demonstrate the proposed method, the stay-cables of the Second Jindo Bridge in South Korea were evaluated, and the analysis results showed that the appropriate selection of vibration control methods and properties could effectively reduce the probability of serviceability failure.

1.1.2. Topic 2: Integrated Vibration Control System [8]

The purpose was to develop an integrated cable vibration control system based on the Arduino platform which has embedded a semi-active control algorithm. As an open-source technology, the Arduino platform is a single-board system, performing both data acquisition and processing functions, with a low-price and low-power consumption. The MEMS accelerometer, also having a low-cost and low-power consumption, was built on the Arduino platform to implement the state-feedback of cable acceleration for the semi-active control. This study selected the magneto-rheological (MR) damper as a semi-active damping device, controlled by a semi-active control algorithm with the clipped-optimal controller embedded in the Arduino platform. To identify the performance of the developed integrated control system, this study installed a cable for a laboratory experiment and conducted a series of tests to estimate the fundamental natural frequency and tension of the cable. A series of experimental studies were carried out to examine the efficiency of the proposed control system based on semi-active control on cable vibration reduction by comparing with passive mode control.

1.1.3. Topic 3: Automated Tension Force Monitoring using Deep Learning [40]

Here, the aim was to develop an automated cable tension monitoring system using deep learning and wireless smart sensors capable of monitoring different tension forces. The automated system design was based on the Raspberry Pi platform, a cost-effective single-board computer, integrated with a MEMS accelerometer. A fully automated peak-picking algorithm was developed using a region-based convolution neural network (R-CNN), which was trained using only numerically generated peaks from the frequency domain representation of cable vibration. The embedded peak-picking algorithm enables the monitoring system to detect peaks automatically from the frequency domain representation. Post-processing was designed to select peaks representing natural modes of the cable by removing undesirable peaks. The developed system features embedded processing on the Raspberry Pi, including acceleration acquisition, power spectral density (PSD) calculation, automated peak-picking, post-processing for peak-selection, and tension force estimation. As the first fully automated monitoring system, the operation was verified through a series of laboratory and field tests.

2. LITERATURE REVIEW

2.1. Serviceability Assessment and Monitoring of Stay-cables

Serviceability of the cable-stayed bridge is the ability of a bridge to be used by the public over a given period of time, while operability is simply the ability of a bridge to continue to function in terms of structural strength [15, 16]. As bridge users tend to recognize a serviceability problem far earlier than an operability problem due to structural damage caused by vibration [15], a serviceability problem can more readily raise public concern regarding the safety of a cable-stayed bridge. Thus, maintaining appropriate serviceability should be emphasized as one of the primary concerns of bridge maintenance efforts [17-19].

This section introduces design codes that specify allowable vibration level satisfying serviceability of the stay-cable. As a vibration amplitude determines the serviceability level, the displacement estimation method based on acceleration data is described subsequently. Lastly, a cable damping is one of the factors closely related to the serviceability level [21-23], and thus methods for damping estimation are introduced in this section.

2.1.1. Allowable Serviceability Levels

Most modern developed countries have design codes that specify allowable serviceability levels for the cables of cable-supported bridges. For example, in Korea, the Korean Highway Bridge Design Code defines a serviceability failure to have occurred when cable vibration amplitude exceeds L/1600 at the middle of a stay-cable under average wind speed of less than 20 m/s, where L is the cable length [4]. The US Department of Transportation classifies the vibration comfort level of bridge users into three levels: ‘not allowable’ when the cable vibration amplitude exceeds 2.0 D, ‘recommended’ when the cable vibration amplitude is near 1.0 D, and ‘preferred’ when the cable vibration amplitude is near 0.5 D, where D is the diameter of the stay-cable [41]. In Japan, the serviceability of bridges with stay-cables is analyzed on the basis of the criterion of the Japanese Railway Bridge Specifications, which defines allowable deflection as L/2000 at mid-span of the bridge deck, where L is the span length in question [42]. In the Chinese Highway Cable-stayed Bridge Design Specification, a serviceability failure is considered to have occurred on a cable-stayed bridge when the deflection at mid-span of the bridge deck is over the allowable deflection of the bridge, defined as L/400, where L is the span length in question [43].

2.1.2. Serviceability Assessment: Displacement Estimation by Acceleration

Various displacement measurement methods have been introduced in the past, including those using contract-type and non-contact-type sensors [44]. Among these, the indirect estimation approach, particularly using an accelerometer, has often been employed to estimate the displacement owing to its convenient installation that is a reference-free and relatively low cost [44]. Theoretically, displacement can be obtained by the double integration of acceleration. However, double integration of the measured acceleration results in the low-frequency drift in the estimated displacement caused by unknown initial conditions, sensor noise, and signal discretization [44]. To avoid this problem, Lee *et al.* [45] proposed a dynamic displacement estimation method, which removes the low-frequency drift error by applying a high-pass filter [45]. The only prior knowledge required is information about the lowest frequency of the stay-cable. This method is appropriate for use with smart sensors, as it avoids low-frequency drift, does not require the initial displacement, provides efficient computation [45], and has been implemented in a wireless displacement estimation system using smart sensors [44, 46]. While this approach cannot estimate the static part of the displacement, dynamic displacement is sufficient to assess the serviceability of a stay-cable using the US criterion [41] employed in this study. Therefore, in this study, the displacement estimation method was applied to develop an automated real-time serviceability assessment system for the stay-cable.

This section briefly describes the displacement estimation method using the measured acceleration proposed by Lee *et al.* [45]. Let u be the estimated displacement, Δt the sampling time of the measurement, and $\bar{a}$ the measured acceleration. The displacement can be estimated by minimizing the following equation:

$$\underset{u}{\text{Min}}\,\Pi(u) = \frac{1}{2}\left\| L_a (L_c u - (\Delta t)^2 \bar{a} \right\|_2^2 + \frac{\lambda^2}{2}\|u\|_2^2 \tag{1}$$

where L_a is the integration operator based on the discretized trapezoidal rule, L_c is the second-order differential operator, $\|\bullet\|$ is the 2-norm of a vector, and λ is the regularization factor that adjusts the degree of regularization as indicated by the second term in the minimization problem. If the regularization factor becomes larger, the zero-displacements are estimated from the measured acceleration [45]. With a low regularization factor, the displacement information becomes meaningless and unstable [45]. Based on the optimal regularization term, the displacement can be derived as Equation (2), which minimizes the difference by the numerical integration of the measured acceleration and considers the regularization term

$$u = (L^T L + \lambda^2 I)^{-1} L^T L_a \bar{a} (\Delta t)^2 \tag{2}$$

where L is equal to $L_a L_c$ and the superscript T denotes the transpose of the matrix. The optimal regularization term is suggested as Equation (3), where N_d denotes the number of data points in a time window, as depicted in Figure 2-1 [45]:

$$\lambda_{\text{optimal}} = 46.81 N_d^{-1.95} \tag{3}$$

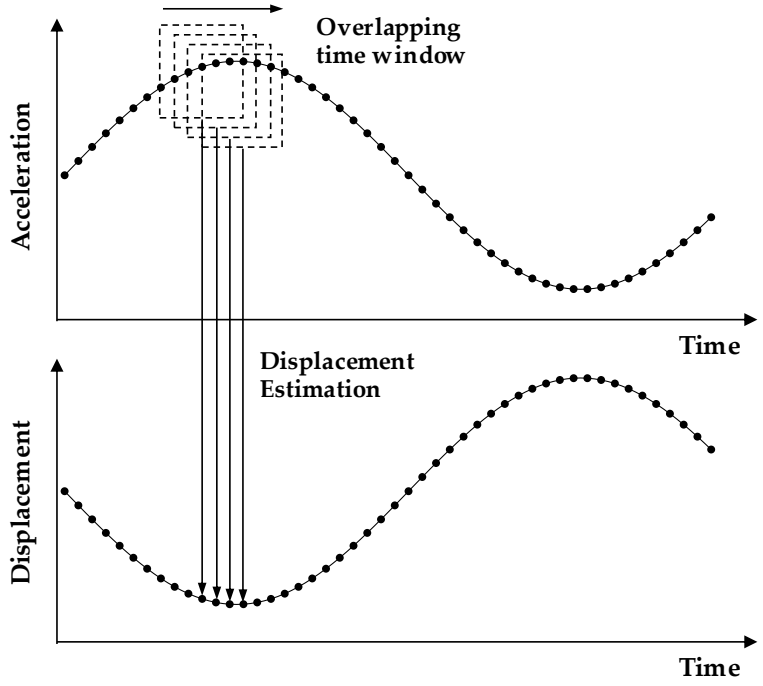

Figure 2-1. Displacement estimation scheme using the overlapping time window

Note that the overlapping moving time window depicted in Figure 2-1 was introduced to estimate the accurate displacement at the center, ignoring the errors that may occur at the beginning and end of the displacements. Each moving window was used to estimate the displacement based on Equation (2), and the full history of displacements is identical to a collection of estimated displacements at the center of each window. The detailed derivation of the estimation of displacement from the measured acceleration can be found in the study by Lee *et al.* [45].

2.1.3. Cable Damping Estimation

Modal analysis is widely conducted to identify dynamic properties of stay-cables, including natural frequency, mode shape, and damping ratio, by using dynamic response data. Cable damping can be estimated by time- or frequency-domain modal analysis. For monitoring cable damping ratio, this study summarizes damping estimation methods categorized into time- and frequency-domain approaches, which include Logarithmic Decrement Ratio, Stochastic Subspace Identification, Eigensystem Realization Algorithm Method, Half-power Bandwidth Method, and Frequency Domain Decomposition.

1) Time-domain Method

- **Logarithmic Decrement Ratio**

This is one of the methods to estimate the damping ratio from time-domain responses of free vibration [47]. This method uses the logarithm decrement between two adjacent peak amplitudes from the time-domain free vibration response as shown in Figure 2-2. When the amplitude of time period n denotes u_n, the logarithm decrement ratio between u_n and adjacent u_{n+1} can be expressed by the following equation.

$$\delta = \frac{1}{n}\ln\left(\frac{u_n}{u_{n+1}}\right) \tag{4}$$

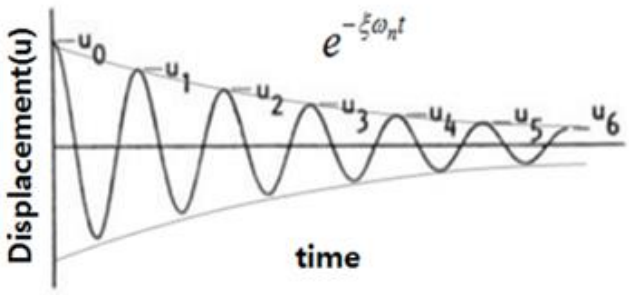

Figure 2-2. Example of free vibration response

Based on the logarithmic decrement ratio, the damping ratio can be derived as follows:

$$\xi = \frac{1}{2\pi n}\ln\left(\frac{u_1}{u_{n+1}}\right) \tag{5}$$

When white noise is added to measured free vibration response as shown in Figure 2-3, it is difficult to estimate damping ratio because of difficulty in identifying 1) locations of peaks and 2) amplitudes of peaks at period *n*. Therefore, white noise can affect the estimated damping ratio by the logarithmic decrement ratio.

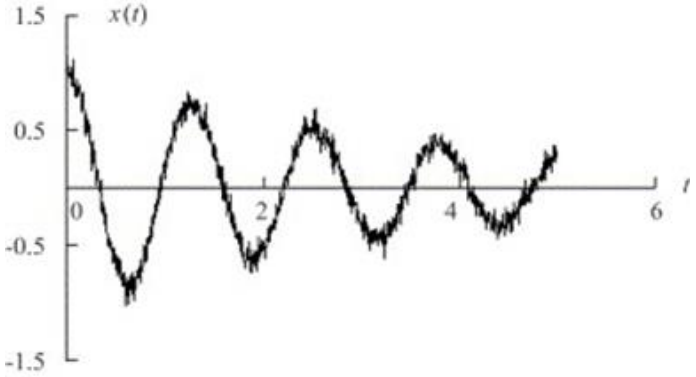

Figure 2-3. Free vibration response with white noise

■ Stochastic Subspace Identification (SSI)

Stochastic Subspace Identification (SSI) is one of the output-only modal analysis methods to estimate the modal properties of structures [48]. The output-only approach uses time-domain structural responses only under the condition of unknown input loading. Two types of SSI exist, which include data-driven SSI and covariance-driven SSI. As the latter method is convenient and fast, covariance-driven SSI is introduced in detail as below.

From a structural equation of motion, a state-space in discrete time can be expressed as follows:

$$\begin{aligned} X_{k+1} &= AX_k + w_k \\ Y_k &= CX_k + v_k \end{aligned} \tag{6}$$

where X denotes a state vector, Y is a response vector, A represents a system matrix, C is an output matrix, w_k is an input vector, especially ambient vibration, and v_k is a measurement noise. Here, two mutually independent w_k and v_k are stochastic random processes that can be represented by white noise. For computing SSI, the state matrix X is assumed to be a time-invariant stochastic process with zero-mean value as follows:

$$E[X_k] = 0 \qquad E[X_k X_k^T] = \Sigma \tag{7}$$

As the output-only modal analysis method, SSI can estimate modal properties by using covariance of measured output responses R_τ. The covariance of responses can be expressed as the following equation with any time delay τ.

$$R_\tau = E[Y_{k+\tau} Y_k^T] \tag{8}$$

Not only the covariance of measured output but also another covariance G which is called "next state-output" is necessary to compute SSI. The new covariance G can be described as follow:

$$G = E[X_{k+1} Y_k^T] = E[(AX_k + w_k)(CX_k + v_k)^T] \tag{9}$$

The covariance, R_τ and G, can be rearranged to estimate system matrix A as follow:

$$R_\tau = CA^{\tau-1}G \tag{10}$$

After defining the maximum time delay ($\tau_{\max}$), a Toeplitz matrix $T_{1:\tau_{\max}/2}$ for all time delay can be constructed using the covariance R_τ as shown in Figure 2-4. It is noted that the covariance R_τ is m x n matrix and the Toeplitz matrix is ($m \times \tau_{\max}/2$) $\times$ ($m \times \tau_{\max}/2$).

$$T_{1:\tau_{\max}/2} = \begin{bmatrix} R_{\tau_{\max}/2} & \cdots & \cdots & R_1 \\ \vdots & R_{\tau_{\max}/2} & \cdots & R_2 \\ R_{\tau_{\max}-1} & \cdots & \ddots & \vdots \\ R_{\tau_{\max}} & \cdots & \cdots & R_{\tau_{\max}/2} \end{bmatrix} = \begin{bmatrix} CA^{\tau_{\max}/2-1}G & \cdots & \cdots & CG \\ \vdots & CA^{\tau_{\max}/2-1}G & \cdots & CAG \\ CA^{\tau_{\max}-2}G & \cdots & \ddots & \vdots \\ CA^{\tau_{\max}-1}G & \cdots & \cdots & CA^{\tau_{\max}/2-1}G \end{bmatrix} \tag{11}$$

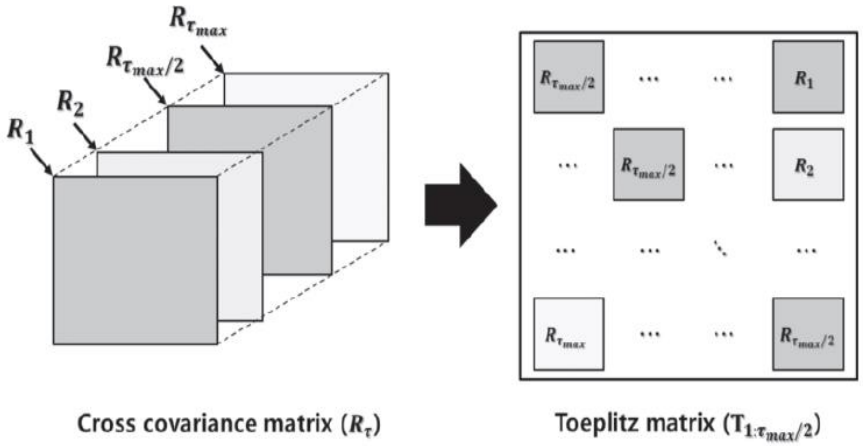

Figure 2-4. Construction of Toeplitz matrix by using covariance matrix R$\boldsymbol{\tau}$ [49]

The Toeplitz matrix can be decomposed into an Observability matrix Q_p and a Controllability matrix C_p as follows:

$$T_{1:\tau_{\max}/2} = \begin{bmatrix} C \\ CA \\ \cdots \\ CA^{\tau_{\max}/2-1} \end{bmatrix} \begin{bmatrix} A^{\tau_{\max}/2-1}G & \cdots & AG & G \end{bmatrix} = O_p C_p \tag{12}$$

The system matrix A can be estimated through the Observability matrix Q_p. Assuming that the upper box indicates Q_p^t and the bottom dotted box denotes Q_p^b in Figure 2-5, the system matrix A can be expressed by multiplying a pseudo-inverse of upper box and the bottom box as follow:

$$A = (O_p^t)^{\dagger} O_p^b \tag{13}$$

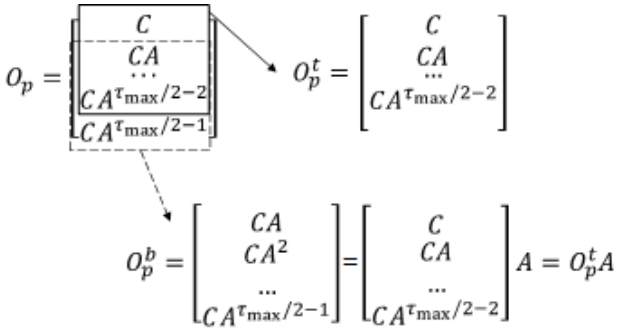

Figure 2-5. Extraction of system matrix from Observability matrix Q_p

The Observability matrix Q_p, a component of system matrix A, can be obtained through Singular Value Decomposition (SVD) of the Toeplitz matrix which results in three matrixes (U, S, V). Based on decomposed matrixes, the Observability matrix, as well as the Controllability matrix, can be derived as the following equation.

$$T_{1:\tau_{\max}/2} = USV^T = \begin{bmatrix} U_1 & U_2 \end{bmatrix} \begin{bmatrix} S_1 & 0 \\ 0 & 0 \end{bmatrix} \begin{bmatrix} V_1^T \\ V_2^T \end{bmatrix} = U_1 S_1 V_1^T = (U_1 S_1^{1/2})(S_1^{1/2} V_1^T) = O_p C_p \tag{14}$$

In summary, the system matrix A can be estimated by using the Observability matrix Q_p represented as $U_1 S_1^{1/2}$ from the SVD of the Toeplitz matrix. By Eigen Decomposition of the system matrix A, the obtained eigenvalue λ_k, natural frequencies ω_k, and damping ratio ξ_k can be represented as follows:

$$\lambda_k = \frac{\ln(\mu_k)}{\Delta t}, \quad \xi_k = -\frac{\mathrm{Re}(\lambda_k)}{abs(\lambda_k)}, \quad \omega_k = abs(\lambda_k) \tag{15}$$

$$Av = \lambda v \qquad (\lambda = diag(\mu_1, \mu_2, \ldots, \mu_N), v = [v_1, v_2, \ldots, v_N])$$

Although the SSI is one of the efficient methods widely applied to system identification and modal analysis when the input loading is unknown, the estimated damping ratio can be affected by types of spectral window because the covariance-driven SSI uses a correlation function between two ambient responses, calculated by the Fourier Transform, to construct the covariance matrix. Furthermore, the size of system matrix A is determined by manual assumption or by checking the estimated values from different system orders, which requires high computation time. In conclusion, the estimated damping ratio is affected by the system order and types of spectral window, and thus human judgment is required to estimate the damping ratio by using the SSI.

■ Eigensystem Realization Algorithm Method (ERA)

Eigensystem Realization Algorithm (ERA) is one of the approaches for system identification and modal analysis by using impulse responses [50]. The state-space model in the discrete-time domain can be expressed as following equation, where X is a state of a structure, Y is a response vector, u represents an input loading, and A, B, C, and D denotes a system, input, output, and feedthrough matrix respectively.

$$\begin{aligned} X_{k+1} &= AX_k + Bu_k \\ Y_k &= CX_k + Du_k \end{aligned} \tag{16}$$

When an impulse loading is applied to the structure, the impulse response vector Y can be represented by a combination of A, B, and C matrixes which are called Markov Parameters.

$$Y_k = CA^{k-1}B \tag{17}$$

The time-history of Y under the impact loading is used to construct a Hankel matrix H, consisting of an Observability matrix Q_p, the system matrix A, and a Controllability matrix C_p.

$$H_{k-1} = \begin{bmatrix} Y_k & Y_{k+1} & \cdots & Y_{k+s} \\ Y_{k+1} & Y_{k+2} & \cdots & Y_{k+s+1} \\ \vdots & \vdots & \ddots & \vdots \\ Y_{k+r} & Y_{k+r+1} & \cdots & Y_{k+r+s} \end{bmatrix} = \begin{bmatrix} C \\ CA \\ \vdots \\ CA^r \end{bmatrix} A^{k-1} \begin{bmatrix} B & AB & \cdots & A^sB \end{bmatrix} = O_p A^{k-1} C_p \tag{18}$$

The system matrix A can be derived by the Singular Value Decomposition (SVD) of the Hankel matrix H_0 at k=1 which results in three matrixes (U, S, V) as follows:

$$H_0 = USV^T = \begin{bmatrix} U_1 & U_2 \end{bmatrix} \begin{bmatrix} S_1 & 0 \\ 0 & S_2 \end{bmatrix} \begin{bmatrix} V_1^T \\ V_2^T \end{bmatrix} = U_1 S_1 V_1^T + U_2 S_2 V_2^T \simeq U_1 S_1 V_1^T = U_1 S_1^{1/2} S_1^{1/2} V_1^T \tag{19}$$

The Observability Q_p and Controllability C_p matrixes are newly defined to be $U_1 S_1^{1/2}$ and $S_1^{1/2} V_1^T$ respectively from the SVD of the Hankel matrix at k=1. The system matrix A can be finally obtained by applying Pseudo Inverse of newly defined the Observability and Controllability matrixes from the $H_1 = O_p A C_p$.

$$A = O_p^{\dagger} H_1 C_p^{\dagger} = (S_1^{-1/2} U_1^T) H_1 (V_1 S_1^{-1/2}) \tag{20}$$

The eigenvalue (λ_k), natural frequencies (ω_k), and damping ratio (ξ_k) can be estimated by the Eigen Decomposition of the system matrix A as the following equation.

$$\lambda_k = \frac{\ln(\mu_k)}{\Delta t}, \quad \xi_k = -\frac{\mathrm{Re}(\lambda_k)}{abs(\lambda_k)}, \quad \omega_k = abs(\lambda_k) \tag{21}$$

$$Av = \lambda v \qquad (\lambda = diag(\mu_1, \mu_2, \ldots, \mu_N), v = [v_1, v_2, \ldots, v_N])$$

The ERA can analyze the system identification and modal analysis based on impulse response data. However, ambient vibration is general in civil engineering structures, and thus Natural Excitation Technique (NExT) is applied to generate impulse vibration from the ambient response by using a correlation function. In general, the correlation function is obtained by an inverse Fourier Transform of a Cross Power Spectral Density (CPSD) of time-history ambient responses. Therefore, the damping ratio obtained by ERA with NExT can be affected by the types of spectral windows and the number of Fourier Transform (NFFT) similar to the result from the SSI.

2) Frequency-domain Method

■ Half-power Bandwidth Method

Half-power bandwidth method is appropriate to estimate the damping parameter when structural responses are forced or ambient vibration [51]. The damping ratio can be calculated by using two frequencies where their locations correspond to $1/\sqrt{2}$ of peak height in the Frequency Response Function of the system as shown in Figure 2-6. When a frequency located in peak denotes ω_n and two frequencies in $1/\sqrt{2}$ of peak height are ω_1 and ω_2 respectively, the damping ratio can be derived as follows:

$$\xi = \frac{w_2 - w_1}{2 w_n} \tag{22}$$

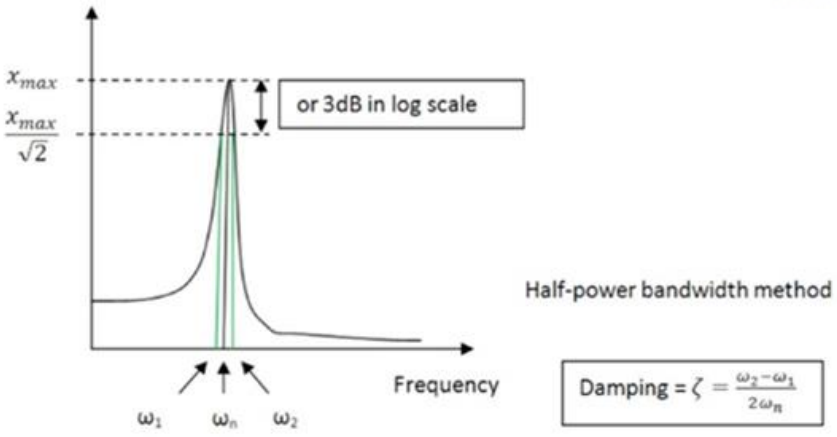

Figure 2-6. Damping estimation using Half-power Bandwidth Method

This method can be applied to the case when the Frequency Response Function of the system is difficult to be derived. Without prior knowledge of an input loading, the damping ratio can be estimated by power spectral density (PSD) from structural responses by forced or ambient vibration. When using the PSD, two frequencies can be selected as points located in 1/2 of peak height instead of $1/\sqrt{2}$.

However, the damping ratio from PSD is affected by types of spectral window which is used to reduce spectral leakage under the PSD calculation. As geometric shapes of peaks are different depending on what types of windows are used as shown in Figure 2-7, the damping ratio can be unreliably estimated.

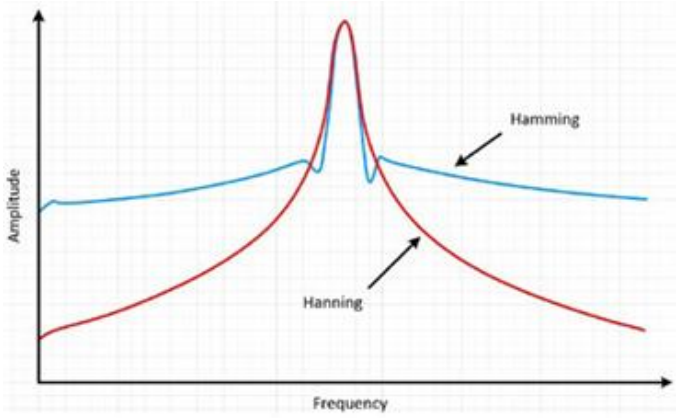

Figure 2-7. Power spectral density by different types of the spectral window

Furthermore, the number of fast Fourier Transform (NFFT) is one of the factors affecting the PSD calculation. If the NFFT is not enough, peaks from PSD can have blunt shapes which result in the overestimation of the damping ratio. Therefore, enough NFFT is necessary to calculate PSD with sharp peaks, and thus empirical study is needed to determine appropriate NFFT.

■ Frequency Domain Decomposition (FDD)

Frequency Domain Decomposition (FDD) is one of the representatives of the output-only system identification method in the frequency domain [52]. From the linear time-invariant system, the input and output can be expressed in the frequency domain as follows:

$$G_{yy}(j\omega) = \bar{H}(j\omega) G_{xx}(j\omega) H(j\omega)^T \tag{23}$$

where, $H(j\omega)$ indicates the frequency response function (FRF), $G_{yy}(j\omega)$ and $G_{xx}(j\omega)$ represent the cross power spectral density (CPSD) of output and input data.

The FRF $H(j\omega)$ can be described by a form of a partial fraction as follows:

$$H(j\omega) = \sum_{k=1}^{n} \left(\frac{R_k}{j\omega - \lambda_k} + \frac{\bar{R}_k}{j\omega - \bar{\lambda}_k} \right) \tag{24}$$

where n is the number of natural modes, λ_k is a pole, R_k is a constant. When the input loading is assumed to be white noise, $G_{xx}(j\omega)$ becomes a constant C, and thus the output CPSD can be expressed as follows:

$$G_{yy}(j\omega) = \sum_{k=1}^{n} \sum_{s=1}^{n} \left(\frac{R_k}{j\omega - \lambda_k} + \frac{\bar{R}_k}{j\omega - \bar{\lambda}_k} \right) C \left(\frac{R_s}{j\omega - \lambda_s} + \frac{\bar{R}_s}{j\omega - \bar{\lambda}_s} \right)^H \tag{25}$$

Here, H implies the conjugate complex number and matrix transpose. By multiplying two partial fractions, the following equation can be obtained.

$$G_{yy}(j\omega) = \sum_{k=1}^{n} \left(\frac{A_k}{j\omega - \lambda_k} + \frac{\bar{A}_k}{j\omega - \bar{\lambda}_k} + \frac{B_k}{-j\omega - \lambda_k} + \frac{\bar{B}_k}{-j\omega - \bar{\lambda}_k} \right) \tag{26}$$

A_k and B_k are residue matrix of output CPSD, and can be expressed as follows:

$$A_k \propto d_k \phi_k \phi_k^T \tag{27}$$

The CPSD of output can be rearranged as following decomposed terms with natural modes. Here, $Dom(\omega)$ denotes the number of natural modes, in general two modes which occupy most energy of a response.

$$G_{yy}(j\omega) = \sum_{Dom(\omega)} \left(\frac{d_k \phi_k \phi_k^T}{j\omega - \lambda_k} + \frac{\bar{d}_k \bar{\phi}_k \bar{\phi}_k^T}{j\omega - \bar{\lambda}_k} \right) \tag{28}$$

The CPSD of output response measured from multiple sensors after the Singular Value Decomposition (SVD) can be depicted as follows:

$$\hat{G}_{yy}(j\omega) = U_i S_i U_i^H \tag{29}$$

where $U_i = [u_{i1}, u_{i2}, \ldots, u_{im}]$ is a unitary matrix and S_i is a vector composed of each singular value. The first singular value of S_i corresponds to the PSD of the first natural mode, and thus the vector u_{i1} represents the first mode shape. After determining PSD of each natural mode by FFD, the damping ratio can be estimated using the Half-power Bandwidth Method. In addition, the Logarithmic Decrement Ratio method can be applied to identify the damping ratio after calculating free responses through inverse Fourier Transform. However, this method can be affected by the types of spectral windows and the number of Fourier Transform, which results in an unstable damping ratio.

3) Summary

The five representative damping estimation methods are summarized in the below table regarding brief explanation, data type, and loading condition.

Table 2-1. Summary of five damping estimation methods

Data type	Method	Explanation	Loading
Time-domain	Logarithmic Decrement Ratio	▪ Damping estimation by using logarithm decrement of peaks between two adjacent periods	Free vibration
	Stochastic Subspace Identification (SSI)	▪ Covariance-based system identification method by singular value decomposition of Toeplitz matrix	Free vibration / Ambient vibration
	Eigensystem Realization Algorithm (ERA)	▪ Impulse response-based system identification method by singular value decomposition of Hankel matrix	Free vibration / Ambient vibration
Frequency-domain	Half-power Bandwidth Method	▪ Damping estimation based on two frequencies located in 1/2 of peak height in PSD	Forced vibration / Ambient vibration
	Frequency Domain Representation (FDD)	▪ Output-only system identification methods based on frequency-domain data	Ambient vibration

2.2. Cable Vibration Control

To keep the serviceability of the cables within an acceptable level, researchers have proposed vibration control methods, including tying multiple cables together, modifying the aerodynamics of cable surfaces, and applying vibration control [11, 12, 24]. Tying cables together is a practical approach for reducing vibration by shifting the natural frequency of the cable to avoid resonance, but this method degrades the aesthetics of the bridge [11]. To avoid exposure to external vibration generating forces, the aerodynamics of the cable surface has also been modified [11]. However, this method is only effective within a specific frequency range, and it is difficult to retrofit existing cables [11]. Due to the drawbacks and limitations of the first two approaches, vibration control such as passive and semi-active control for stay-cables has emerged as an effective and practical alternative [6, 11, 12, 24, 25].

In this section, the cable dynamics are derived from the motion of a taut string proposed by Irvine [53], followed by passive and semi-control algorithms.

2.2.1. Cable Dynamics

This section describes the vibration-controlled cable dynamics using an analysis that considers cable characteristics including sag, inclination, static deflection, and flexural rigidity. Consider an inclined cable with a vibration control device, as shown in Figure 2-8. Based on previous studies [11, 53, 54], a cable system with a damper can be expressed as a non-dimensional partial differential equation of motion for the transverse displacement $v(x,t)$ in the domain $0 \le x \le 1$ with boundary conditions $v(0,t) = v(1,t) = 0$ for all t as:

$$\ddot{v}(x,t) + c\dot{v}(x,t) - \frac{1}{\pi^2} v''(x,t) + \frac{\lambda^2}{\pi^2}\left[\int_0^1 v(\xi,t)d\xi\right] = f(x,t) + F_d(t)\delta(x - x_d) \tag{30}$$

where c is the non-dimensional viscous damping per unit length; x_d is the location of the damper; $F_d(t)$ is the transverse damping force at $x = x_d$; $v''(x,t)$ is the second-order partial derivative of displacement v with respect to x; $\ddot{v}(x,t)$ and $\dot{v}(x,t)$ denote partial derivatives with respect to t; $f(x,t)$ is the distributed load along the cable; λ^2 is the non-dimensional sag parameter, and $\delta(x\text{-}x_d)$ is the Dirac-delta function. The non-dimensional quantities describing the cable are related to their corresponding dimensional quantities, which can be found in the previous study [11].

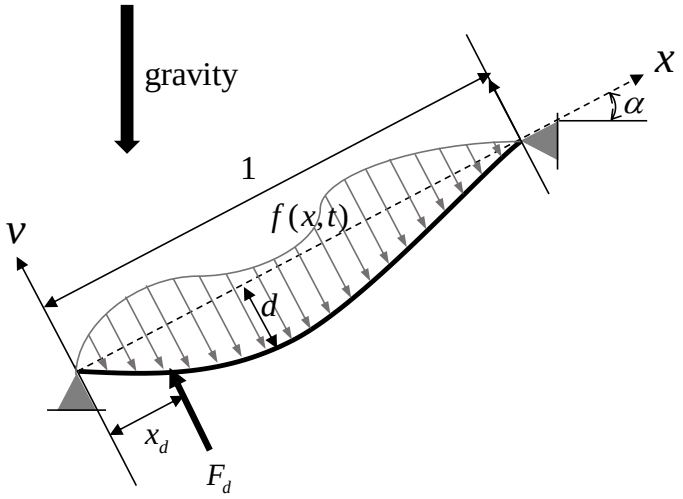

Figure 2-8. Inclined cable with sag and damper

The non-dimensional parameter λ^2 considers the effect of cable sag, inclination, and axial stiffness on the cable dynamics [11, 54] as follows:

$$\lambda^2 = \left(\frac{\rho g L \cos\alpha}{T}\right)\frac{EAL}{TL_e} = 64\left(\frac{\bar{d}}{L}\right)^2\frac{EAL}{TL_e}$$
$$L_e = L\left[1+\frac{1}{8}\left(\frac{\rho g L\cos\alpha}{T}\right)^2\right], \quad \bar{d} = Ld = \frac{\rho g L^2\cos\alpha}{8T} \tag{31}$$

where ρ is the cable mass per unit length; α is the inclination angle; L is the cable length; L_e is the stretched length of the cable; T is the cable tension in the longitudinal direction along the x-axis; d is the peak dimensional sag of the cable; g is the gravity; E is Young's modulus of the cable; and A is a cross-sectional area of the cable. Note that the non-dimensional sag parameter λ^2 becomes zero when the effect of cable sag is ignored.

The transverse cable motion $v(x,t)$ can be assumed using a finite series, formed of a combination of generalized coordinates $q_j(t)$ and a set of shape functions $\phi_j(x)$, that satisfies the boundary conditions $\phi_j(0) = \phi_j(1) = 0$, where j represents the mode number, as follows:

$$v(x,t) = \sum_{j=1}^{m} q_j(t)\phi_j(x) \tag{32}$$

The shape functions of a cable without a damper $\phi_{un,j}(x)$ can be assumed to be sinusoidal [55], while those of a cable with a damper $\phi_{con,j}(x)$ include static deflection as the first shape function and sinusoidal functions for the rest of the modes [11, 55]. The shape functions for a cable without and with a damper are as follows, where m is the number of assumed modes.

$$\phi_{un,j}(x) = \sin j\pi x \quad (0 \le x \le 1, \quad j = 1, \cdots, m) \tag{33}$$

$$\begin{aligned} \phi_{con,1}(x) &= \begin{pmatrix} x/x_d & (0 \le x \le x_d) \\ (1-x)/(1-x_d) & (x_d \le x \le 1) \end{pmatrix} \\ \phi_{con,j+1}(x) &= \sin j\pi x \quad (0 \le x \le 1, \quad j = 1, \cdots, m-1) \end{aligned} \tag{34}$$

The equation of motion in Equation (30) can be expressed in matrix form by substituting the cable motion in Equation (32), multiplying by the shape functions, then integrating over the length of the cable. Considering the damper force $F_d(t)$ and the additional tension due to cable sag, a cable system with a damper can be described in matrix form as [11, 54]:

$$\mathrm{M}\ddot{\mathrm{q}} + \mathrm{C}\dot{\mathrm{q}} + \mathrm{K}\mathrm{q} = \mathrm{f} + \phi F_d(t) \tag{35}$$

$$\begin{aligned} m_{ij} &= \int_0^1 \phi_i(x)\phi_j(x)dx, \qquad c_{ij} = cm_{ij} \\ k_{ij} &= \lambda^2 k_i^{sag} k_j^{sag} + k_{ij}^{tension}, \quad f_i(t) = \int_0^1 f(x,t)\phi_i(x)dx \\ k_i^{sag} k_j^{sag} &= \frac{1}{\pi^2}\int_0^1 \phi_i(x)dx \int_0^1 \phi_j(x)dx, \quad k_{ij}^{tension} = -\frac{1}{\pi^2}\int_0^1 \phi''_i(x)\phi_j(x)dx \end{aligned} \tag{36}$$

where the mass M = $[m_{ij}]$, damping C = $[c_{ij}]$, stiffness due to sag and tension K = $[k_{ij}]$, generalized coordinates q = $[q_1, q_2 \cdots q_m]^T$, externally applied force f = $[f_1, f_2 \cdots f_m]^T$, and damper load vector ϕ = $[\phi_1(x_d), \phi_2(x_d) \cdots \phi_m(x_d)]^T$.

The state-space form of cable dynamics can be formulated as follows where X=$[\mathrm{q}^{\mathrm{T}} \quad \dot{\mathrm{q}}^{\mathrm{T}}]^{\mathrm{T}}$ is the system state, Y=$[\mathrm{v}(\mathrm{x_d},\mathrm{t}) \quad \ddot{\mathrm{v}}(\mathrm{x_d},\mathrm{t})]^{\mathrm{T}}$ +v is a vector including displacement and acceleration at damper location, v is a vector of sensor noise.

$$\begin{aligned} \dot{\mathrm{X}} &= \mathrm{A}\mathrm{X} + \mathrm{B}F_d + \mathrm{G}\mathrm{f} \\ \mathrm{Y} &= \mathrm{C}\mathrm{X} + \mathrm{D}F_d + \mathrm{H}\mathrm{f} + v \end{aligned} \tag{37}$$

$$\begin{aligned} \mathrm{A} &= \begin{bmatrix} 0 & \mathrm{I} \\ -\mathrm{M}^{-1}\mathrm{K} & -\mathrm{M}^{-1}\mathrm{C} \end{bmatrix}, \qquad \mathrm{B} = \begin{bmatrix} 0 \\ \mathrm{M}^{-1}\varphi \end{bmatrix} \\ \mathrm{C} &= \begin{bmatrix} \varphi^{\mathrm{T}} & 0 \\ -\varphi^{\mathrm{T}}\mathrm{M}^{-1}\mathrm{K} & -\varphi^{\mathrm{T}}\mathrm{M}^{-1}\mathrm{C} \end{bmatrix}, \quad \mathrm{D} = \begin{bmatrix} 0 \\ \varphi^{\mathrm{T}}\mathrm{M}^{-1}\varphi \end{bmatrix} \\ \mathrm{G} &= \begin{bmatrix} 0 \\ \mathrm{M}^{-1} \end{bmatrix}, \qquad \mathrm{H} = \begin{bmatrix} 0 \\ \varphi^{\mathrm{T}}\mathrm{M}^{-1} \end{bmatrix} \end{aligned} \tag{38}$$

2.2.2. Passive Control

Several studies have proposed passive control using viscous dampers attached transversely to stay-cables near the deck anchorages [6, 11, 24]. When well-tuned, such passive viscous dampers can provide supplemental damping to a cable without requiring external power [6]. As a result, this type of damper has been widely applied to many cable-stayed bridges worldwide, including the Brotonne Bridge in France (1983), the Sunshine Skyway Bridge in Florida (1988), and the Aratsu Bridge in Japan (1989) [11]. The use of this scheme in long-span bridges, however, has revealed that, despite its effectiveness, it has installation challenges. Owing to aesthetic and practical reasons, the damper location is restricted to a location close to the cable anchor, within 5% [12, 56]. For a bridge having a short cable, the passive damper can provide sufficient damping by being installed at feasible location, whereas for a long-stay bridge having a cable that is over 1,000 m, the passive damper alone has difficulty in meeting the control requirement of the cable because of insufficient damping to eliminate the vibration [11, 12, 57].

When a passive viscous damper is used to control the cable vibration, the non-dimensional damper force can be expressed as:

$$F_d(t) = -c_d \dot{v}(x_d, t) \tag{39}$$

where the c_d is non-dimensional damping constant and $\dot{v}(x_d, t)$ is the non-dimensional velocity at the location of the damper $\dot{v}(x_d, t) = \phi^T \dot{\mathbf{q}}$ [11, 55]. In the case of a cable without a damper, the non-dimensional damping constant c_d is zero.

The cable dynamics in Equation (35) can be expressed as different form by substituting the damper force $F_d(t)$ and rearranging the formula where damping matrix C contains the $F_d(t)$ together as follows:

$$\mathrm{M}\ddot{\mathrm{q}} + \mathrm{C}\dot{\mathrm{q}} + \mathrm{K}\mathrm{q} = \mathrm{f} \tag{40}$$

$$\begin{gathered} m_{ij} = \int_0^1 \phi_i(x)\phi_j(x)dx, \qquad c_{ij} = cm_{ij} + c_d \phi\phi^T \\ k_{ij} = \lambda^2 k_i^{sag} k_j^{sag} + k_{ij}^{tension}, \quad f_i(t) = \int_0^1 f(x,t)\phi_i(x)dx \\ k_i^{sag} k_j^{sag} = \frac{1}{\pi^2}\int_0^1 \phi_i(x)dx \int_0^1 \phi_j(x)dx, \quad k_{ij}^{tension} = -\frac{1}{\pi^2}\int_0^1 \phi''_i(x)\phi_j(x)dx \end{gathered} \tag{41}$$

Based on the rearranged formula in Equation (40), the state-space form of cable dynamics in Equation (37) can be reformulated as a form that B and D matrixes are merged into A and C matrixes.

2.2.3. Semi-active Control

The semi-active control as an alternative to passive control has received considerable attention as a new solution for vibration reduction of long stay-cables [12, 57]. With a semi-active control, the magnetorheological (MR) damper has become a promising semi-active damping device in civil engineering, especially in the cable-stayed bridge for vibration reduction [6, 24, 57, 58]. Compared to the passive control with viscous damper, the semi-active MR damper has outstanding features for cable vibration reduction [25, 57, 59]. Owing to the advantages of the semi-active MR damper, theoretical studies have been conducted to implement the MR damper in cable vibration control [24, 60]. Wu and Cai [24] conducted a performance test of the MR damper with different frequencies, temperatures, and input currents, and identified the effectiveness of the passive mode MR damper on cable vibration reduction based on the test using scaled laboratory cable. Li, Liu [12] installed the combined stay-cable/MR damper system and conducted a series of tests to identify the efficiency of the MR damper on cable vibration control under sinusoidal excitation with the first two modal resonant frequencies. The experiments were carried out with different control strategies, passive-off (without input current), passive-on (with maximum input current), and semi-active control (based on state feedback of response), and the MR damper with semi-active control indicated better control efficacy than the passive mode. Because the stay-cable has low damping, Zhou and Sun [28] conducted free vibration-damping tests on a full-scale cable, attaching a pair of MR dampers to the cable to examine the effect of the MR damper on the cable damping. Compared to the free cable without the MR damper, the free cable with the MR damper experienced increased cable damping events though there was no applied voltage. When the passive-on voltage was transmitted to the MR damper, the damping of the cable greatly increased. The MR damper was applied not only in theoretical studies but also to real stay-cables of a bridge. The first application of MR damper to a real stay-cable was carried out in 2002 on the Dongting Lake Bridge in China [5]. Since then, the MR damper has been applied to the Eiland Bridge in the Netherlands [27], Third Qiantang River Bridge [26], and Bingzhou Yellow River Highway Bridge in China [12].

While many controllers are known to be used for semi-active control [61], the clipped-optimal controller based on state feedback of acceleration for semi-active control is widely used because this controller is known to be suitable for the MR damper [62]. To make the MR damper generate the desired damping force, the clipped-optimal controller determines the appropriate command input voltage applied to the current driver for the MR damper. The desired control force f_c is provided based on the Linear Quadratic Gaussian (LQG) control. The control of cable vibration is treated as an optimization problem, and LQG control is used to solve this problem. A quadratic cost function is defined based on the LQR theory as follows:

$$J_t = \int_0^\infty [X(t)^T Q X(t) + R f_c^{\,2}(t)] dt \tag{42}$$

where Q is a state weight matrix, R is a weight factor for control, X(t) is a system state, and f_c is the desired control force. The desired control force is determined by minimizing a quadratic cost function based on the constraints imposed by the state-space matrix of cable dynamics as follows.

$$f_c = -K\hat{X}(t) \tag{43}$$

where K is the control gain, satisfying the algebraic Riccati equation, and $\hat{X}(t)$ is an estimated system state X(t), calculated by the Kalman filter based on the measured cable displacement at the location of the damper.

The command input voltage is determined by the relationship between the damping force generated by the MR damper and the desired optimal control force. When the magnitude of damping force is smaller than that of the desired control force with the same sign, the command voltage is increased to the maximum level in order to match the damping force with the desired control force by increasing the damping force of the damper. If the damping force is the same as the desired control force, the command voltage remains constant. Otherwise, the command voltage is set to zero. The clipped-optimal algorithm can be summarized in a simple equation as follows.

$$V = V_{max} H\{(f_c - F_d) F_d\} \tag{44}$$

where V is the command voltage to the current driver, V_{max} is the maximum voltage saturating magnetic field in the MR damper, f_c is the desired optimal control force, F_d is the damping force generated by the MR damper, and H(.)is the Heaviside step function. The detailed graphical explanation is in Figure 2-9.

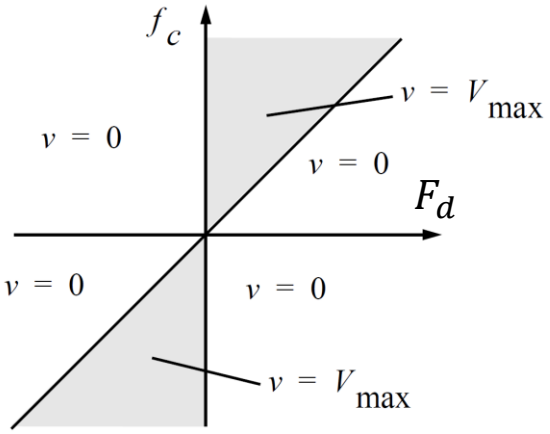

Figure 2-9. Command voltage determined by semi-active damper

2.3. Cable Tension Monitoring

Previous studies have measured cable tension forces by using direct and indirect techniques. The direct method has used load-measurement devices such as load cells, optical fiber Bragg grating (OFBG) sensor, and electromagnetic (EM) sensor to measure the tension force [1, 2, 30, 34]. The load cell and OFBG sensor have the advantages of measuring tension force accurately. However, these devices are mainly installed during the construction stage, i.e., they have problems such as difficult to be replaced and not appropriate to be applied in the existing cable without these sensors before [1, 34]. The EM sensor can measure the tension force of a cable exposed to the air by measuring wave speed generated by EM induction, whereas this sensor cannot measure the tension of a cable that is filled with grouting or grease [1]. Owing to the drawbacks of the direct method, the indirect method has received significant attention as a reliable, cost-effective, and convenient approach to measure tension force [2, 30-34]. The cable tension can be estimated indirectly by measuring cable responses such as acceleration, strain, and ferromagnetic magneto-elasticity [2]. Among various indirect methods, a vibration-based method with an acceleration data has been commonly used in practice to estimate the tension force of a cable by using the relationship between modal parameters and the tension force [2, 30-34].

2.3.1. Vibration-based Estimation of Cable Tension Force

As one of the commonly used the vibration-based method by Shimada [63], this algorithm can estimate the cable tension force T by using an explicit relationship with natural frequencies f_n and corresponding mode number n of the cable. Assume that the cable is inclined with constant tension force T, cable length L, bending stiffness EI, weight per unit length w, gravitational constant g and deflection d at the middle span as shown in Figure 2-10. The equation of motion of the inclined cable can be expressed as Equation (45).

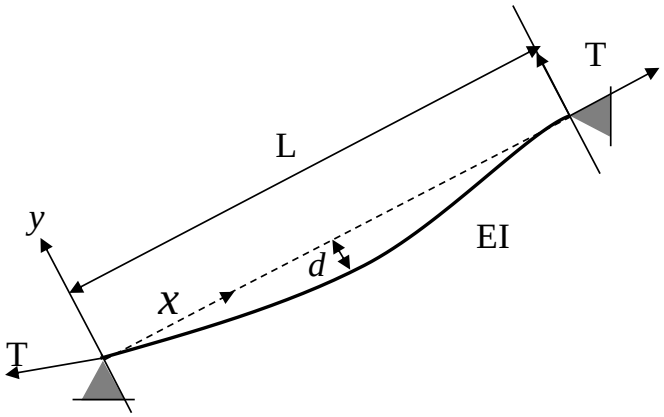

Figure 2-10. Inclined cable with tension force T

$$\frac{w}{g}\frac{\partial^2 y}{\partial t^2} + EI\frac{\partial^4 y}{\partial x^4} - T\frac{\partial^2 y}{\partial x^2} = 0 \tag{45}$$

If both ends of the cable are simply supported, a cable tension T can be written as a linear form in terms of $(f_n/n)^2$ and n^2 as shown in Equation (46).

$$T = \frac{4wL^2}{g}\left(\frac{f_n}{n}\right)^2 - \frac{EI\pi^2}{L^2}n^2 \tag{46}$$

This equation can be rearranged as a form of linear regression as below, and graphical representation is shown in Figure 2-11. Based on the least-square method, $(f_n/n)^2$ can be estimated by the linear regression of n^2 with slope a, and y-intercept b. It is noted that slope a is related to bending stiffness EI. The cable tension force can be estimated by the y-intercept b, which is identical to $(4wL^2/g)\times b$.

$$\left(\frac{f_n}{n}\right)^2 = \frac{EIg\pi^2}{4wL^4}n^2 + \frac{g}{4wL^2}T = an^2 + b \tag{47}$$

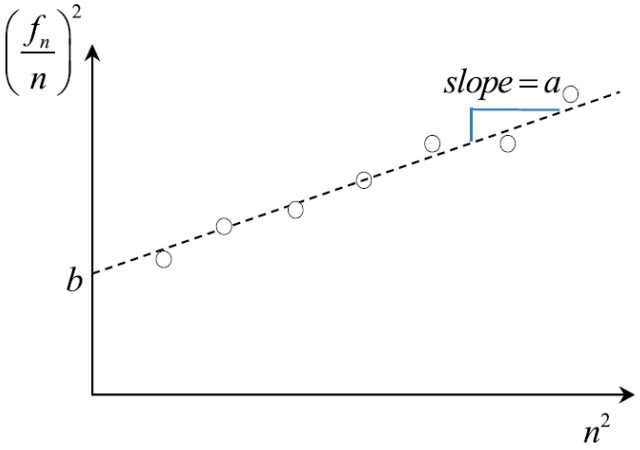

Figure 2-11. Least-square method to estimate cable tension force

The cable tension can be estimated using Equation (2) by following steps: 1) cable acceleration is measured, 2) measured acceleration is converted into frequency domain representation (e.g., PSD), 3) peak-picking is conducted to extract modal properties, including natural frequencies and corresponding mode numbers, and 4) cable tension is estimated by the linear regression of modal properties, especially $(f_n/n)^2$ and n^2. Linear regression of modal properties on cable tension enables a low-frequency response caused by cable-deck interaction to be ignored [35].

As locations of peaks in the frequency domain of a cable response represent modal properties of the cable, a peak-picking method can be implemented to determine the natural frequencies and

corresponding mode numbers. If peaks are detected automatically, natural frequencies of the cable could be identified. As natural frequencies of a cable are proportionally increasing with integer multiple [31], the mode number of each detected natural frequency can be extracted subsequently. Finally, automation in tension force estimation could be achieved by a linear relationship with modal properties automatically identified by peak-picking. In the next section, this study introduces an automated peak-picking algorithm based on Faster R-CNN used to find natural frequencies of a cable and corresponding mode numbers.

2.3.2. Automated Cable Tension Estimation

As an effort to monitor the cable tension force, previous works have proposed a cable tension monitoring system implementing the vibration-based approach [9, 30, 31]. These studies have shown a possibility of monitoring cable tension force automatically by identifying natural frequencies through a peak-picking method. For example, Cho *et al* [30] initially developed a wireless system for automated cable tension estimation using an accelerometer. To estimate cable tension, the first three natural frequencies were identified automatically through a peak-picking method. This method initially estimated the first peak greater than a predefined threshold value and searches the local maxima point within the prescribed frequency range. The maximum point was considered as the first natural frequency and the other two modal frequencies were obtained by multiple times the first mode. The different approach of peak-picking was proposed by Kim *et al* [9], which searches the local maxima of the power spectrum within preselected frequency ranges to determine natural frequencies. Predefined frequency bands were believed to include natural frequencies of the cable. The tension monitoring system utilized piezoelectric strain sensors to measure cable responses and applied the peak-picking method to identify the natural frequencies. When the variation of cable tension is within 20 % of the designed force, modal properties were successfully extracted automatically through the monitoring system which embedded the peak-picking. For long term monitoring of cable tension, Sim *et al* [31] constructed a wireless sensor network using a MEMSIC's Imote2 smart sensor which featured power harvesting and sleeping mode for inactive sensors to save the operation power. To monitor the cable tension automatically, the peak-picking identified the natural frequencies by searching the highest points around the approximate value of natural frequencies. For successful identification of peaks, natural frequencies of the cable are assumed to be 1) well separated and recognized, and 2) almost constant over time. The cable tension monitoring system was applied to the in-service cable-stayed bridge in the Republic of Korea and successfully performed monitoring cable tension about 1 month. Overall, the previous monitoring system has implemented the peak-picking to identify natural frequencies automatically by selecting maximum peaks which are larger than the user-defined threshold or within prescribed frequency ranges.

2.3.3. Automated Peak-picking using a Faster R-CNN

As a method to identify locations of salient peaks in the graphical data, peak-picking is widely used to extract modal parameters such as natural frequency, mode shape, and damping ratio from the structural responses in the frequency domain [9, 30, 31, 37]. Many attempts have been conducted to propose the peak-picking method to estimate cable tension automatically [9, 30, 31]. However, these methods require user-defined thresholds or prescribed frequency ranges to search peaks and thus can be applied to specific applications [22, 37, 38]. Recently, previous work has shown the potential of deep learning technique in developing automated peak detector which can distinguish cable peaks from undesirable peaks [37].

In the civil engineering field, deep learning has been recognized as a promising tool to solve structure-related problems, including automated crack detection, structural damage identification and structural component recognition [64]. Especially, a region-based convolutional neural network (R-CNN) has been implemented to detect objects in images such as concrete cracks, steel corrosion, and components of the structure [65, 66]. Among various R-CNN methods, the Faster R-CNN has received significant attention in the field of object detection, which features a combination of a region proposal network (RPN) and Fast R-CNN [67]. Fast R-CNN can detect multiple objects from an image by passing the image through several convolutional and max-pooling layers to obtain a feature map and implementing selective search to generate possible object locations from the feature map [67]. However, the computational time is huge to generate the possible object locations through the selective search method despite the better performance of multiple-object detection than that of CNN-based detection which uses a fixed sliding window to extract regions of the full image. Instead of selective search, RPN is proposed as an alternative way to generate possible object locations from the feature map with less computational time incorporated with the implementation of a graphics processing unit (GPU). RPN uses a rectangular sliding window to extract region from a feature map, and a set of nice anchors are applied to an extracted region to localize possible objects. A more detailed explanation of Fast R-CNN and RPN can be found in the previous study [67].

Based on the previous work [37], this study develops an automated peak-picking algorithm tailored to the stay-cable using the Faster R-CNN. Automated peak-picking in this work is designed to have two object classes, peaks or non-peaks, and determine peaks based on not RGB color information but the geometric shape of peaks from cable responses. In the next section, automated peak-picking tailored to a stay-cable is explained with the cable tension estimation method.

3. SERVICEABILITY ASSESSMENT AND MONITROING

For serviceability assessment and monitoring of stay-cables, this chapter 1) develops an automated serviceability monitoring system using smart sensors, 2) presents an automated cable damping monitoring strategy, and 3) proposes a serviceability assessment method considering failure probability. The automated serviceability monitoring system is designed to assess the level of serviceability in real-time based on vibration amplitude at the mid-span of stay-cables. Cable damping is related to the serviceability of stay-cables because cables have inherently less damping ratio resulting in vulnerable to vibration. The monitoring damping ratio enables the inspector to diagnose the serviceability level of cables and evaluate the performance of the damper attached to the cables in terms of reducing vibration. The proposed serviceability assessment method aims to inform the failure moment necessary to block the service of cable-stayed bridges under external excitations such as wind and traffic. A more detailed explanation of this chapter is as below.

3.1. Automated Real-time Serviceability Monitoring System

In this study, an automated real-time monitoring system for cable serviceability assessment is developed using wireless smart sensors (Figure 3-1). Note that the smart sensors are expected to provide the functions of wireless communication and on-board computation with small size, low cost, and low power consumption [25]. The system is designed to measure the structural acceleration response using a MEMS accelerometer and conduct on-board processing for the estimation of displacement and subsequently evaluate the serviceability. The system consists of two types of nodes—a gateway node and a leaf node, as shown in Figure 3-1. The gateway node is connected to the leaf node through wireless communication and remotely controls it to monitor the serviceability (Figure 3-1). The leaf node, installed in the mid-span of the cable, assesses the serviceability after the command from the gateway node is received, and features embedded on-board processing using smart sensors that measure the acceleration of the cable and estimate the displacement from the measured acceleration and assess the serviceability of the stay-cable.

3.1.1. Sensor Hardware Platform

The system is composed of hardware and software in both the gateway and the leaf nodes. When it comes to the hardware of the gateway node, a Bluetooth device is used to implement the wireless system. Other wireless communication modules such as LoRa, WiFi, and Zigbee can also be applied to

implement wireless communication between the gateway and leaf nodes. Among the various devices that consist of the Bluetooth module, a smartphone was selected—an efficient, user-friendly portable device to check the serviceability condition of the stay-cable. A Samsung Galaxy S10 smartphone equipped with Bluetooth version 5, which can communicate with other devices wirelessly up to 100 m, was selected as the gate node. As the main hardware of the leaf node, a single-board platform, the Raspberry Pi 3 Model B+, was selected for on-board processing (Figure 3-1). This low-cost and low-power single-board computer is equipped with a 1.4 GHz Quad-Core 64-bit ARMv8 CPU and 1 GB LPDDR2 SDRAM, which demonstrates the capability to carry out the entire embedded processing, from acceleration measurement to serviceability assessment. Furthermore, this hardware possesses HDMI, four USB 2.0 ports, 5 V/2.5 A DC power input, extended 40-pin GPIO headers, 2.4 GHz wireless LAN, Bluetooth 4.2, and a micro SD port for loading the operating system and storing data. Users can access and control the Raspberry Pi 3 Model B+ easily using a keyboard, mouse, and display through HDMI and USB ports. As this single-board computer is equipped with a Bluetooth module, the gateway node can be wirelessly connected to the leaf node, the main hardware of which is the Raspberry Pi 3 Model B+. Further, extended 40-pin GPIO headers aid the single-board computer to control and monitor the external sensors, such as the accelerometer through connections with the electronic circuits. To measure the acceleration, an ADXL335 smart sensor—a small tri-axial MEMS-based analog accelerometer with low cost and low power consumption (Figure 3-1)—is selected. This MEMS accelerometer is known to measure accelerations up to 3*g* (270 mV/g sensitivity) with sampling rates of 0.5–1600 Hz for the *X*- and *Y*-axis and 0.5–550 Hz for the *Z*-axis. With the analog-based ADXL335 accelerometer, an ADS1115—a 16-bit analog-to-digital converter (ADC)—is used to convert analog acceleration into digitalized acceleration because the Raspberry Pi 3 Model B+ is equipped with GPIO headers with digital input only (Figure 3-1). The MEMS accelerometer with the ADC sensor can be installed in the mid-span of the stay-cable to measure the vibration of the cable, and these sensing devices are connected to the GPIO headers of the Raspberry Pi model through a jump cable.

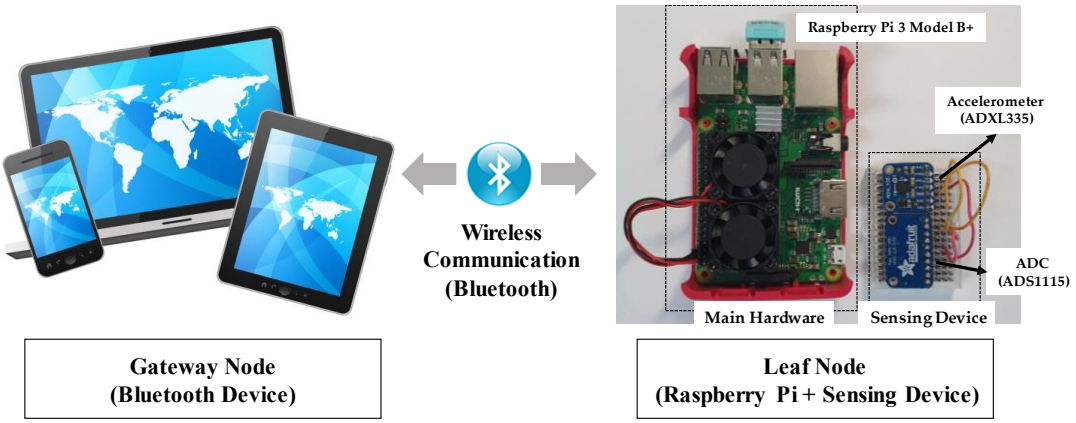

Figure 3-1. Design of wireless automated real-time cable serviceability assessment system

3.1.2. Operating Software

The software layer is designed depending on the functions of the gateway and leaf nodes. *BT Chat*, which is a free mobile software application used to implement Bluetooth connections between available devices, is installed in the gateway node. When the gateway node is connected to the leaf node, it commands the leaf node to assess the serviceability level. After the leaf node carries out the assessment, the gateway node receives the status of serviceability from it wirelessly. Inspectors can monitor the serviceability level of a subject cable automatically and in real-time using BT Chat, which communicates the maximum amplitude of the cable vibration and a warning message when serviceability is a failure.

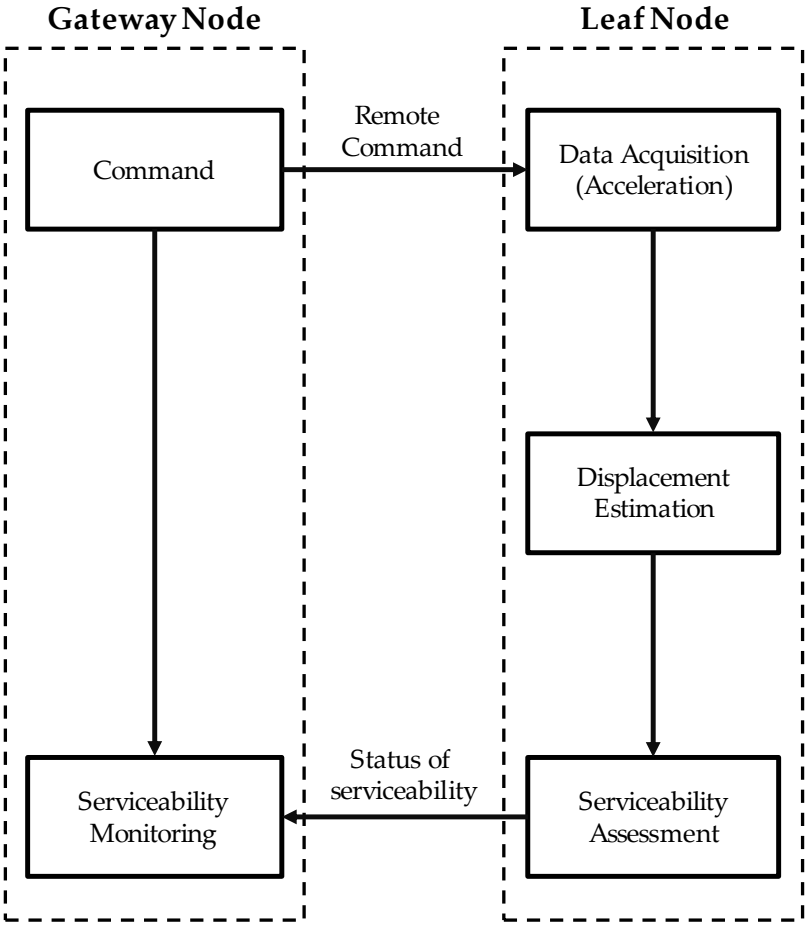

Figure 3-2. Flowchart for automated real-time cable serviceability assessment

In the case of leaf nodes, the software algorithm is implemented using Python and embedded to the Raspberry Pi 3 Model B+ running on a Linux operating system. In detail, the software of the leaf node works as follows: when the gateway node commands the leaf node to start monitoring, the leaf

node first measures the vibration of the cable in the mid-span using the MEMS accelerometer with an ADC sensor at a sampling rate of 100 Hz. It should be noted that in this study, the sampling time was set to 5 s to assess the serviceability, which can be changed depending on the users' requirements. Subsequently, the acceleration measured for 5 s is converted into displacement using the displacement estimation algorithm, and the leaf node evaluates whether the maximum amplitude of the estimated displacement exceeds the serviceability criterion which is twice the diameter of the target cable provided by the United States [16]. Thereafter, the leaf node transmits the results, i.e., the maximum displacement and serviceability status, to the gateway node through Bluetooth communication. As mentioned, this system is designed to monitor the serviceability level of the stay-cable every 5 s. The procedure for monitoring the serviceability is graphically described in Figure 3-2.

3.1.3. Laboratory-scale Experiment for Automated System

A laboratory-scale experiment was conducted using a cable to verify the performance of the serviceability assessment system, as presented in Figure 3-3. The physical and geometric properties of the cable are listed in Table 3-1. The target cable, an IWRC type, has 6.95 m of length with 43° inclination, 0.314 kg/m of mass density, 5.46 Ton of the break load, and 10 mm of the diameter. The tension force of the cable was set to be 457.8 N that is measured using the vibration-based tension estimation method proposed by Shimada [26]. The leaf node was installed on the center of the cable to measure the vibration and assess the serviceability level (Figure 3-3). Because the single-board computer with the MEMS sensor has low power consumption, the leaf node can also operate with power from an external battery. In the experiment, an attempt was made to command the leaf node every 5 s by locating the gateway node 10 m away from the leaf node. Note that the sampling time for serviceability assessment can be adjusted depending on the inspector's requirements or the criticality of maintenance. A fan located under the cable was used to induce vibration in it with ambient motion, as shown in Figure 3-3.

Table 3-1. Properties of laboratory-scale cable

Length (m)	Inclination (°)	Tension (N)	Mass (kg/m)	Diameter (mm)	Break load (Ton)	Cable type
6.95	43	457.8	0.314	10	5.46	IWRC

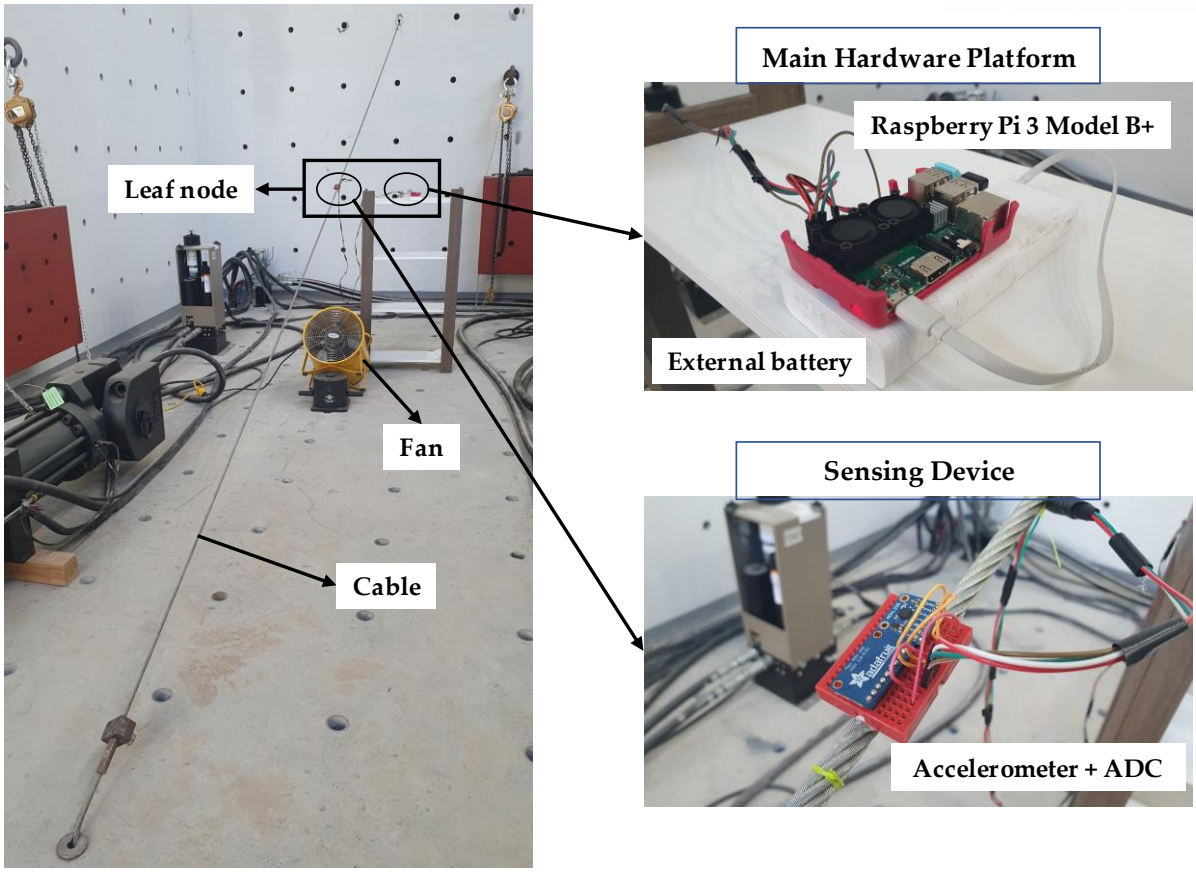

Figure 3-3. Laboratory setup for monitoring serviceability

3.1.4. Test of the Automated Real-time Cable Serviceability Assessment System

A series of laboratory experiments were carried out to test the developed automated real-time serviceability assessment system. These experiments were designed to assess the serviceability level of the stay-cable in mid-span every 5 s. The test results are displayed in Figure 3-4. The gateway node commanded the leaf node to measure the cable vibration in terms of the acceleration every 5 s, as shown in Figure 3-4 (a). The leaf node automatically computed the acceleration-based displacement conversion algorithm to estimate the dynamic displacement every 5 s (Figure 3-4 (b)). Finally, the maximum absolute amplitude of the converted dynamic displacement was used to assess the serviceability level, which can be either allowed or disallowed depending on the serviceability criterion (the amplitude should be less than twice the diameter of the target cable; Figure 3-4 (c)). The serviceability level was evaluated based on the "Max Abs Amp", which denotes the maximum absolute amplitude of the estimated displacement for 5 s. From the results depicted in Figure 3-4, this study verified that the developed system functioned well to measure the cable response in terms of acceleration, estimate the displacement from the measured acceleration, and assess the serviceability level based on the defined threshold.

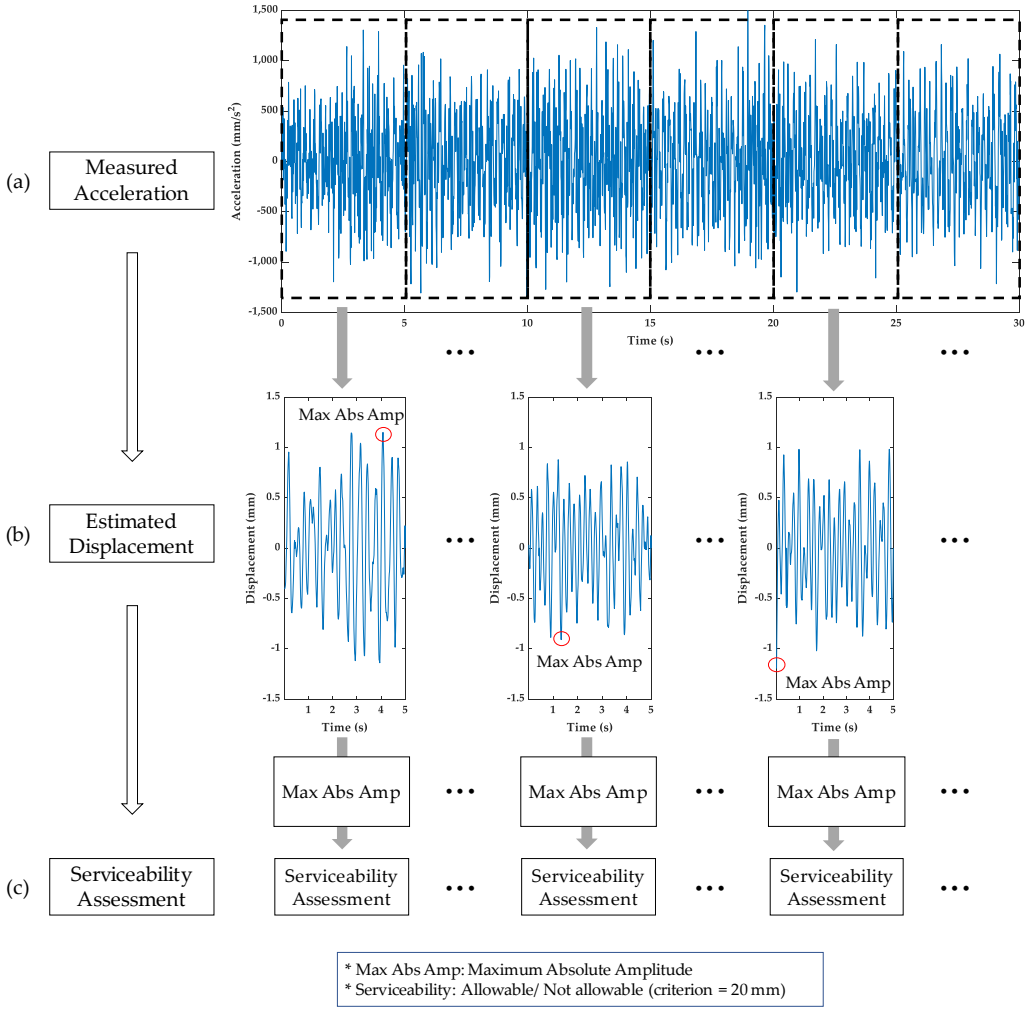

Figure 3-4. Automated real-time serviceability assessment results for 30 s

Furthermore, the wireless communication between the gateway node and the leaf node was tested to verify the system for serviceability assessment. The result of the wireless communication test between the two nodes is depicted in Figure 3-5. Because the fan was not sufficiently strong to induce vibrations greater than the failure level of 20 mm, the serviceability threshold was adjusted to 1 mm just for the purpose of verification. As shown in Figure 3-5 (a), wireless communication can be activated after the gateway and leaf nodes are connected through Bluetooth communication by pressing the "Scan for devices" button and selecting the "raspberrypi" as the pairing device in the "Select a device to connect" list of the *BT Chat* application. After the activation of wireless communication, the gateway node commanded the leaf node to measure the acceleration of the stay-cable under the fan vibration, estimate the displacement from the measured acceleration, and assess the serviceability level every 5 s. The serviceability status, as well as the maximum absolute amplitude of the estimated displacement for 5 s, were communicated to the gateway node through wireless communication, as shown in Figure 3-5 (b). Note that "ua_max" denotes the maximum absolute amplitude of the estimated displacement for 5

s and the serviceability level is printed as either “Allowable” or “Not allowable” based on the defined threshold of 1 mm. The stay-cable experienced both serviceability allowable and not allowable conditions depending on the assessment cases. For example, in the third assessment case (Figure 3-5 (c)), the maximum absolute displacement was 0.909 mm at 1.33 s, which indicates allowable serviceability. In the second example, the maximum absolute displacement was 0.914 mm at 0.24 s, which is also within the serviceability threshold (Figure 3-5 (d)). The third example, however, indicated that the serviceability was a failure because the maximum absolute displacement was 1.230 mm at 1.68 s, which exceeds the defined threshold (Figure 3-5 (e)). Thus, this study verified that the developed wireless system can assess the serviceability of the stay-cable automatically and in real-time under the defined serviceability threshold through wireless communication between the gateway and leaf nodes.

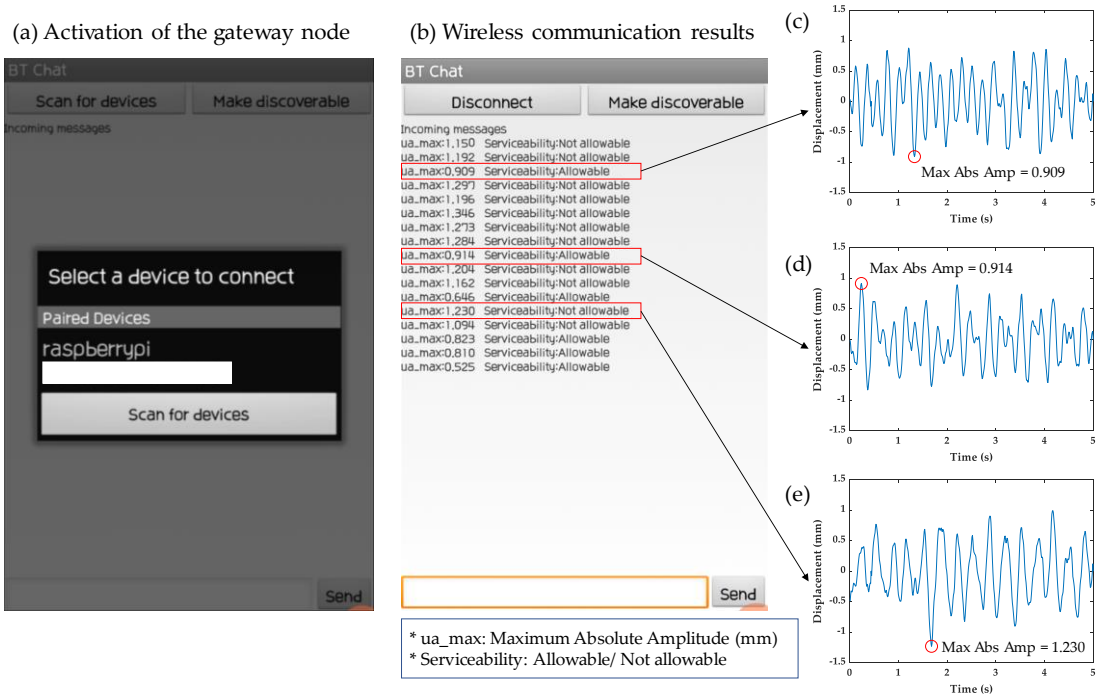

Figure 3-5. Wireless communication results of serviceability assessment

As a new pioneering study implementing wireless smart sensors for the maintenance of stay-cables, the developed system can be applied not only for monitoring serviceability but also for other maintenance purposes. For example, a damper system such as a passive, active, and magneto-rheological damper has been widely applied to enhance the damping performance of the stay-cable as a means to reduce the cable vibration [4, 8]. The developed system can be used to evaluate the performance of the damper in terms of reducing vibration by monitoring the vibration of the cable before and after the damper installation. When the serviceability of the stay-cable fails continually despite the installation of the damper, the developed system allows inspectors to adjust the damper performance to reduce the vibration enough to meet the serviceability criterion.

3.2. Automated Damping Estimation Method

3.2.1. Selection of Appropriate Method for Damping Automation

Five representative methods widely used for damping estimation were described as shown in Table 3-2 based on the literature review in Section 2. As the optimal method for damping automation has not been reported, this study set the criteria to select an appropriate automated damping estimation method. First, a loading condition is one of the important criteria. In real-world bridges, it is difficult not only to apply impulse loading to cables artificially but also to identify characteristics of input loading. Second, the selected method is required to perform damping estimation with less computation power. The computation burden of the frequency-domain method is less than that of the time-domain approach. Third, a method, possible to extract properties of natural modes easily, is appropriate for damping automation. Based on three criteria, this study selected the 'Half-Power Bandwidth Method' for damping automation which satisfied below three conditions.

Condition 1. Output-only modal identification method based on ambient vibration

Condition 2. A simple method with less computation time to identify damping ratio

Condition 3. Easy to identify peaks from the frequency domain representation (i.e., Power Spectral Density (PSD))

Table 3-2. Selection of an appropriate method for damping automation

Data type	Method	Explanation	Loading condition	Condition 1	Condition 2	Condition 3
Time-domain	Logarithmic Decrement Ratio	▪ Damping estimation by using logarithm decrement of peaks between two adjacent periods	Free vibration	X	O	X
	Stochastic Subspace Identification (SSI)	▪ Covariance-based system identification method by singular value decomposition of Toeplitz matrix	Free vibration / Ambient vibration	O	X	X

	Eigensystem Realization Algorithm (ERA)	▪ Impulse response-based system identification method by singular value decomposition of Hankel matrix	Free vibration / Ambient vibration	O	X	X
Frequency-domain	Half-Power Bandwidth Method	▪ Damping estimation based on two frequencies located in 1/2 of peak height in PSD	Forced vibration / Ambient vibration	O	O	O
	Frequency Domain Representation (FDD)	▪ Output-only system identification methods based on frequency-domain data	Ambient vibration	O	O	X

3.2.2. Automated Damping Estimation Method

The automated damping estimation is designed to conduct data acquisition, PSD calculation, peak-picking, and damping ratio estimation. A more detailed automation process is as follows:

Step 1: Measure the cable response in terms of acceleration
Step 2: Transform a time-history cable response into a frequency domain representation (e.g., PSD)
Step 3: Detect peaks which correspond to natural modes
Step 4: Apply Half-Power Bandwidth Method to identify damping ratio

It is noted that the peaks are detected by searching local maxima with ten spectral lines around predefined natural frequencies. After peak-picking, the Half-Power Bandwidth Method is applied to estimate the damping ratio. The Half-Power Method with user-defined peak-picking can identify structural damage in a stay-cable by monitoring an estimated damping ratio. When peak locations are shifting owing to structural damage, geometric shapes of peaks around predefined ranges are changing, and thus estimated damping ratio has different values. As damping estimation by Half-Power Method depends on geometric shapes of predefined peaks, this peak-picking method is efficient to monitor cable damage as well as damper activation.

3.2.3. Case Study: The Hwatae Bridge

The proposed automated damping estimation method was applied to one of the stay-cables in the Hwatae Bridge. This bridge is located in the city of Yeosu, a southern region of the Korean Peninsula, connecting Dolsan Island and Hwatae Island (Figure 3-6). This bridge was constructed in December 2015 with a 130 m height of pylon, 500 m span between two pylons, and 1,345 m total bridge length, which has the highest pylon and the third-longest span in Korea. The bridge is supported by a total of 136 stay-cables composed of three different types of cables.

Figure 3-6. Field experiment site (Hwatae Bridge)

This study selected the largest cable located in Dolsan Island direction, CM17 shown in Figure 3-7, as a target cable to monitor the damping ratio automatically under the different wind conditions. The geometric and physical properties of the selected cable are shown in Table 3-3.

Table 3-3. Geometric and physical properties of the stay-cable

	Cable length (m)	Weight per length (N/m)	Sectional area (mm2)	Inclined angle (°)
CM17	271.803	559.0	6,000	26.693

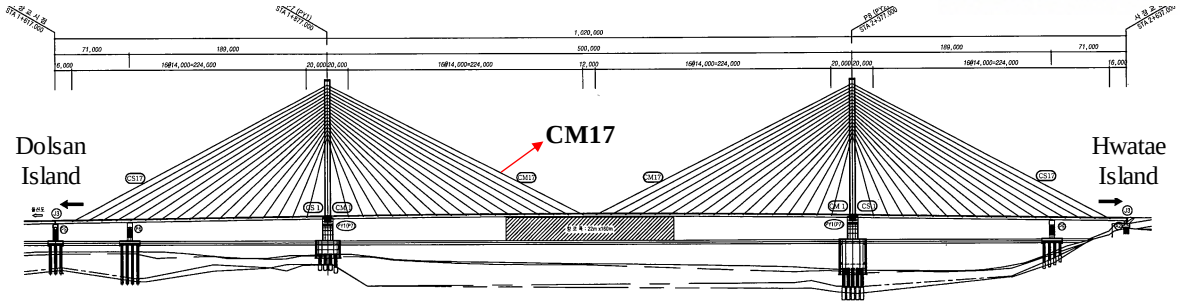

Figure 3-7. Longitudinal sectional profile of the Hwatae Bridge with the target stay-cable

At the target cable, an accelerometer (CAC_I05) was installed to acquire an acceleration response as shown in Figure 3-8. This study obtained the cable responses, especially a total of five datasets with different wind conditions (Table 3-4) from this sensor, and then applied the proposed automated damping estimation method. All collected datasets are composed of acceleration data recorded by every 10 min with a 100 Hz sampling rate. For example, the cable response dataset from September 8, 2019, has a total of 144 data files recorded by every 10 min for 24 hours. The dataset from July 20, 2019, and September 7, 2019, were measured when typhoon *Danas* and *Lingling* struck to the bridge respectively.

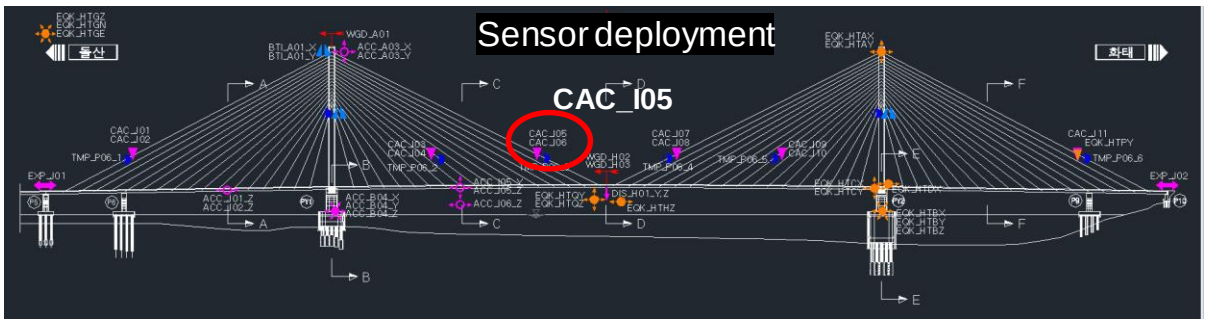

Figure 3-8. Sensor deployment in the Hwatae Bridge

Table 3-4. Five datasets with different ambient wind conditions

	Date	Mean Wind Speed at the Deck (m/s)	Mean Wind Speed at the Top of Pylon (m/s)	Description
Ambient	20190908	1.1686	0.7871	24 Hours, 00:00-24:00
	20190703	3.2045	1.5265	9 Hours, 09:00-18:00
	20180110	8.5543	8.9954	6 Hours, 00:00-06:00
	20190720	17.3990	18.8834	2 Hours, 06:00-08:00
	20190907	21.2124	22.7014	3 Hours, 03:00-06:00

3.2.4. Application of Automated Damping Monitoring

The calculation of PSD is affected by the number of fast Fourier Transform (NFFT) and types of the spectral window as mentioned in Section 2.1.3. Before applying the Half-power method to monitor the damping ratio, this study examined the optimal value of NFFT and the appropriate type of spectral window. In the case of the spectral window, three types of windows, boxcar, hanning, and hamming, were considered to select the appropriate window used to avoid spectral leakage when calculating the PSD of responses. These windows were applied to one of the time-history cable acceleration response for 10 min from the CAC_I05 sensor, and the corresponding PSD graph with one peak is shown in Figure 3-9. Compared with the boxcar window, two windows, hanning and hamming, showed the similar geometric shape of a peak in the PSD illustration. As the boxcar window cannot reduce the spectral leakage, this study selected one of two windows (i.e., hanning window) to apply the calculation of PSD.

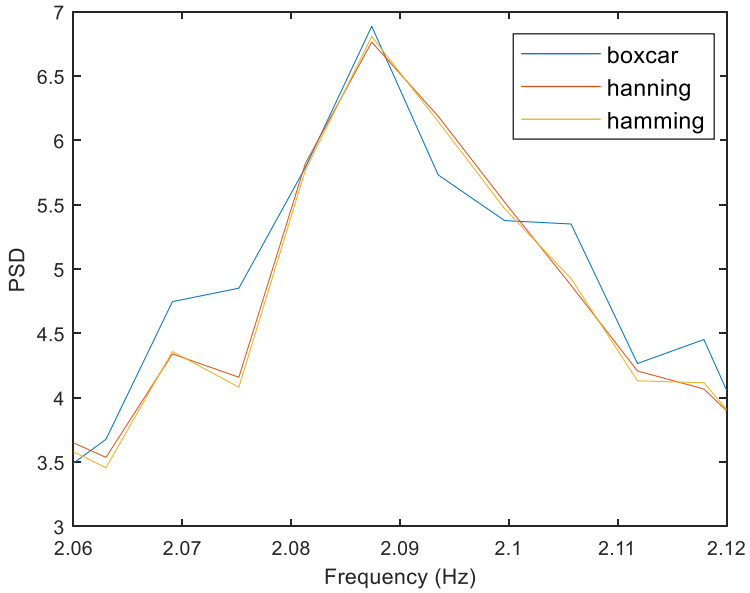

Figure 3-9. Power spectral density with different spectral windows

When it comes to the NFFT, this study increased the NFFT value from 2^{10} to 2^{15} to calculate the PSD of a time-history cable acceleration data for 10 min from the CAC_I05 sensor. The higher NFFT value is used to obtain the PSD graph, the sharper peaks we can obtain as shown in Figure 3-10. However, the geometric shapes of peaks have become not clear when the 2^{15} of NFFT value was used compared to other values. In conclusion, this study selected the 2^{14} of NFFT as an appropriate number for calculating PSD. It is noted that the optimal value of NFFT can be different by characteristics of response data.

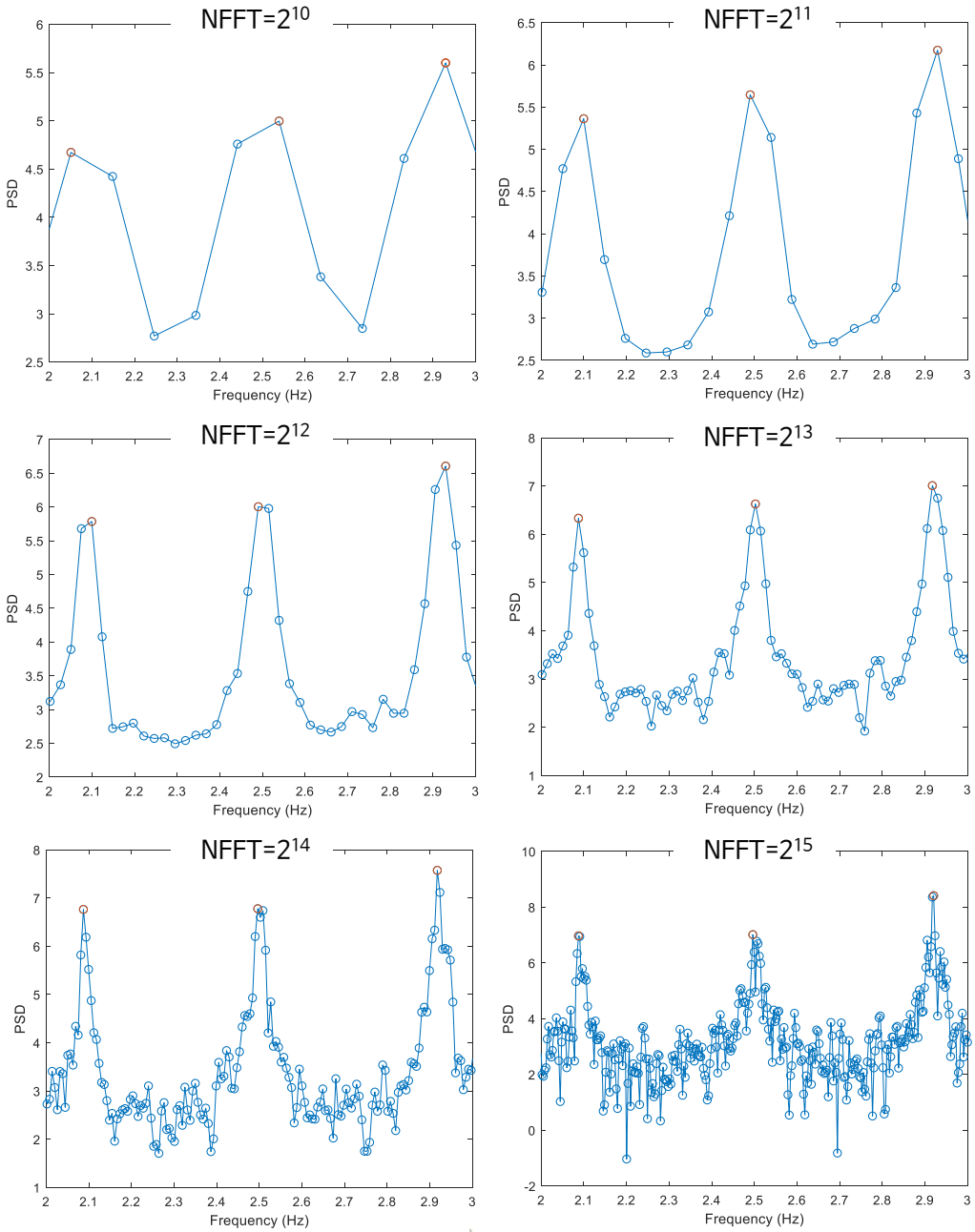

Figure 3-10. Power spectral density of a cable response with different NFFT

The collected response datasets from the CAC_I05 accelerometer were analyzed by following four steps introduced in Section 3.2.2 to monitor the damping ratio. For calculating the PSD of each data file containing the acceleration response for 10 min, this study used the hanning window and 2^{14} of NFFT with the overlap of NFFT/2. The peak-picking was applied to the PSD graph by searching local maximum point around predefined natural frequencies of the Cable CM17. The example PSD graph of a cable response measured from September 8, 2019, is shown in Figure 3-11 with ten predefined natural frequencies identified manually from one of cable response data (2^{nd}: 0.830 Hz, 3^{rd}: 1.245 Hz, 4^{th}: 1.660

Hz, 5th: 2.075 Hz, 6th: 2.490 Hz, 7th: 2.905 Hz, 8th: 3.320 Hz, 9th: 3.760 Hz, 10th: 4.175 Hz, and 11th: 4.590 Hz). Note that the first natural frequency was not considered in the estimation of the damping ratio owing to high noise in the low-frequency range. The ten natural modes, within predefined frequency ranges, were extracted (Figure 3-11), and then the damping ratio of each mode was calculated automatically by the half-power method. The estimated damping ratio showed similar trends with the result of the NExT-ERA technique as shown in Table 3-5, which can be successfully verified to estimate reliable damping ratio.

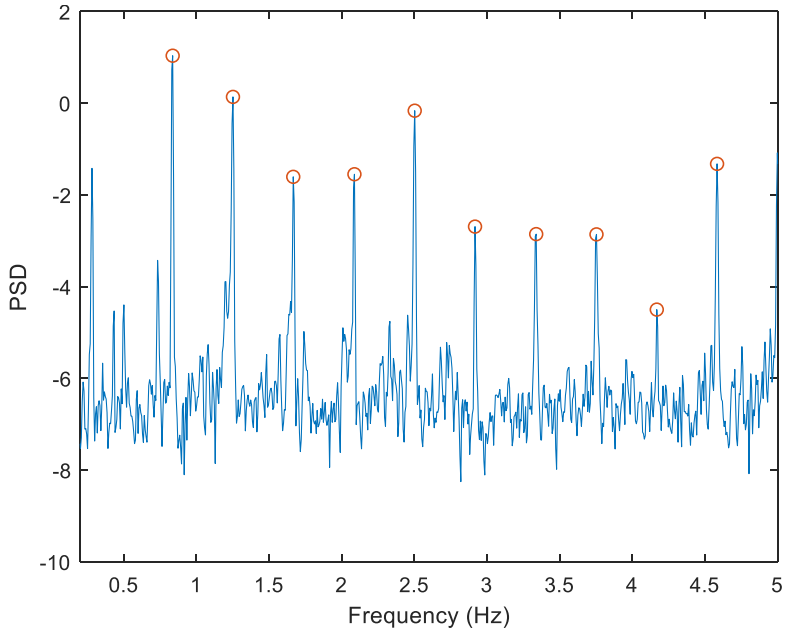

Figure 3-11. Peak-picking with ten identified natural frequencies (September 8, 2019)

Table 3-5. Estimated damping ratio by different two methods

Method	Damping ratio (%)				
	2nd	**3rd**	**4th**	**5th**	**6th**
Half-Power method	0.4993	0.3669	0.2623	0.2101	0.1725
NExT-ERA	0.5196	0.3863	0.2485	0.1980	0.1870

The same process was repeated to every data file for 10 min measured from September 8, 2019, and the monitoring results with five natural modes for 24 hours are shown in Figure 3-12. As some data files had over/less-estimated damping ratio, this study removed outlier estimated values that are out of outlier criterion (10 % variation of a representative damping ratio). The average value of monitored damping ratio is indicated in Table 3-6 and Figure 3-13, which shows 0.514 %, 0.267 %, 0.262 %, and 0.217 % of damping ratio for 2nd, 3rd, 4th, and 5th natural modes.

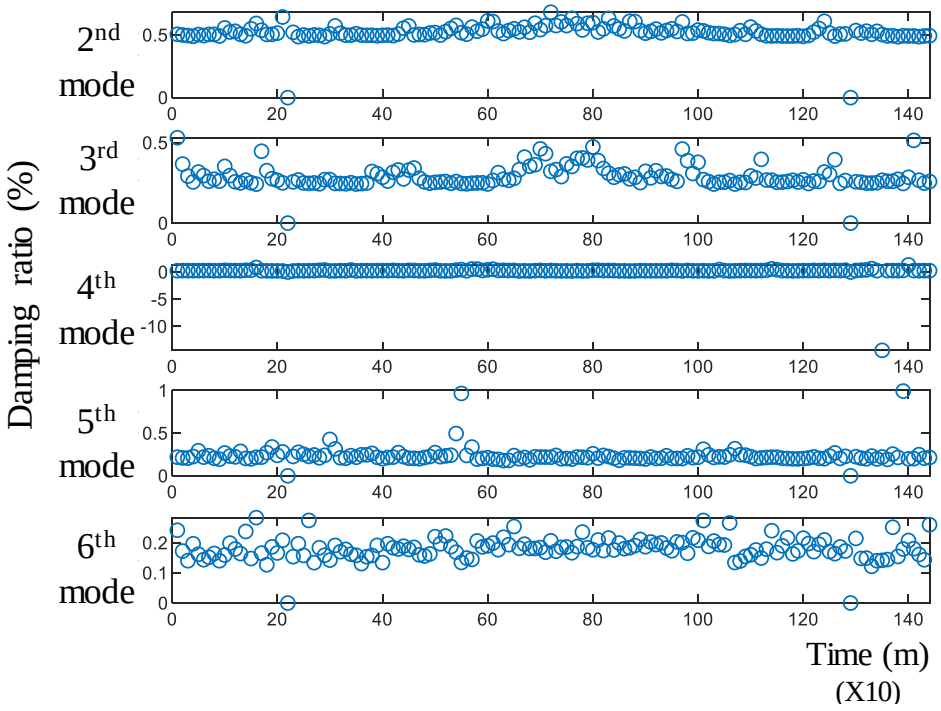

(a) Damping monitoring before outlier removal

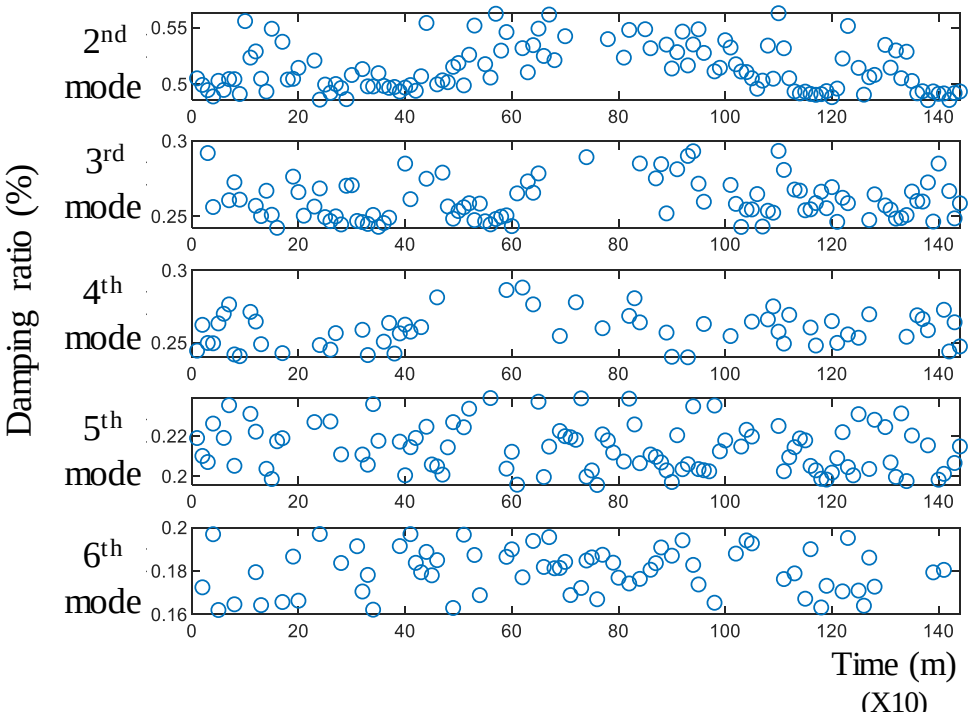

(b) Damping monitoring after outlier removal

Figure 3-12. Monitoring results of damping ratio for 24 hours (September 8, 2019)

This study repeated the same process of damping monitoring for other data sets with different wind conditions, and the mean damping ratio from monitored results is indicated in Table 3-6 and Figure 3-13. When the wind speed was faster, the damping ratio tended to be higher as shown in Table 3-6 and Figure 3-13. This finding showed that a damper installed to the Cable CM17 operated owing to wind force, and thus the damping ratio was increasing consequently.

Table 3-6. Mean damping ratio with acceleration responses by five cable response datasets

Date	1st	2nd	3rd	4th	5th	Wind speed at the deck (m/s)	Acc. (Max)	Acc. (S.D)
20190908	*n.d	0.514	0.267	0.262	0.217	1.169	954.63	1.88
20190703	*n.d	0.584	0.398	0.296	0.231	3.205	1,178.15	7.86
20180110	*n.d	0.685	0.410	0.296	0.247	8.554	1,100,64	35.83
20190720	*n.d	0.758	0.493	0.414	0.262	17.399	1,319.25	69.57
20190907	*n.d	0.763	0.538	0.519	0.333	21.212	1,373.27	81.47

*n.d: Not determined

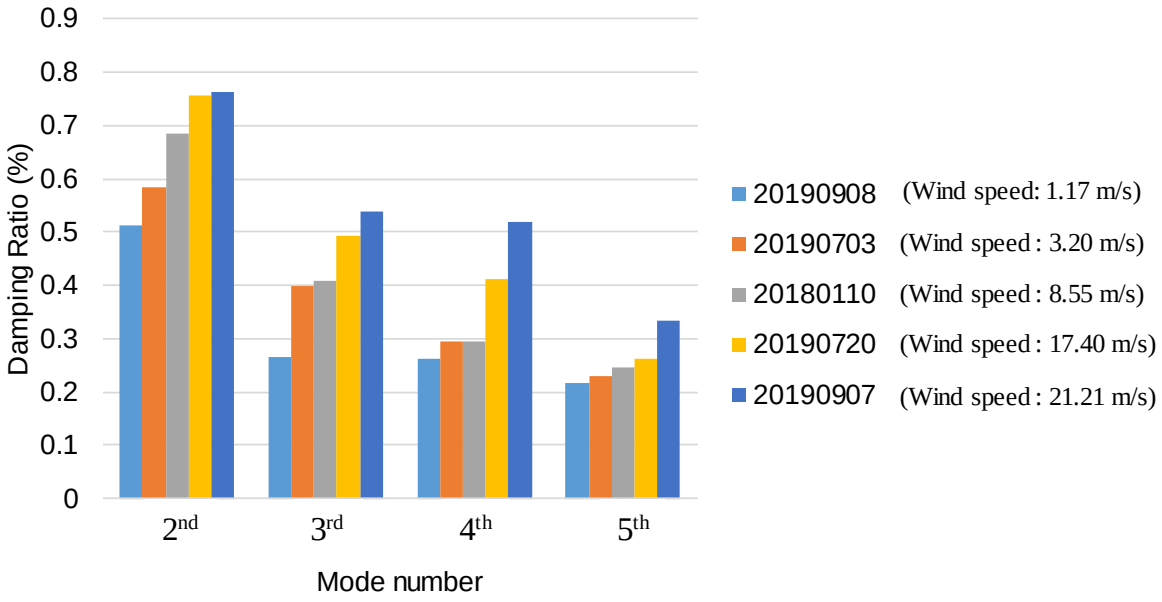

Figure 3-13. Monitored damping ratios with different wind conditions

3.3. Serviceability Assessment Method with Vibration Control

3.3.1. Serviceability Assessment using VanMarcke's First-passage Probability

This section describes the proposed serviceability assessment method for stay-cables equipped with vibration control measures. Most modern developed countries have design specifications that define the serviceability failure of stay-cables [4, 41-43]. For example, the Korean design code states that the maximum allowable deformation of a stay-cable must be less than 1/1600 of the cable length at the middle of the cable under the external wind of mean speed less than 20 m/s for 10 minutes [4]. The proposed framework was accordingly designed to assess cable serviceability based on such design specifications that define the point of serviceability failure.

The serviceability failure probability can be determined as a first-passage problem using time history data of cable vibration with and without vibration control. Let $P_f(x_s;\tau)$ be the first-passage failure probability of $X(t)$ over a given double-sided threshold $|x| = x_s$ during a time interval $t\epsilon(0,\tau)$, where $X(t)$ indicates the cable displacement. Note that the threshold value x_s is generally specified by the appropriate design guideline. The approximated form of this probability is as follow [68]:

$$P_f(x_s;\tau) \cong 1 - A\exp\left[-\int_0^\tau \alpha(x_s;t)dt\right] \tag{48}$$

where A is the probability of $X(t)$ in the safe domain at $t = 0$, and $\alpha(x_s;t)$ is the conditional mean crossing rate at time t, given no prior crossings.

Under VanMarcke's approximation [69], the unconditional mean crossing rate of the envelope process $\eta(x_s;t)$ is used instead of the conditional crossing rate $\alpha(x_s;t)$ because the conditional crossing rate depends on the bandwidth of the process and duration time in the unsafe region. Additionally, A is replaced with B, which indicates the probability that the envelope process is in the safe domain at $t = 0$. Using this approximation, the first-passage probability of the cable response can be determined from the following equations:

$$\begin{aligned} P_f(x_s;\tau) &\cong 1 - B\exp\left[-\int_0^\tau \eta(x_s;t)\,\mathrm{d}t\right] \\ B &= P\left[E(0) < x_s\right] = \int_0^{x_s} f_E(e;0)\,\mathrm{d}e \\ \eta(x_s;t) &= \frac{P\left[E(t) \ge x_s\right]\nu(0;t)}{P\left[E(t) < x_s\right]}\left[1 - \exp\left(\frac{-\nu_E^{+}(x_s;t)}{P\left[E(t) \ge x_s\right]\nu(0;t)}\right)\right] \end{aligned} \tag{49}$$

where $E(t)$ is the envelope process of $X(t)$; $\nu(x_s;t)$ is the unconditional mean crossing rate of $|X(t)|$ over x_s under the Poisson approximation; $f_E(e;t)$ is the marginal probability density function of $E(t)$; and $\nu_E^+(x_s;t)$ is the unconditional mean up-crossing rate of $E(t)$.

When $X(t)$ has a stationary and zero-mean Gaussian distribution, $\eta(x_s;t)$ and $\nu(x_s;t)$ are functions of x_s only. By employing the envelope defined by [70], B and $\eta(x_s;t)$ in Equation (49) can be replaced with:

$$B = 1 - \exp\left(-r^2/2\right) \tag{50}$$

$$\eta(x_s) = \nu(x_s)\left\{\left[1-\exp(-\sqrt{\pi/2}\,\delta^{1.2}r)\right]/\left[1-\exp\left(-r^2/2\right)\right]\right\} \tag{51}$$

where $r = x_s/\sigma_X$ is the normalized threshold and σ_X is the standard deviation of $X(t)$. The safety factor characterizing the bandwidth of the process can be defined as $\delta = (1-\lambda_1^2/\lambda_0\lambda_2)^{1/2}$, where λ_m is the spectral moment for $m = 0, 1, 2$ defined by the frequency domain of the cable response as:

$$\begin{aligned}\lambda_0 &= \int_{-\infty}^{\infty} G_{XX}(\omega)d\omega = \sigma_X^2 \\ \lambda_1 &= \int_{-\infty}^{\infty} |\omega| G_{XX}(\omega)d\omega \\ \lambda_2 &= \int_{-\infty}^{\infty} \omega^2 G_{XX}(\omega)d\omega\end{aligned} \tag{52}$$

where $G_{XX}(\omega)$ is the power spectral density in the frequency domain of the vibration $X(t)$.

Using the VanMarcke's first-passage failure probability, this study determined the probability of cable system serviceability failure, allowing the effect of vibration control on the cable serviceability to be examined. The procedure used in this study for the serviceability assessment of stay-cables equipped with vibration control is described in Figure 3-14.

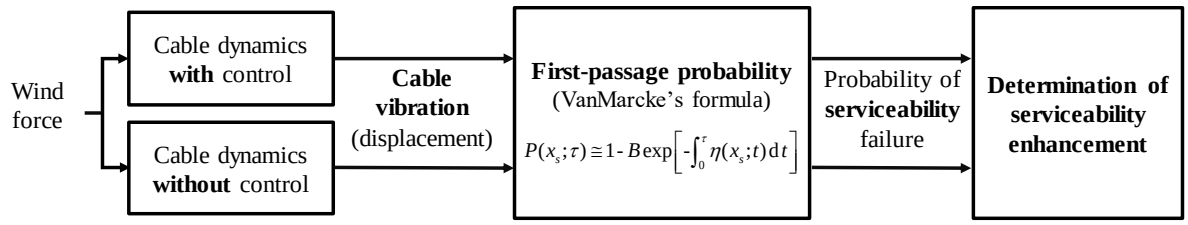

Figure 3-14. Flowchart of stay-cable serviceability assessment considering vibration control

3.3.2. Case Study for Serviceability Assessment: The Second Jindo Bridge

■ **Bridge Description**

The Second Jindo Bridge was selected as the case study for the proposed method of assessing cable serviceability considering vibration control. The Second Jindo Bridge, shown in Figure 3-15, is a 484-m long cable-stayed bridge in Korea connecting Jindo Island to the town of Haenam, a southwestern inland region of the Korean Peninsula. In all, 15 different types of cables constitute the 60 total stays that support the bridge. The properties of three representative cables are summarized in Table 3-7 [71]. Despite the high-velocity tidal currents at this bridge site, the bridge does not suffer from any scour problem as the pylons were constructed on the land. However, the bridge is only lightly damped and thus vulnerable to both wind-rain and traffic-induced vibrations.

Figure 3-15. Jindo Bridges (the Second Jindo Bridge is on the left)

Table 3-7. Cable properties of the Second Jindo Bridge [47]

Cable		Total length	Diameter	Unit mass	Tension force
ID	Type	(m)	(m)	(ton/m)	(tonf)
C10	Ø7 X 109	96.515	0.095	0.0347	110.2
C11	Ø7 X 109	110.940	0.095	0.0347	130.6
C14	Ø7 X 139	157.880	0.106	0.0439	174.4

This study investigated Cables C10, C11, and C14 shown in Table 3-7 to demonstrate the proposed serviceability assessment method. A total of 20 shape functions, including one static deflection term and 19 sine functions, were assumed to construct the combined cable-damper model, which is known to approximately represent the damped cable model [55]. The cable sag due to self-weight was also considered in the cable model in order to provide a more realistic numerical simulation. The passive viscous damper was assumed to be installed at 2% of the cable length and to have a damping constant

c_d = 1.5, providing a 0.5% additional damping ratio to the cable. Note that the damper is required to produce at least 0.5% of the critical damping according to the bridge design criteria in Korea [4].

■ Aerodynamic Wind Force

Aerodynamic wind force applied to the cable is generated in this study. Let the external force $f(x,t)$ in Equation (53) be assumed to be the aerodynamic wind force $W(t)$, which is uniformly distributed on the cable as:

$$f(x,t) = W(t) \tag{53}$$

The wind force $W(t)$ on the cable can be derived as a combination of lift and drag forces caused by the oncoming relative wind speed (U_{rel}) as [72]:

$$\begin{aligned} W(t) &= \frac{1}{2}\rho_{air} D U^2 C_y = W_L(\psi_t)\cos(\psi) + W_D(\psi_t)\sin(\psi) \\ W_L(\psi_t) &= \frac{1}{2}\rho_{air} D U_{rel}^2 C_L(\psi_t), \quad W_D(\psi_t) = \frac{1}{2}\rho_{air} D U_{rel}^2 C_D(\psi_t) \end{aligned} \tag{54}$$

where ρ_{air} is the air density; D is the diameter of the cable; W_L and W_D are the lift and drag forces, respectively; C_L and C_D are the lift and drag coefficients, respectively; and ψ_t is the summation of ψ, θ_0, and θ, where ψ is the angle between the direction of the relative wind speed (U_{rel}) and the horizontal plane of the cable surface, θ_0 is the initial angle of the rainwater rivulet, and θ is the instantaneous angle of the rivulet.

The oncoming wind is composed of two components of varying magnitude depending on its direction: one perpendicular to the cable axis and the other parallel to the cable axis. As the wind blowing on the cable in the parallel direction has less of an effect on wind-rain induced vibration, this study considered only the oncoming wind in the direction perpendicular to the cable axis, denoted by U. The oncoming wind causing the cable vibration (U) can then be derived by a function of the inclined angle of the cable (α) and the oncoming wind speed (U_0) for a wind direction angle (β) as follows:

$$\begin{aligned} U &= U_0\sqrt{\cos^2\beta + \sin^2\alpha\sin^2\beta} = U_0\sqrt{\sin^2\alpha + \cos^2\alpha\cos^2\beta} \\ \gamma &= \arcsin\left(\frac{\sin\alpha\sin\beta}{\sqrt{\cos^2\beta + \sin^2\alpha\sin^2\beta}}\right) \end{aligned} \tag{55}$$

where γ is the angle between the wind direction of U and the horizontal plane of the cable surface. The relative wind speed U_{rel} with respect to a cable velocity $\dot{y}$ is indicated for an included angle ψ by:

$$U_{rel} = \sqrt{(U\cos\gamma)^2 + (\dot{y} + U\sin\gamma)^2}$$
$$\psi = \arctan\left(\frac{\dot{y} + U\sin\gamma}{U\cos\gamma}\right) \tag{56}$$

Thus, given the time history data of wind speed U and its associated angles, the wind force $W(t)$ can be obtained. More details regarding the derivation of wind force can be found in the previous study [72].

3.3.3. Dynamic Simulation for Wind-rain Induced Cable Vibration

Three oncoming wind speed (U_0) cases consisting of different 10-minute mean wind speeds (V_{10}), shown in Table 3-8, were considered to generate the simulated displacement responses. All wind forces were assumed to be uniformly applied to the cables. The time history wind data for the three cases were obtained from the NatHaz On-line Wind Simulator (NOWS) [73] for Exposure Category D, a cut-off frequency of 5 Hz, and time duration of 18,000 s. Note that Exposure Category D is the case for the open ocean according to ASCE 7-98. Based on a previous study [72], the numerical analysis in this section simulated wind-rain induced aerodynamic wind force under assumptions of a cable inclination angle α of 30°, wind direction angle β of 35°, initial angle θ_0 of 20°, and instantaneous angle θ of 25°.

Table 3-8. Three evaluated oncoming wind speed cases (U0)

Wind case	10-minute mean wind speed (V_{10})	Description
Case 1	12.89 m/s	Mean wind speed when typhoon COMPASU was closest to the Jindo Bridge (2010.09.01 PM 09:42-09:51) [27]
Case 2	20 m/s	Mean wind speed criterion for serviceability failure as defined in the Korean Highway Bridge Design Code [21
Case 3	36 m/s	Maximum mean wind speed when typhoon RUSA (2002.08.31, the most powerful typhoon in Korea) passed through the Korean peninsula [28]

The simulated responses in Case 1 were compared with the actual measurements acquired during typhoon COMPASU to compensate for possible errors in the dynamic simulations. Then, the generated wind force was modified by matching the standard deviations of the simulated and measured displacements so that the generated results matched the collected data. Let Cable C14 be taken as an example for generating realistic wind forces. When typhoon COMPASU was closest to the Jindo Bridge (Case 1), the dynamic displacement response of Cable C14, which was converted from the measured acceleration, indicated a standard deviation of 0.0036 m over 60 s for a wind speed of 12.89 m/s. The modified wind forces $W(t)$ of Cable C14 for the three wind cases in Table 3-8 from 8,000 to 10,000 s

of the 18,000 s evaluation period are provided in Figure 3-16. The wind forces on the other cables were generated using the same procedure.

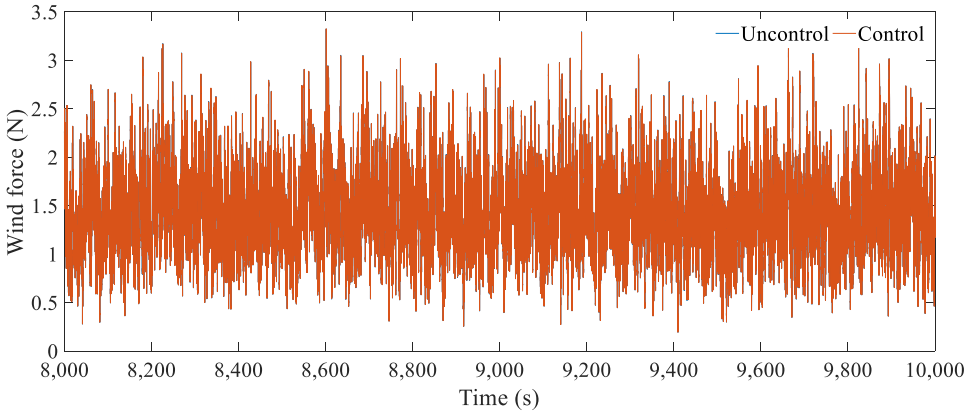

(a) Case 1 (V_{10} = 12.89 m/s)

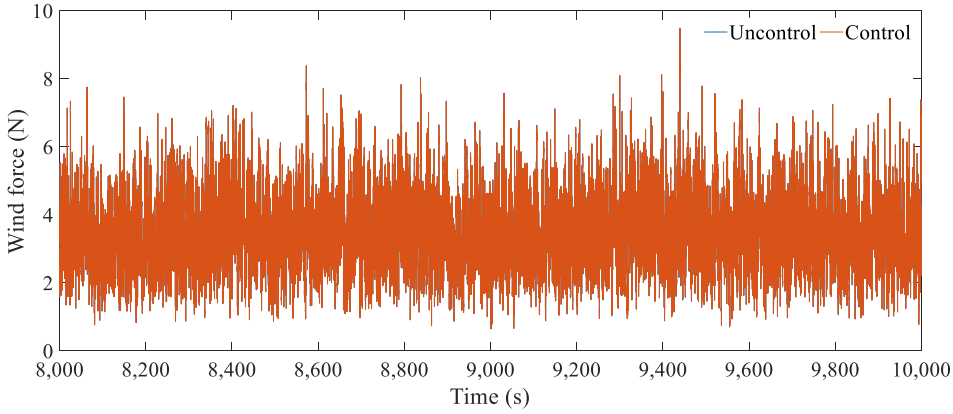

(b) Case 2 (V_{10} = 20 m/s)

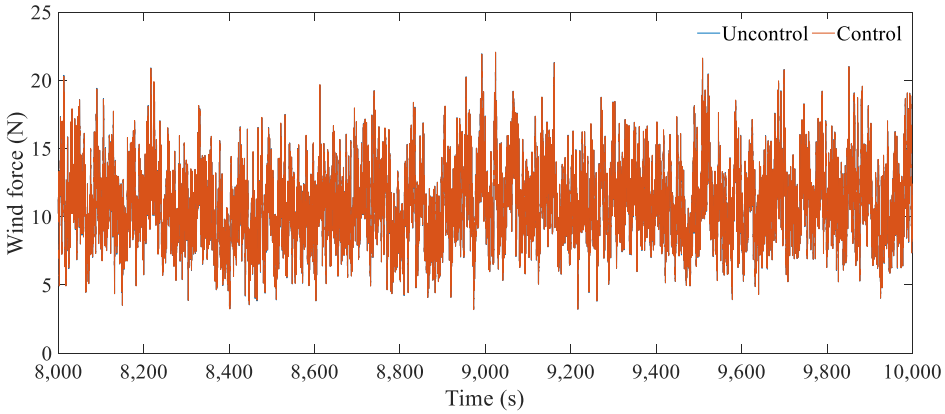

(c) Case 3 (V_{10} = 36 m/s)

Figure 3-16. Time histories of wind force W(t) for each wind case on Cable C14

A time history analysis was conducted to obtain the displacement responses of the cables with and without vibration control. Figure 3-17 shows the resulting displacement responses of Cable C14 and Table 3-9 summarizes the standard deviation, maximum displacement, and control efficacy for each

wind case. Note that the passive viscous damper with c_d = 1.5 was observed to reduce the cable vibration by 40–50% in most cases, as shown in Table 3-9.

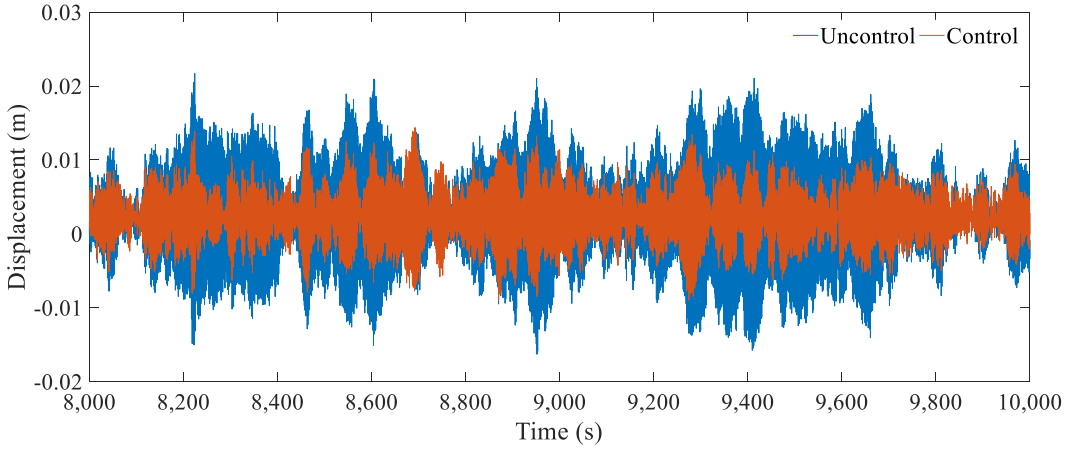

(a) Case 1 (V_{10} = 12.89 m/s)

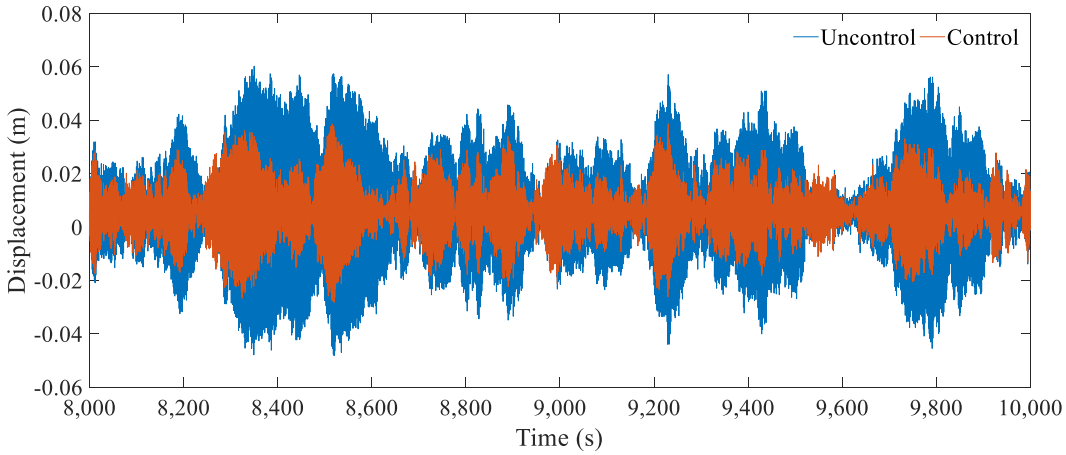

(b) Case 2 (V_{10} = 20 m/s)

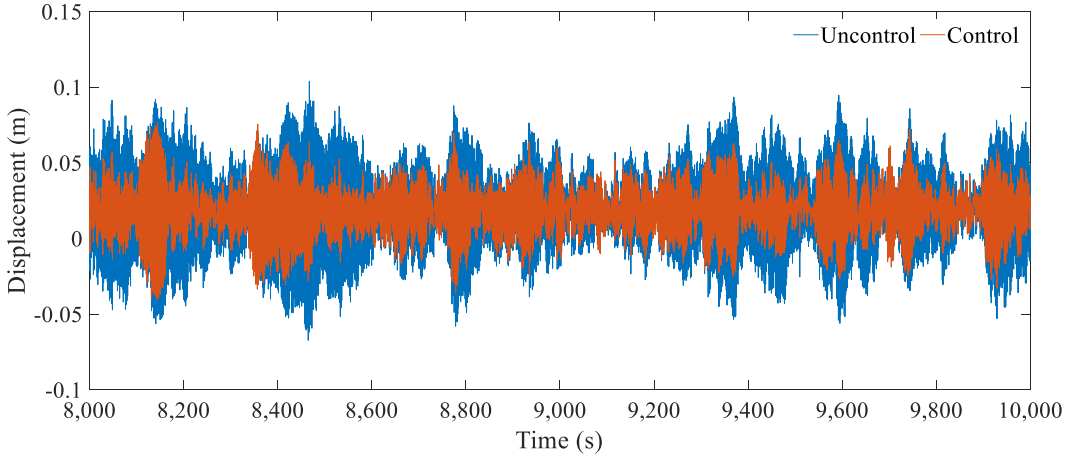

(c) Case 3 (V_{10} = 36 m/s)

Figure 3-17. Time histories of cable vibration for cd = 1.5 on Cable C14

Table 3-9. Numerical results of cable vibration with/without vibration control on Cable C14.

Wind cases	Standard deviation			Maximum displacement (m)		
	Un-controlled	Passive control (c_d =1.5)	Control efficacy (%)	Un-controlled	Passive control (c_d =1.5)	Control efficacy (%)
Case 1 (V_{10} = 12.89 m/s)	6.45×10^{-3}	3.32×10^{-3}	48.53	2.71×10^{-2}	1.38×10^{-2}	49.01
Case 2 (V_{10} = 20 m/s)	1.72×10^{-2}	9.21×10^{-3}	46.45	7.10×10^{-2}	3.82×10^{-2}	46.20
Case 3 (V_{10} = 36 m/s)	2.82×10^{-2}	1.64×10^{-2}	41.84	1.17×10^{-1}	8.41×10^{-2}	28.12

3.3.4. Serviceability Assessment

The probability of serviceability failure was evaluated for the three target cables (C10, C11, and C14) with and without vibration control under the three wind cases as shown in Table 3-10. Note that the serviceability failure criteria used in this study were adopted from the Korean Highway Bridge Design Code [4], defined as a displacement of over 1/1600 of the cable length at the middle of the cable when the wind speed is less than 20 m/s for 10 minutes. Using Cable C14 as an example, the cable can be observed to bear the external wind force without serviceability failure (P_f= 0) in Case 1 regardless of the presence of the passive damper. In Case 2, the probability of serviceability failure over one hour was 1.65×10^{-1} when uncontrolled but was lowered to 1.15×10^{-12} when the passive damper was included. Under the conditions of the most powerful wind measured in Korea (Case 3), the serviceability of the uncontrolled cable exhibits definite failure, while the passively controlled cable exhibits relatively high failure probabilities of 3.59×10^{-1} and 5.89×10^{-1} for T = 3,600 s and 7,200 s, respectively.

The probability of serviceability failure can be adjusted by changing the non-dimensional damping constant (c_d) as it describes the performance of the passive viscous damper. The probability of serviceability failure for Cable C14 in Case 3 is shown in Figure 3-18 for damping constants from 0 to 5.0 for T = 3,600 s. As would be expected, increasing the damping constant of the passive damper mitigates the cable vibration and results in a lower probability of serviceability failure. Clearly, the probability of serviceability failure can be effectively controlled to meet design guidelines by adjusting the performance of the installed passive viscous dampers.

Table 3-10. Calculated probability of serviceability failure (P_f)

Case parameters			Probability of serviceability failure (P_f)		
			Cable C10	Cable C11	Cable C14
Case 1 (V_{10} = 12.89 m/s)	Uncontrolled	T = 3,600 s	8.92×10^{-6}	0	0
		T = 7,200 s	1.78×10^{-5}	0	0
	Passive control (c_d =1.5)	T = 3,600 s	0	0	0
		T = 7,200 s	0	0	0
Case 2 (V_{10} = 20 m/s)	Uncontrolled	T = 3,600 s	1	9.23×10^{-1}	1.65×10^{-1}
		T = 7,200 s	1	9.94×10^{-1}	3.04×10^{-1}
	Passive control (c_d =1.5)	T = 3,600 s	4.91×10^{-1}	6.20×10^{-7}	1.15×10^{-12}
		T = 7,200 s	7.40×10^{-1}	1.24×10^{-6}	2.30×10^{-12}
Case 3 (V_{10} = 36 m/s)	Uncontrolled	T = 3,600 s	1	1	1
		T = 7,200 s	1	1	1
	Passive control (c_d =1.5)	T = 3,600 s	1	1	3.59×10^{-1}
		T = 7,200 s	1	1	5.89×10^{-1}

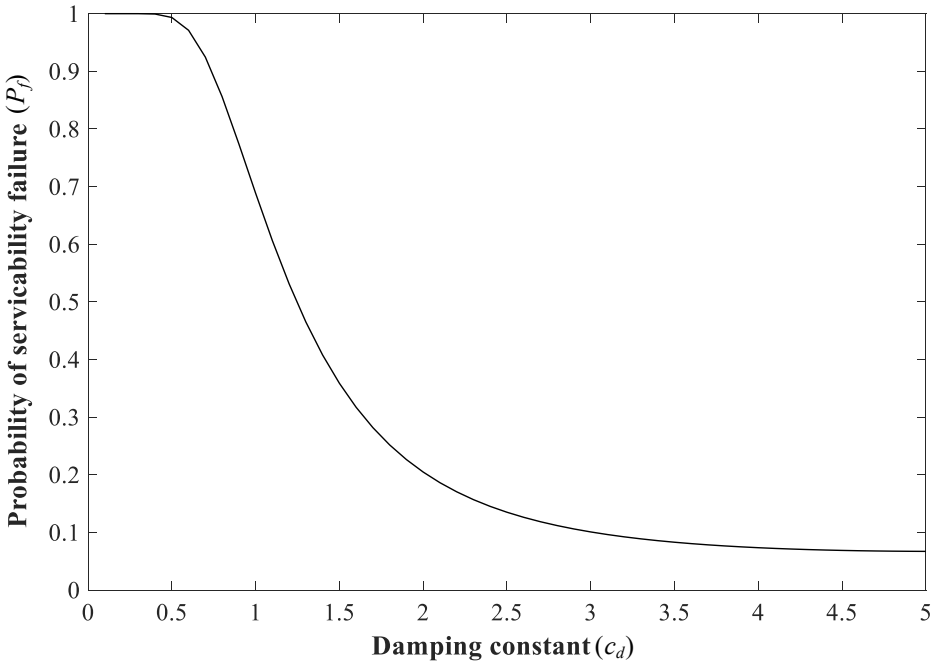

Figure 3-18. Probability of serviceability failure of Cable C14 versus non-dimensional damping constants (c_d) in Case 3

3.4. Summary

The present topic consisted of three parts: 1) developing an automated real-time serviceability assessment system, 2) presenting an automated cable damping monitoring strategy, and 3) proposing a serviceability assessment method with consideration of vibration control. First, the automated real-time serviceability assessment system using wireless smart sensors was developed to monitor the serviceability of the stay-cable in a cable-stayed bridge, which operates at low cost and consumes low power. The developed system consists of a gateway node and a leaf node connected to each other through Bluetooth communication. The gateway node commands the leaf node to assess the serviceability and monitor the serviceability level, and the leaf node assesses the serviceability of the stay-cable. The gateway node was designed using a Bluetooth device to check the serviceability condition of the stay-cable. Smart sensors with low cost and low power consumption were used to develop the leaf node, which is based on the Raspberry Pi 3 Model B+ single-board computer and MEMS accelerometer with ADC sensor. The system features embedded on-board processing to measure the acceleration, estimate the displacement from the measured response, and diagnose serviceability failure based on the US design code [16]. Note that the measured acceleration of the stay-cable is converted into dynamic displacement based on a previous study [22]. A series of experiments were conducted using a laboratory-scale cable to verify the developed system, and the results indicate that the system can monitor the serviceability of the stay-cable using a single type of measurement data with the Raspberry Pi-based single-board computer. In addition, the leaf node installed on the cable can be remotely commanded by the gateway node, in particular, using the Bluetooth device, which aids inspectors in monitoring the serviceability level of the stay-cable conveniently.

Second, an automated cable damping monitoring strategy was presented. For complement, this study examined various damping estimation methods, which can be classified into time- and frequency-domain methods. The criteria were set to determine the appropriate method for damping automation, which can be possible to conduct output-only modal identification with less computation time. The half-power method was selected, satisfying predefined conditions for automation tailored to the stay-cable, to estimate damping ratio from PSD calculation. As the estimated damping ratio by the half-power method is affected by the NFFT and types of spectral window, this study investigated the optimal NFFT and spectral window to calculate PSD with less spectral leakage. The PSD of cable responses were calculated based on the determined NFFT and spectral window. Peak-picking was applied to detect natural frequencies in the PSD graph based on predefined ranges which are assumed to include natural modes. After that, the proposed automated damping estimation method was applied to cable responses, obtained from in-service bridges in Korea under the different wind conditions, and successfully verified to monitor cable damping ratio continually.

Third, a serviceability assessment method for vibration-control equipped stay-cables was proposed and evaluated when subjected to external wind forces causing wind-rain induced vibration. The cable serviceability failure event used in this method was defined according to when the cable response reached either the upper or lower bound given in the relevant bridge design code. Treating the cable behavior as a first-passage problem, the probability of serviceability failure was assumed to be the probability of the cable response first moving outside the defined limits during a prescribed time interval. The cable dynamics were simulated considering not only cable sag but also inclination angle, flexural rigidity, and static deflection to construct a realistic cable model, and a passive viscous damper was selected as the damping device. By using VanMarcke's approximation, this study then assessed the probability of serviceability failure of the cables used in the Second Jindo Bridge in Korea depending on the presence of vibration control. According to the Korean Highway Bridge Design Code, the cable vibration serviceability failure threshold was set to 1/1600 of the cable length [4]. The proposed method showed a clear correlation between the behavior calculated using the proposed method and data collected under the same wind speed event. The results demonstrate that the proposed serviceability assessment method can be used to provide a guideline to determine the possibility to use of a cable-stayed bridge and the appropriate damping systems given the wind environment and can serve as a criterion to establish the appropriate time interval for assessing the probability of serviceability failure.

4. INTEGRATED VIBRATION CONTROL SYSTEM

Cable vibration control is one of the important topics to keep the allowable serviceability level under external loadings. This study aims to develop an integrated cable vibration control system using the Arduino platform and MR damper implementing a semi-active control and clipped optimal algorithm. A more detailed explanation of the system is introduced below.

4.1. Design of the Integrated Cable Vibration Control System

4.1.1. Sensor Hardware Platform

This study develops an integrated cable vibration control system () that performs two main functions, sensing the cable response and controlling the damping device. As a low-cost and low-power single microcontroller board, the Arduino Due is selected as a platform for the integrated vibration sensing and control system. The Arduino Due is the first Arduino product based on the 32-bit ARM core microcontroller, meeting the needs for vibration sensing and control in this study. This board has 54 digital input/output pins, 12 analog inputs, 84 MHz clock, a USB OTG capable connection, two DAC, and a 3.3 V operating voltage. For programming Arduino, an interface named the 'Integrated Development Environment (IDE)' is provided, which is capable of writing, debugging, and uploading code based on C and C++ to the board.

As the component for sensing the cable response, this study selects a tri-axial accelerometer ADXL 335 based on the MEMS accelerometer. The ADXL 335 is small and low-cost; moreover, it has a low-power consumption (350 μA), the minimum measurement range of ±3g in tri-axis, and 270 mV/g of sensitivity. The sampling rate of this sensor ranges from 0.5 Hz to 1,600 Hz for the X and Y axes, and from 0.5 Hz to 550 Hz for the Z axis.

As a damping device for semi-active control, the MR damper, RD-1097-01 model, produced by Lord Corporation is selected. This model is designed to generate 100 N as its maximum damping force under 1 A of current and 51 mm/s of piston velocity. Under the passive-off mode, the damping force is less than 9 N at a piston velocity 200 mm/s. This damper has a stroke from – 25 mm to 25 mm, and a response time that is less than 25 ms (response speed = 40 Hz) under a step change of the current from 0 A to 1 A for 51 mm/s piston velocity [6]. Details of damper characteristics in terms of displacement, loading velocity, and input current can be found in the previous study [24]. As the MR damper is controlled by the current signal, this study uses the Wonder Box to convert the command voltage produced by the semi-active control to current.

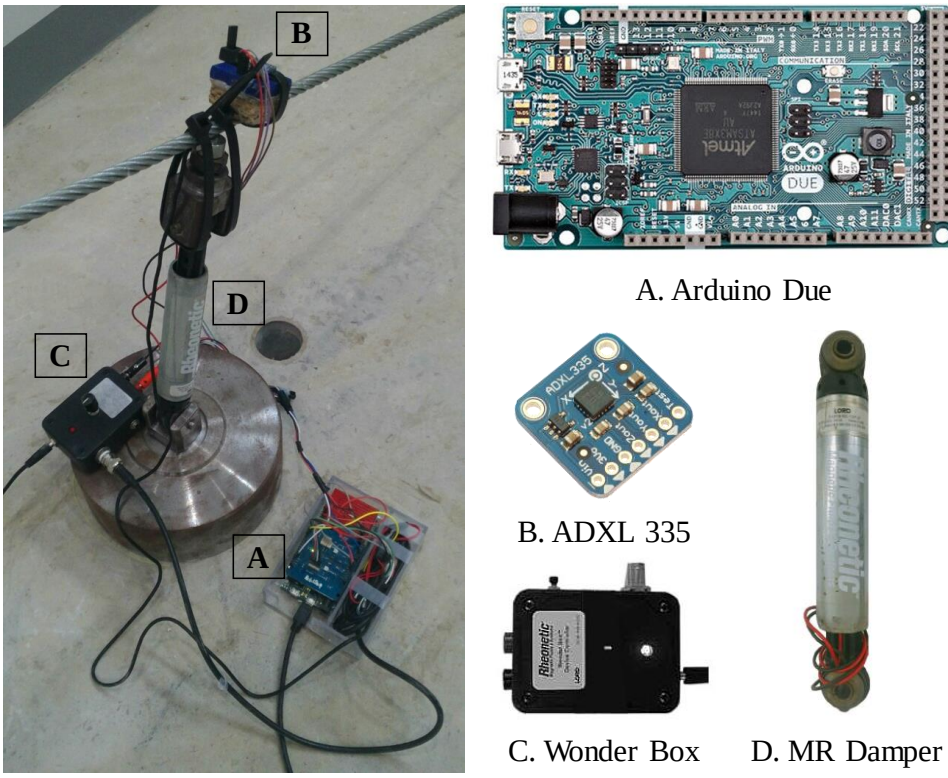

Figure 4-1. Integrated control system with semi-active damping device

4.1.2. Operating Software

The semi-active control algorithm is implemented on the Arduino Due through the IDE interface. For semi-active control, the LQG control algorithm is first programmed to estimate the system state using the measured cable response and provide control gain used to calculate the control force. While 20 shape functions are known to be effective for determining the control force of a cable [55], cable dynamics in this study are constructed using one shape function, focusing on reducing the first mode of vibration because of the limited performance of the Arduino board. The cable's tension is also measured to construct cable dynamics using vibration-based methods, finding the linear relationship between natural frequencies and cable tension proposed by Shimada [63]. Because of limited operating speed, the sampling rate of the Arduino board is set to 20 Hz as a maximum speed when the semi-active control is embedded. To control the MR damper's performance, the clipped-optimal controller is implemented on the Arduino board to determine the command input voltage to the MR damper.

The procedure for cable vibration control is summarized in Figure 4-2. At the damper location, the acceleration sensed by the low-cost MEMS accelerometer is measured. This is the first cable response that is measured. The measured cable response is transmitted to the Arduino Due and used to calculate

the desired control force through LQG control. The command voltage is generated by the clipped-optimal algorithm based on the relationship between the control force and damping force measured by a load cell at the damper location. The control voltage is converted to current, and this current is applied to the MR damper to control cable vibration.

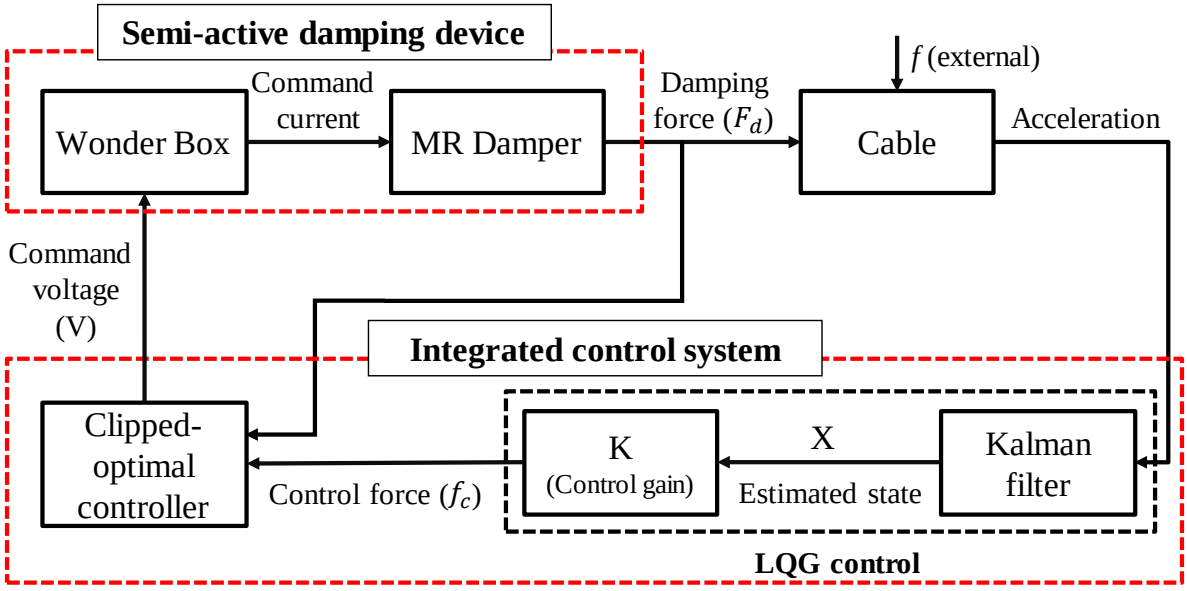

Figure 4-2. Block diagram of the control process

4.2. Laboratory-scale Experiment

4.2.1. Experimental Setup

In this study, a cable/MR damper system for a laboratory experiment is developed to examine the effectiveness of the proposed system on cable vibration reduction (Figure 4-3). The geometric and mechanical properties of the cable are indicated in Table 4-1. The MR damper is located 15% of the total length of the cable from the lower anchorage. An exciter (B&K Exciter 4808) is installed in the mid-span of the cable to impose in-plane sinusoidal excitation to the cable in a perpendicular direction. To measure the cable response, an accelerometer (PCB 353B33, 101.9 mv/g) is installed in the middle span of the cable. The force of the MR damper is measured by a load cell located in between the MR damper and the cable. The cable tension is fixed at 379.2 N, and its value is estimated by the vibration-based methods proposed by Shimada [63].

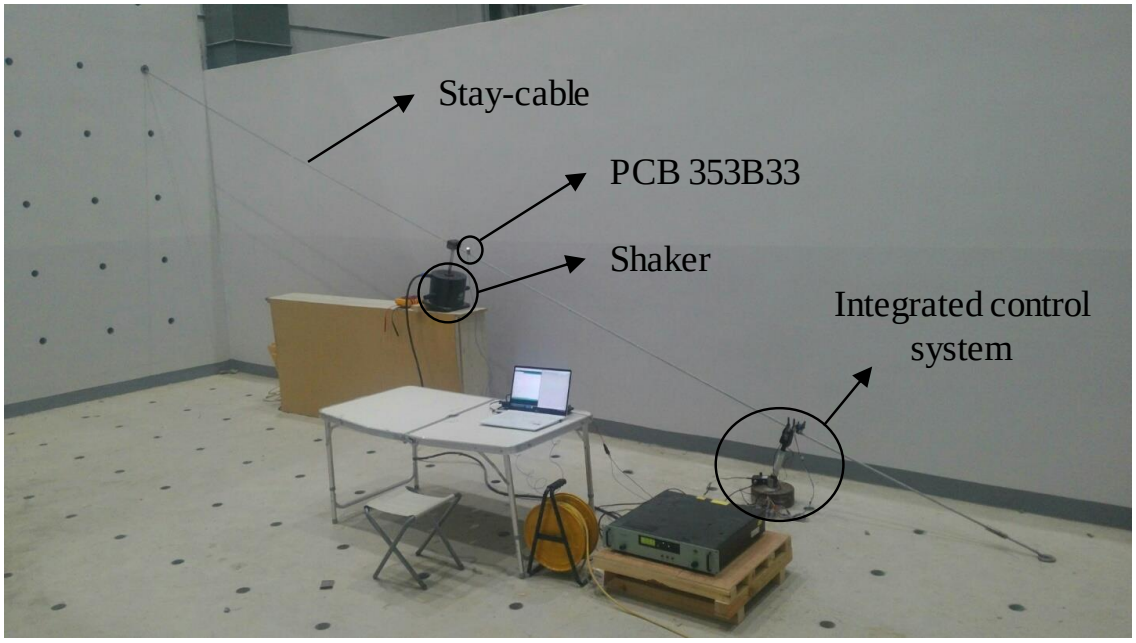

Figure 4-3. Experimental setup for cable vibration control

Table 4-1. Properties of the model cable

Length (m)	Inclined angle (°)	Tension (N)	Mass (kg/m)	Diameter (mm)	Break load (Ton)	Cable type	Natural frequency (Hz)		
							First	Second	Third
6.95	43	379.2	0.314	10	5.46	IWRC	2.5	5.0	7.5

4.2.2. Test of the Integrated Cable Vibration Control System

A series of experiments to validate the performance of the proposed system were conducted with the following four control schemes: (1) without the MR damper (namely, “uncontrolled”), (2) with the MR damper having no applied current (namely, “passive-off” control), (3) with the MR damper having constant applied current (namely, “passive-on” control), and (4) with the MR damper having an inconstant current controlled by the semi-active control algorithm. The four tests were carried out with the same excitation condition under constant amplitude and the third natural frequency (7.5Hz). The exciter was not able to induce sufficient vibration in the first and second natural modes of the cables, whereas the third mode could be excited.

Before conducting a series of tests, the performance of the system was evaluated. In particular, the system’s stability, time delay, and command signal were investigated. First, as the response speed of the MR damper (40 Hz) is higher than that of the developed control system (20 Hz), the damper can be controlled by the system with sufficient time to be saturated, showing the same result in the experiment. Therefore, the developed control system could provide control voltage to the damper stably. Second, the existence of the time delay when the Arduino-based control system is operating was investigated.

The time delay was not identified in the Arduino platform because the integrated control system was designed to have a maximum sampling rate of 20 Hz, running the semi-active control fully. Third, a signal of the control voltage was examined to verify whether the MR damper is well controlled or not based on a clipped optimal algorithm. The spatial distribution of control voltage is indicated in Figure 4-4 for the first ten seconds of operation time with a relationship between the optimal control force and damping force. This study confirmed that the MR damper is correctly controlled by the Arduino-based integrated control system satisfying the clipped optimal algorithm.

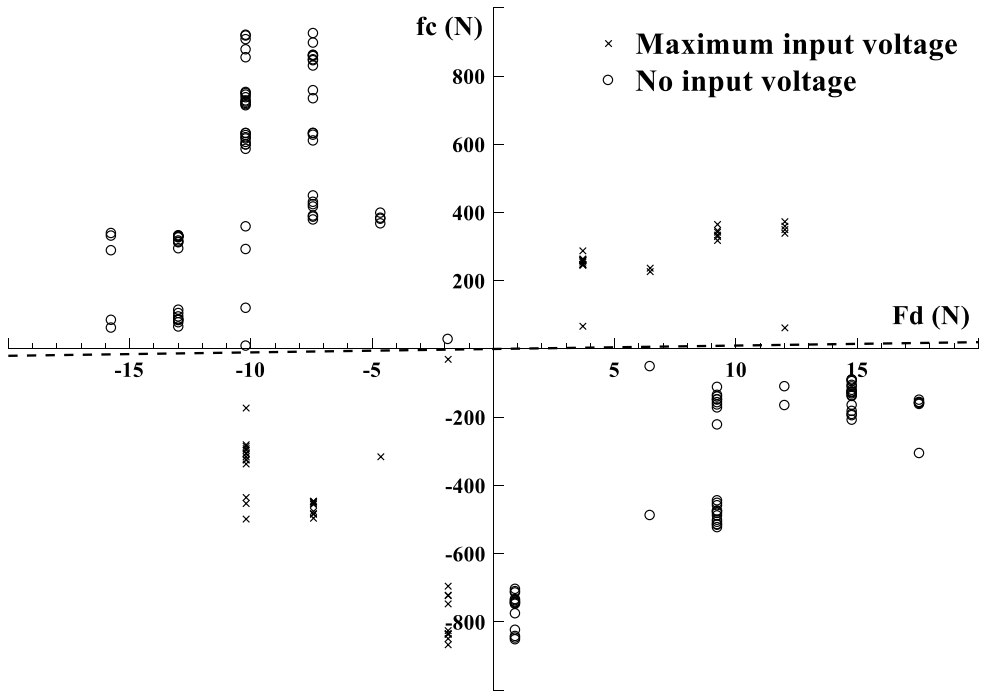

Figure 4-4. Spatial distribution of control voltage depending on optimal control force and damping force (the dashed line represents $f_c = F_d$)

Figure 4-5 represents the time histories of cable accelerations with the four different control schemes when the driving frequency of the exciter is 7.5 Hz. The obtained acceleration responses showed that all the MR dampers with passive-off, passive-on, and semi-active control reduced the cable vibration compared to the uncontrolled case. Supporting the result from Figure 4-5, Table 4-2 shows that all passive-off, passive-on, and semi-active control schemes reduce the level of maximum acceleration compared with the uncontrolled case. Note that whereas the standard deviation of the passive-on control is larger than that of the uncontrolled case, the passive-on scheme has a lower maximum acceleration. Both passive-off and semi-active control showed a lower variation in acceleration than the uncontrolled case.

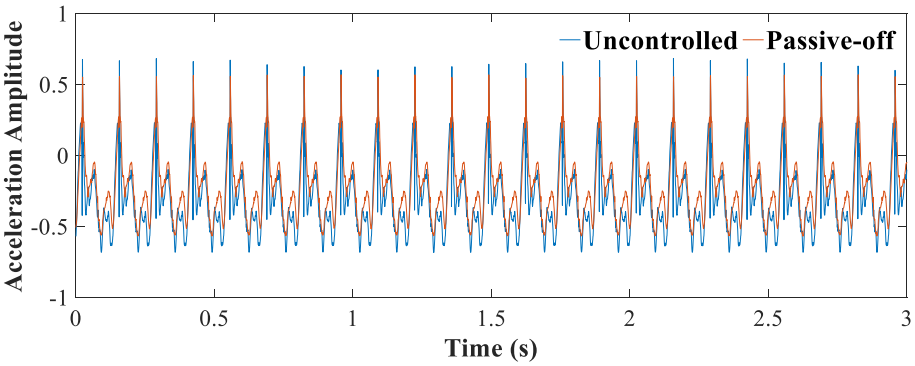

(a) uncontrolled and passive-off

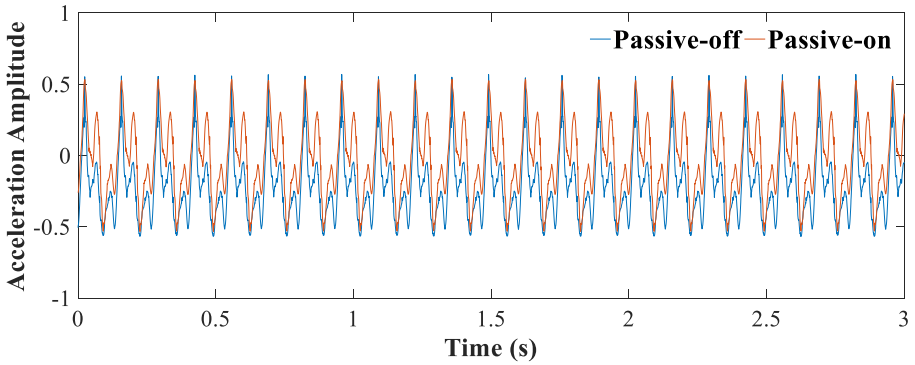

(b) passive-off and passive-on

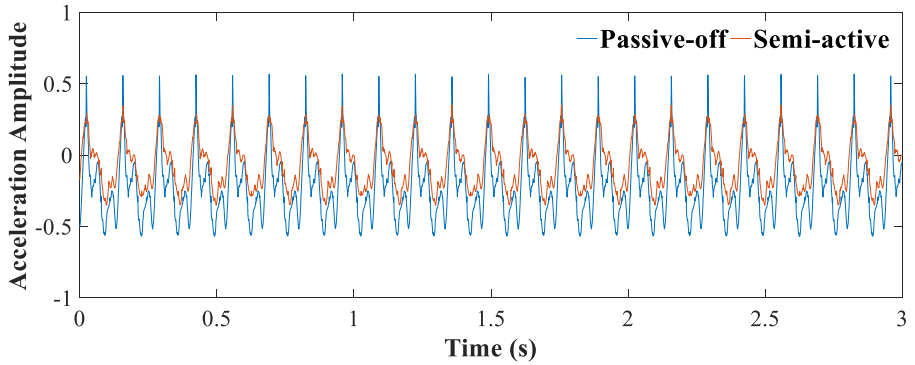

(c) passive-off and semi-active

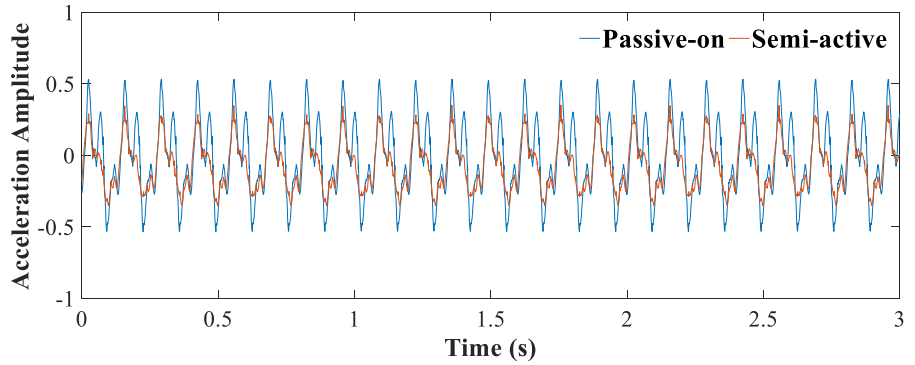

(d) passive-on and semi-active

Figure 4-5. Time histories of the acceleration response of the cable

Table 4-2. Experimental results of the cable vibration control with/without control

Cases	Standard deviation	Maximum acceleration (m/s^2)	Control efficacy (%)
Uncontrolled	0.2440	0.6834	/
Passive-off	0.2306	0.5682	16.86
Passive-on	0.2645	0.5336	21.02
Semi-active	0.1731	0.3513	48.60

This study calculated the power spectral density of cable accelerations to show a dominant mode vibration and to identify the effect of semi-active control on vibration reduction (Figure 4-6). Two effective control schemes, showing large vibration reduction, were chosen to compare the power spectral density of a cable response to each other. Both control schemes indicated the same dominant excitation frequency (7.5 Hz). Compared to a passive-on control, a semi-active control showed more energy reduction in the excitation frequency, indicating good performance in vibration reduction.

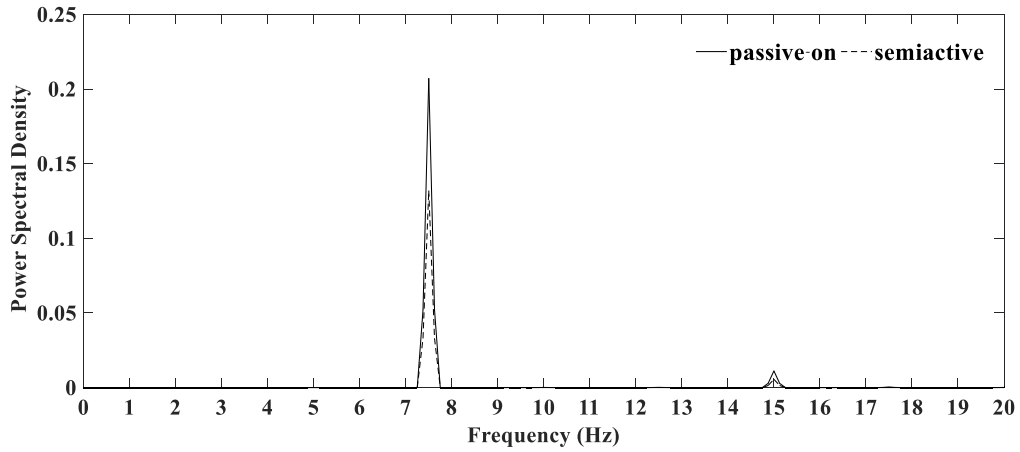

Figure 4-6. Power spectral density of cable accelerations from passive-on and semi-active control

The following conclusions can be drawn from the results. First, semi-active control most effectively reduced the cable vibration in terms of acceleration compared with passive-off and passive-on control. The cable response by semi-active control exhibits less vibration than other controls, and the control efficacy also supported the finding that semi-active control can reduce the maximum acceleration about 2.5 times more than passive-off and passive-on control. Second, both passive-on and passive-off control could reduce the cable response while showing a similar vibration reduction.

To apply the developed control system to real-world applications, it is important to identify the appropriate capacity of a power source that provides the operating power for the integrated control system. Measuring the power consumption of this system is needed to design the appropriate power source. Arduino Due, which is a platform for this system, has two components, a microcontroller, and

a power regulator, which consume power. During normal operation, the Arduino Due micro-controller (SAM3X, 84 MHz) uses 75 mA/h, and the power regulator consumes 10 mA/h. Under the input voltage with 9 V, it is concluded that the integrated control system consumes 0.765 W/h and 18.36 W/d.

4.3. Summary

The objective of this study was to develop an integrated cable vibration control system, embedding a semi-active control. The integrated system was constructed based on the Arduino Due platform, which known to be low-cost and has low-power consumption. This system was designed to function in two ways, i.e., sensing the cable response and controlling the MR damper to reduce cable vibration. A low-cost, low-power MEMS accelerometer was employed to sense the cable vibration, and a semi-active control algorithm was implemented in this system to reduce cable vibration. For controlling the damping device, this study implemented the clipped-optimal controller known to be effective for performing semi-active control. An experimental test was carried out using a stay-cable installed for the laboratory experiment to identify the utility of the proposed system on vibration reduction and the effectiveness of semi-active control compared with passive control.

5. AUTOMATED TENSION MONITROING USING DEEP LEARNING

The tension force provides useful information for stay-cable during the construction of cable-stayed bridges and in-service status as mentioned in the literature review. To monitor cable conditions, this study develops an automated cable tension monitoring system using smart sensors and deep learning. A more detailed description is introduced in this chapter.

5.1. Automated Cable Tension Force Estimation

The cable tension force can be estimated by using the vibration-based method which utilizes the relationship between modal parameters and tension force. If natural frequencies and mode numbers of a cable are extracted automatically, cable tension can be estimated consequently through the vibration-based method. This section introduces a process of automated cable tension estimation which can be specified into 1) developing automated peak detector tailored to a stay-cable using a Faster R-CNN and 2) selecting peaks representing natural modes of the cable for estimating cable tension force.

5.1.1. Faster R-CNN for Peak Detector

The numerical model of a stay-cable introduced in previous studies [4, 55] is used to obtain training data for developing the automated peak detector using a Faster R-CNN. The cable system at the middle span can be transformed into frequency response function H as shown in Equation (57) where n is the number of the natural modes, ω is the frequency, and j, k is the number of natural modes, and m, c, k indicate mass, damping, stiffness per unit length of a cable.

$$H(\omega) = \sum_{j=1}^{n} \sum_{k=1}^{n} \frac{1}{(k_{jk} - m_{jk}\omega^2 + ic_{jk}\omega)} \tag{57}$$

Peaks with different geometric shapes can be generated using the frequency response function as shown in Equation (57) by changing cable properties. After generating frequency response functions of the stay-cable, a quantitative definition of the peak is required to train the automated peak detector. This study refers to the peak definition scheme proposed by the previous work [37], which defined the peak size in terms of relative width W_p and relative height H_P as shown in Equation (58) and Figure 5-1.

$$W_P = \frac{N_W}{M_W} \le W_{\max} \quad , \quad H_P = \frac{N_H}{M_H} \ge H_{\min} \tag{58}$$

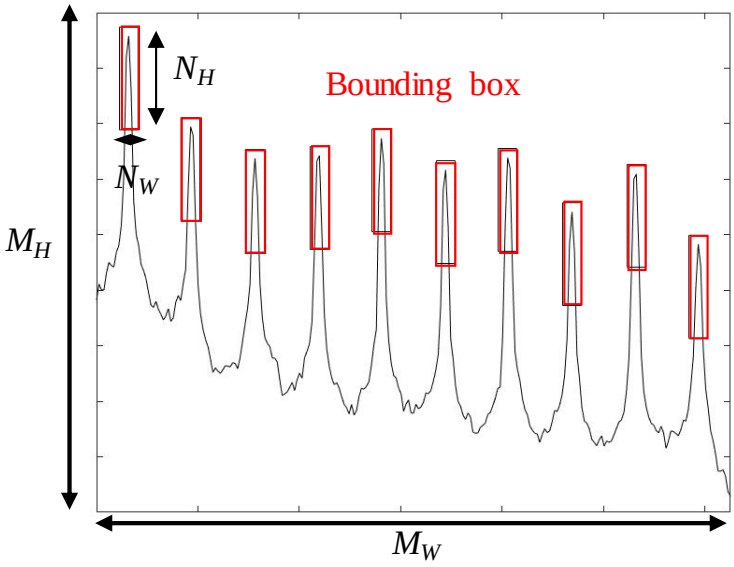

Figure 5-1. Frequency domain representation of a cable with predefined bounding boxes of peaks

where N_W and N_H indicate the number of pixels in each peak's width or height; and M_W and M_H represent the total number of pixels along the x-axis and y-axis of an image. This study regards that peak is detected by bounding boxes from the Faster R-CNN which satisfies the predefined peak size with relative height and width as shown in Equation (58).

All frequency response functions with quantitatively defined peaks are converted into image format to generate training data for automated peak detector tailored to the stay-cable. In this study, the automated peak detector is developed using the Faster R-CNN over inception v2 pre-trained on the COCO dataset through the *TensorFlow Object Detection* API, which is an open-source framework provided by *Google*. Note that an automated peak detector is designed to extract two object classes, peaks or non-peaks and localize bounding boxes where peaks exist. Of total peaks, 80% of peaks are selected as training data and others are used to test the automated peak detector. The developed automated peak detector is optimized through quantizing weights which reduces a model size to be embedded into an automated cable tension monitoring system. A more detailed explanation of the proposed automated peak detector is indicated in Figure 5-2.

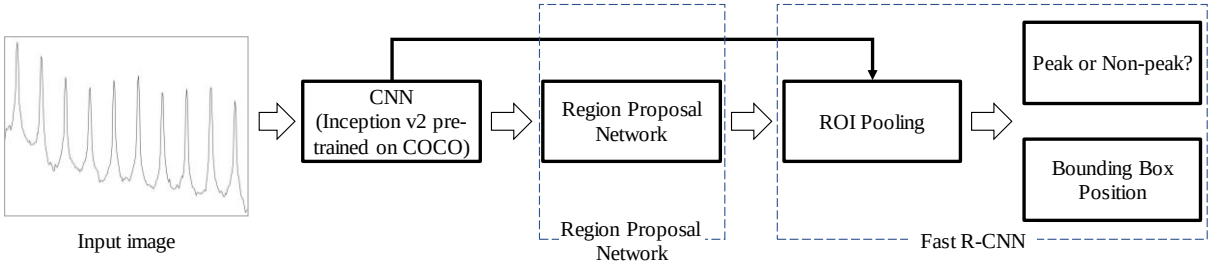

Figure 5-2. Schematic of the proposed automated peak detector based on Faster R-CNN

In this study, training data are generated through frequency response functions with 12.5 Hz as the maximum *x*-axis containing various geometric shapes of peaks by changing the value of damping per unit length *c*. A total of 14,000 frequency response functions are numerically obtained by the fixed *m, L, n*, and *T* and the varying *c* from 0.03 to 1.75 with 0.0001 intervals to make various geometric shapes (Table 5-1). Note that 0.03 of *c* corresponds to 0.1% damping of the first mode and 1.75 is equal to 0.5% damping of the first mode in this model, which is based on the bridge design criterion in Korea [4]. As the cable response in the middle span contains ten peaks among twenty peaks due to the assumed number of natural modes, this study obtains a total of 140,000 peaks which contains different geometric shapes by varying *c*.

Table 5-1. Cable characteristics used to generate training data

Mass per unit length (*m*)	Damping per unit length (*c*)	Cable length (*L*)	Cable tension (*T*)	Number of natural modes (*n*)
43.9 kg/m	0.03-1.75 kg/m/s	157.880 m	1,709.120 kN	20

Although the selection of peak size is a subjective task, this study attempts to define the size of peaks based on measurement data of cable responses from in-service cable-stayed bridges. Sixty cable responses are collected from two different cable-stayed bridges (the 1st, and 2nd Jindo Bridge) in the Republic of Korea, and cable responses are plotted in the frequency domain. This study manually examines the size of peaks from sixty cable data, and the geometric size of cable peaks are finally defined as 20 pixels of width (N_W) and 110 pixels of height (N_H) that can be distinguished by human judgment as shown in Figure 5-1. Note that bounding boxes have height with 100 pixels, and this study adds an additional 10% of height from the highest point to make peak points within the bounding boxes. As M_W and M_H are set to be 677 pixels and 534 pixels, $W_{\max}$ and $H_{\min}$ correspond to 0.03 and 0.21 respectively.

5.1.2. Peak-selection for Natural Modes

After applying the automated peak detector to the frequency domain data, peaks are detected as a form of bounding boxes. Each peak is assumed to have a point with the highest value of the energy spectrum within the bounding box. However, the automated peak-picking may detect undesirable peaks that fail to satisfy the characteristic of cable responses in that natural frequencies are increasing with the almost same interval.

Accordingly, post-processing for removing undesirable peaks is required to select peaks representing natural modes of the cable. Undesirable peaks can exist mainly as two forms: 1) when detected peaks exist in the adjacent natural modes as shown in Figure 5-3 (a), and 2) when detected

peaks exist in the low-frequency range caused by cable-deck interaction as indicated in Figure 5-3 (b). Using the characteristic of the cable that peaks tend to exist with the almost same interval, an interval which fails to meet this characteristic is removed as outlier interval by using an idea from random sample consensus (RANSAC). Note that RANSAC is used to determine an optimal statistical model that well represents a dataset with outliers based on proximity to the statistical model [74].

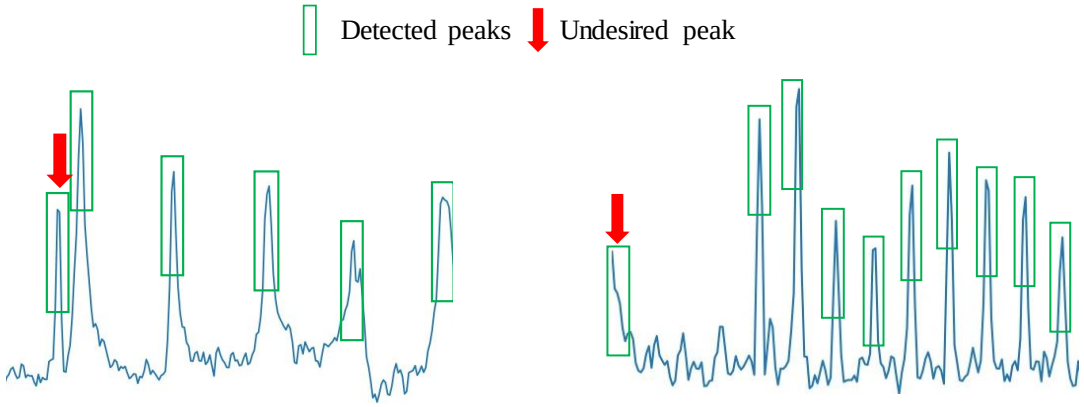

(a) Undesirable peak case 1 (b) Undesirable peak case 2

Figure 5-3. Types of undesirable peaks among detected peaks

The peaks which represent natural modes are selected as the following steps. After applying the automated peak-picking to the frequency domain image, this study plots frequency intervals of each adjacent detected peak and assumes a constant function that crosses one of the collected intervals. Then, frequency intervals, within the prescribed threshold (10 %) of the assumed constant function, are identified as inliers, and others are considered as outliers. These two processes are repeated for every interval, and the number of inliers and outliers are calculated for each process (Figure 5-4). Then, this study selects the optimal constant function which well explains the frequency intervals the most based on the line model with the largest number of inliers. The determined optimal constant function is regarded as the frequency interval which explains the natural frequencies of the cable. Based on the determined frequency interval, this study selects peaks which meet the characteristic of the cable with similar frequency interval by removing undesirable peaks located in adjacent natural modes (undesirable peak condition 1). If the detected peaks are less than 90% of determined interval frequency, this peak is regarded as undesirable peaks located in the low-frequency range (undesirable peak condition 2). The process of a peak-selection for identifying natural modes is summarized by four steps as below:

Step 1: Calculate and plot frequency intervals between each adjacent detected peak

Step 2: Perform the outlier removal from frequency intervals to select frequency interval

Step 3: Remove undesirable peaks located in adjacent natural modes (Undesirable peak case 1)

Step 4: Remove undesirable peaks located in the low-frequency range (Undesirable peak case 2)

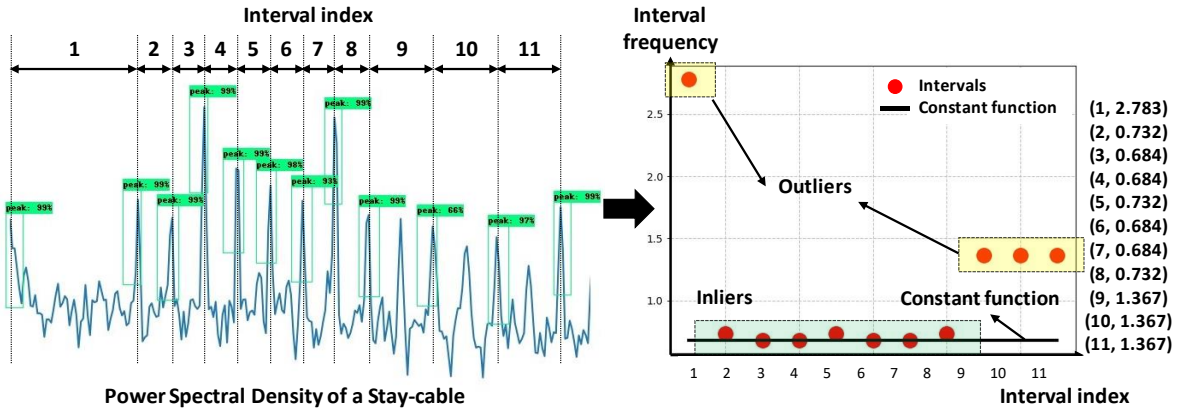

Figure 5-4. Process of selecting optimal frequency interval of the stay-cable

5.1.3. Automated Cable Tension Force Monitoring

In conclusion, automated tension force estimation is designed to conduct a data acquisition of cable responses, automated peak-picking, peak-selection for identifying natural modes, and estimation of cable tension force by using the vibration-based method as shown in Figure 5-5. A more detailed process is as follow:

Step 1: Acquire the cable response in terms of acceleration

Step 2: Transform a time-history of the cable response into a frequency domain data (e.g., PSD), which is in turn saved as an image

Step 3: Apply the automated peak detector to the frequency domain image to find candidates of natural frequencies and mode numbers

Step 4: Select cable peaks by removing undesirable peaks based on the characteristic of the cable response that natural frequencies increase proportionally with an integer multiple

Step 5: Estimate the cable tension based on identified natural frequencies and mode numbers

Figure 5-5. Flowchart of automated cable tension estimation

5.2. Design of Automated Cable Tension Monitoring System using Smart Sensors

This work develops the automated cable tension monitoring system using deep learning and wireless smart sensors. Wireless smart sensors have been widely adopted to construct a system for structural health monitoring [8, 31, 39, 46, 75, 76]. The smart sensor is regarded to have an ability to communicate with other sensors wirelessly and compute on-board processing with small size, low-cost and low-power consumption [31]. The developed system is composed of two types of nodes: a gateway node and multiple sensor nodes as shown in Figure 5-6. The gateway node remotely controls sensor nodes to monitor cable tension force through wireless communication. Under the command operation from the gateway node, sensor nodes, installed on stay-cables, start to estimate the cable tension force and transmit results to the gateway node wirelessly. Among various wireless communication modules, this study utilizes a Bluetooth module to connect the gateway node and sensor nodes wirelessly. The wireless system network can be also constructed through other wireless modules, including LoRa, WiFi, and Zigbee.

5.2.1. Sensor Hardware Platform

Appropriate hardware platforms are selected for the gateway and sensor nodes, considering the algorithm implementation and wireless communication. In the case of the gateway node, the Bluetooth device is used to control sensor nodes wirelessly. Among various devices with Bluetooth module, this study selects a smartphone, one of the commonly used devices with Bluetooth module. As the smartphone is one of the portable mobile devices widely used, this device is an efficient tool to build the gateway node for the cable tension monitoring system. In this study, a Samsung Galaxy S10 smartphone is used to build the gateway node, which is equipped with Bluetooth version 5 capable of communicating with other devices up to 100 m wirelessly.

As the hardware platform of sensor nodes, this study selects one of the single-board computers, Raspberry Pi 3 Model B+, which has a small-size with an external dimension of 86 x 54 mm (Figure 5-6). This single-board computer features 1.4 GHz Quad-Core 64-bit ARMv8 CPU and 1 GB LPDDR2 SDRAM, which has enough capability to compute automated peak-picking trained by Faster R-CNN. In addition, this model possesses Bluetooth version 4.2, 2.4 GHz wireless LAN, HDMI, 4 USB 2.0 ports, extended 40-pin GPIO headers, and a micro SD port for installing the operating system and storing data. Bluetooth module embedded in this Raspberry Pi enables sensor nodes to communicate with the gateway node wirelessly. Through HDMI and USB ports, users can access this computer easily using a mouse, keyboard, and monitor. The sensor node is operating by a Raspbian, an official operating system for the Raspberry Pi model, by installing the system in a micro SD card. Deep learning library

(i.e., *Tensorflow* in this study) can be installed in the Raspberry Pi owing to the operating system. To activate the Raspberry Pi, the recommended input power is 5 V input voltage with 2 A current. Under the recommended power input, this computer consumes approximately 2.5 W/h during the system idling status and 7 W/h during the main operation which uses 80 % memory [77]. This study develops a prototype that can prove the concept of fully automated tension monitoring; a complete long-term monitoring system with low power consumption can be realized when more energy-efficient sensor hardware is advent in the future.

The sensor nodes measure cable responses by using a tri-axial MEMS-based analog accelerometer, ADXL335 which is small size, low-cost, and low-power consumption (Figure 5-6). This MEMS accelerometer can measure acceleration up to 3 g with 270 mV/g sensitivity and sampling rate from 0.5 Hz to 1,600 Hz for the X- and Y-axis and from 0.5 Hz to 550 Hz for the Z-axis. To measure acceleration responses using the Raspberry Pi, an ADS1115, which is an analog-to-digital converter (ADC) with 16-bit precision, is utilized with the ADXL 335 analog accelerometer as shown in Figure 5-6. The MEMS accelerometer with ADC, installed on stay-cables, measures cable responses, and transmit the measurement data to the Raspberry Pi through GPIO header.

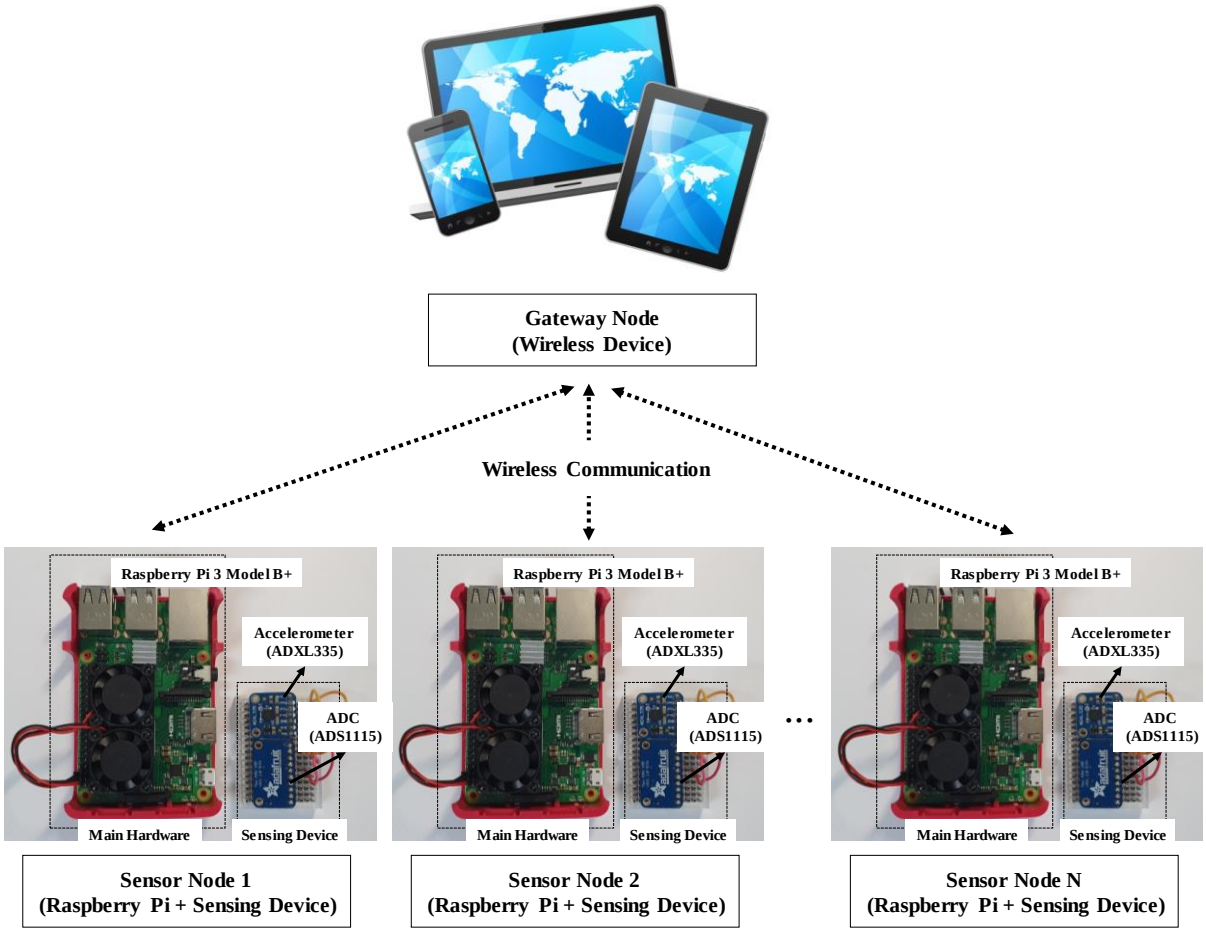

Figure 5-6. Design of wireless automated cable tension monitoring system

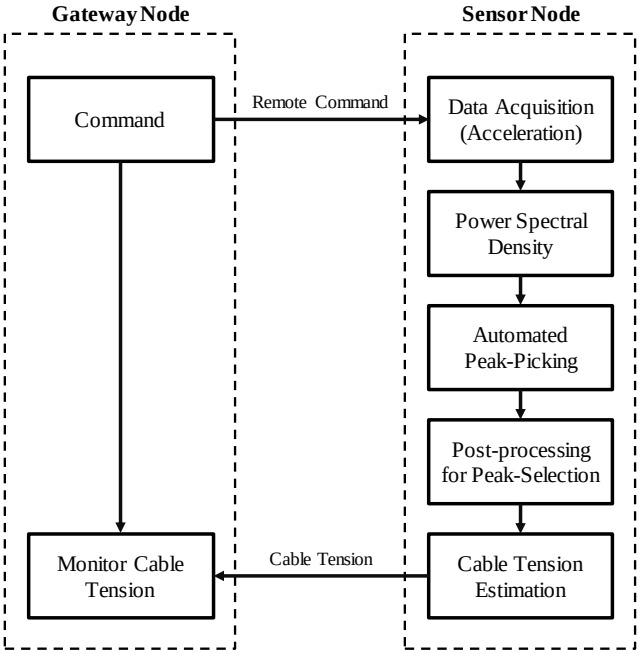

Figure 5-7. Procedure for wireless automated cable tension estimation

5.2.2. Operating Software

Each node has a different functional operation to monitor cable tension forces. The gateway node commands sensor nodes to measure cable tension forces automatically and receives results through wireless communication. In this study, the gateway node is connected to sensor nodes through the Bluetooth module by using one of the free mobile applications, *BT Chat* [78]. Inspectors can control the gateway node using this application to command sensor nodes.

Sensor nodes have embedded software in the Raspberry Pi platform including acceleration acquisition, PSD calculation, automated peak-picking, peak-selection for natural modes, and tension estimation, which is realized by Python language. The operation process of sensor nodes is as follows and summarized in Figure 5-7: First, sensor nodes start to measure a cable response in terms of acceleration after receiving a command from the gateway node. Measured acceleration data is converted to the power spectrum. The automated peak-picking algorithm identifies possible locations of natural frequencies from PSD of cable responses. Post-processing to select peaks representing natural modes is conducted by removing undesirable peaks. Based on the determined natural frequencies and mode numbers, sensor nodes calculate tension forces using the vibration-based tension estimation method. Lastly, sensor nodes transmit the estimated tension force to the gateway node through Bluetooth communication.

As aforementioned in Section 5.1.3, the automated peak detector is designed using the Faster R-CNN through the *TensorFlow Object Detection* API. The training and test processes to develop this

detector are conducted by a desktop with Intel i7-8700 CPU, 16 GB DDR4 RAM, and one NVIDIA GTX-1080 GPU, which takes ten hours approximately. As sensor nodes have not enough computation power to compute the Faster R-CNN, this study optimizes the size of automated peak detector by quantizing weights which reduces a model size to be embedded into the Raspberry Pi platform.

5.3. Laboratory-scale Experiment

5.3.1. Experimental Setup

To test the developed system, this study selected a laboratory-size IWRC type wire cable that has a 6.95 m of a length with 43° inclined angle, 0.314 kg/m of mass per unit length, 10 mm of diameter, and 5.46 Ton of break load (Table 5-2). The cable was installed at the laboratory by fixing the ends of the cable at the reaction wall and floor. The sensor node was installed 4 m from the lower end of the cable as shown in Figure 5-8. A rechargeable battery was attached to the sensor node to provide the power. Located about 10 m from the cable, the gateway node commanded the operation of the sensor node to measure cable tension and received estimated tension value through Bluetooth communication. The cable was excited by a fan under the cable as shown in Figure 5-8 to generate random vibration. A total of three cases with different tension forces were considered by changing the tightening levels of the cable, and the same test procedure was repeated for each tension case.

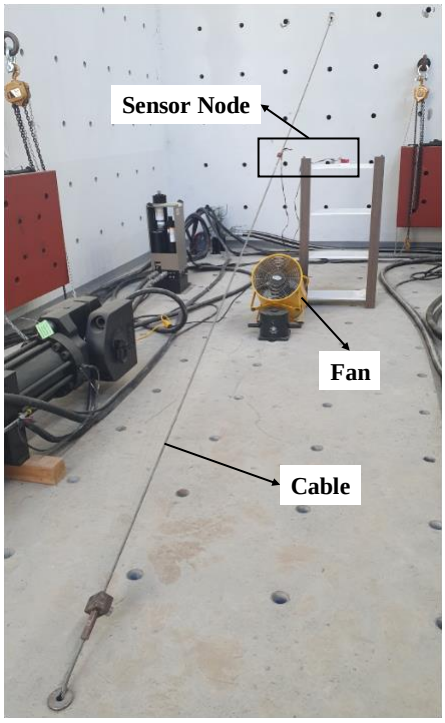

Figure 5-8. Experimental setup for wireless cable tension monitoring system in the laboratory

Table 5-2. Geometric and physical properties of the stay-cable in laboratory

Length (m)	Inclined angle (°)	Mass (kg/m)	Diameter (mm)	Break load (Ton)	Cable type
6.95	43	0.314	10	5.46	IWRC

5.3.2. Test Results and Discussion

This study carried out a series of laboratory experiments to verify the performance of the developed automated cable tension monitoring system. In this experiment, the sensor node was set to measure acceleration for 300 s with a sampling rate of 100 Hz. The five steps to automate the cable tension estimation shown in Figure 5-5 were conducted for each tension case. Figure 5-9 illustrates the automated operation of the sensor node for Case 2. The measured acceleration was converted to PSD, from which the automated peak detector identified six peaks. Post-processing to select peaks representing cable natural modes was conducted by removing an undesirable peak as shown in Figure 5-9. Note that the first natural frequency was not detected because the excitation was insufficient to induce the first mode vibration. Using the natural frequencies and mode numbers, the cable tension force was determined to be 156.2 N.

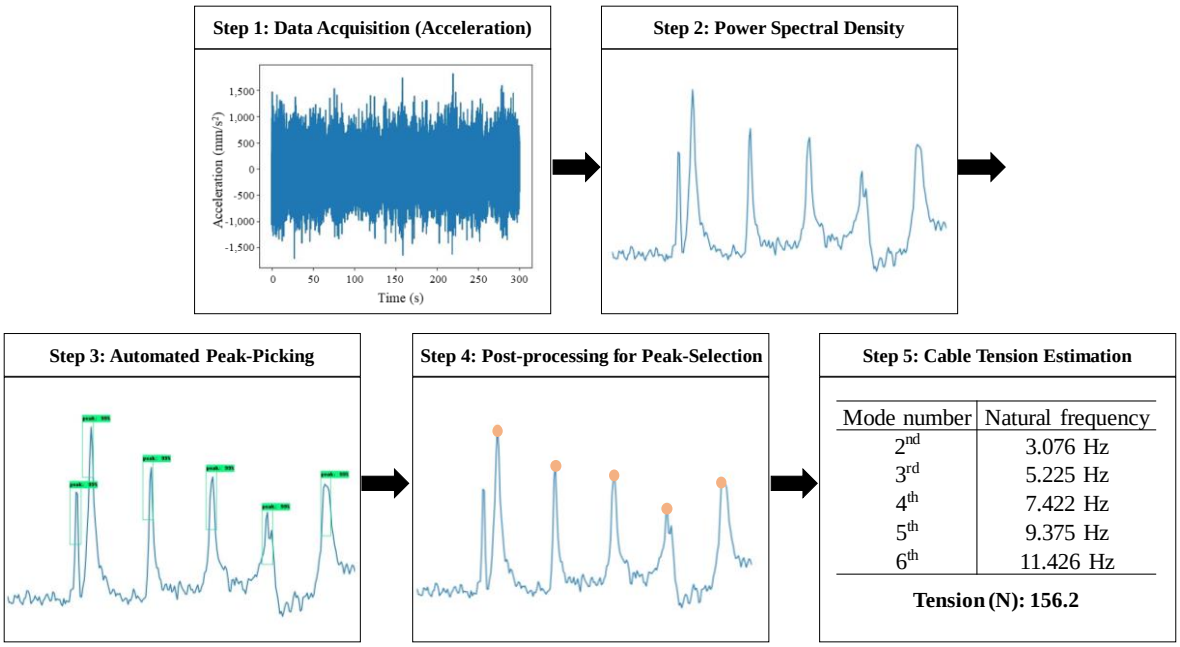

Figure 5-9. Illustration of automated cable tension estimation for Case 2

Three tests for each tension case were carried out, showing consistent tension estimation results in all three cases as shown in Figure 5-10. The standard deviations of the three cases were 0.16, 0.37, and 1.60, which were up to 0.8 % of the average tension forces. In conclusion, a total of nine tests in

laboratory experiments confirmed that developed wireless monitoring system can perform cable tension estimation with high consistency under different tension forces.

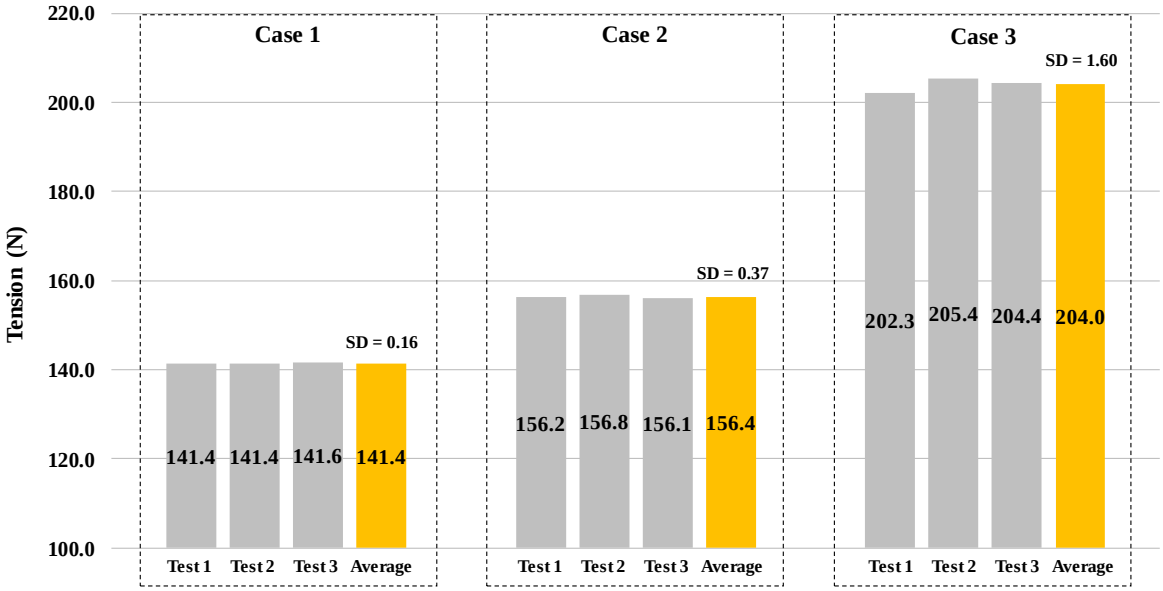

Figure 5-10. Estimated tensions from three tests under different tension forces

5.4. Field Experiment

5.4.1. Description of the Hwatae Bridge

For further verification of the developed system, the Hwatae Bridge was selected as the field experimental site in this study. A more detailed explanation of this bridge is described in Section 3.2.3. This study selected three stay-cables (CM07, CM08, and CM09) to conduct field tests for verification of the developed system. Detailed geometric and physical properties of the three cables are summarized in Table 5-3. The locations of the cables are shown in Figure 5-11. The known design tension forces of the cables were used as a reference to compare with the estimated values from the proposed system.

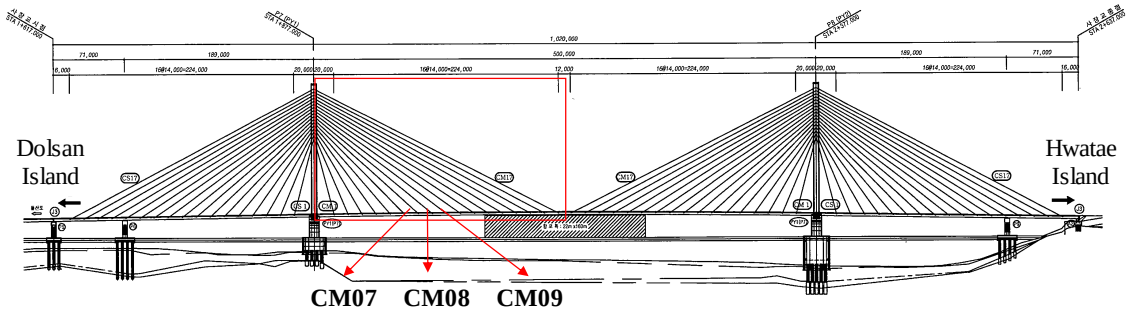

Figure 5-11. Longitudinal sectional profile of the Hwatae Bridge with three stay-cables

Table 5-3. Geometric and physical properties of three stay-cables for field tests

	Designed tension (kN)	Cable length (m)	Weight per length (N/m)	Sectional area (mm2)	Inclined angle (°)
CM07	2,129	138.235	447.0	4,800	41.857
CM08	2,330	150.803	447.0	4,800	39.158
CM09	2,557	163.652	447.0	4,800	36.875

5.4.2. Experimental Setup

The cable tension monitoring system was installed on the three cables of the Hwatae Bridge to verify the performance and reliability. The sensor node was attached to the stay-cables near the lower anchorages with a rechargeable battery for power supply as shown in Figure 5-12. The gateway node was prepared near the cables to send command signals and retrieve the estimated tension forces under the ambient vibration from wind and traffic.

Figure 5-12. Field test setup for automated cable tension monitoring (Cable: CM09)

5.4.3. Test Results and Discussions

Field tests were conducted to verify the operation of the automated cable tension monitoring system. The cable tension force of each cable was estimated automatically following five steps in Figure 5-5.

One operation example of the sensor node is illustrated in Figure 5-13 for Cable CM09. The sensor node measured acceleration during 300 s with a sampling rate of 100 Hz. The measured acceleration was converted to PSD. Automated peak-picking detected twelve peaks from the PSD image, and eleven peaks were finally selected as natural modes of the cable. Using selected peaks representing modal properties, the cable tension force was estimated to be 2458.8 kN.

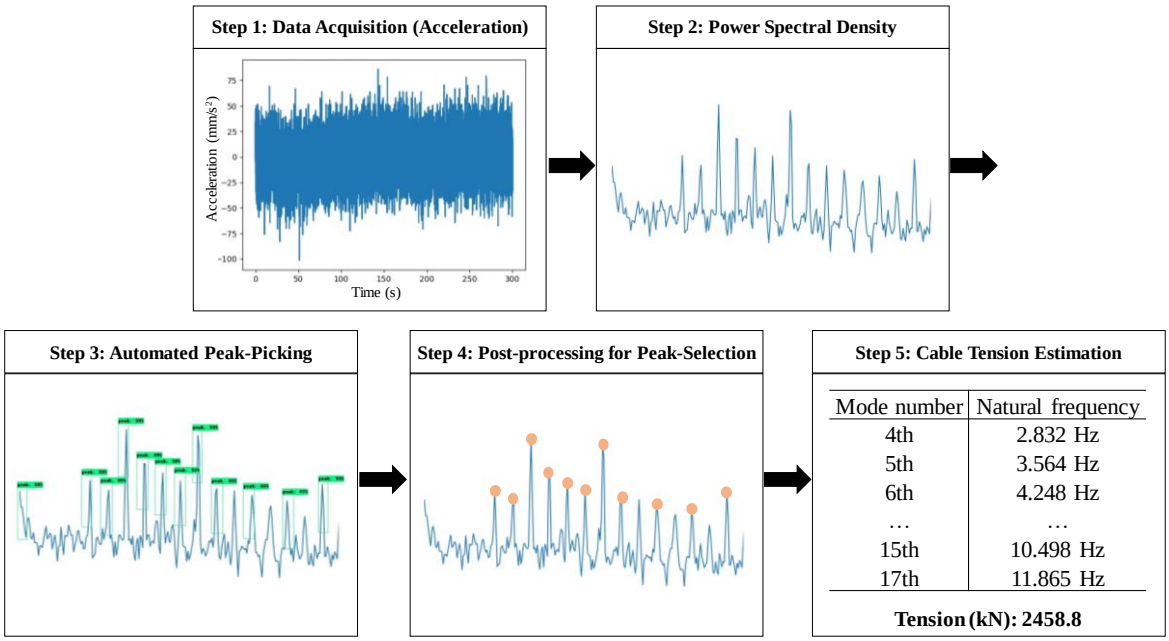

Figure 5-13. Illustration of automated cable tension estimation for CM09 cable

Three tests for each cable were repeated, showing consistent tension estimation results in all three cables as shown in Figure 5-14. The standard deviations of estimated tension forces on three cables were 7.05, 12.32, and 0.87, which were up to 0.5 % of the average tension forces. Furthermore, estimated tension forces by the developed system were close to design tension forces. Cable CM07 showed a 5.5% difference between estimated average tension force from three tests and design tension force, and Cables CM08 and CM09 showed 0.2% and 3.8%, respectively (Table 5-4). In conclusion, a total of nine tests in three stay-cables on the Hwatae Bridge verified that the developed system could automatically estimate cable tension forces consistently under various tension forces.

Table 5-4. Comparison between estimated tension and designed tension

Cable	Test1 (kN)	Test2 (kN)	Test3 (kN)	**Average (kN)**	**Design (kN)**	**Error (%)**
CM07	2241.1	2253.8	2242.0	**2245.7**	**2129.0**	**5.5**
CM08	2325.0	2348.3	2329.8	**2334.4**	**2330.0**	**0.2**
CM09	2458.8	2460.4	2460.1	**2459.7**	**2557.0**	**3.8**

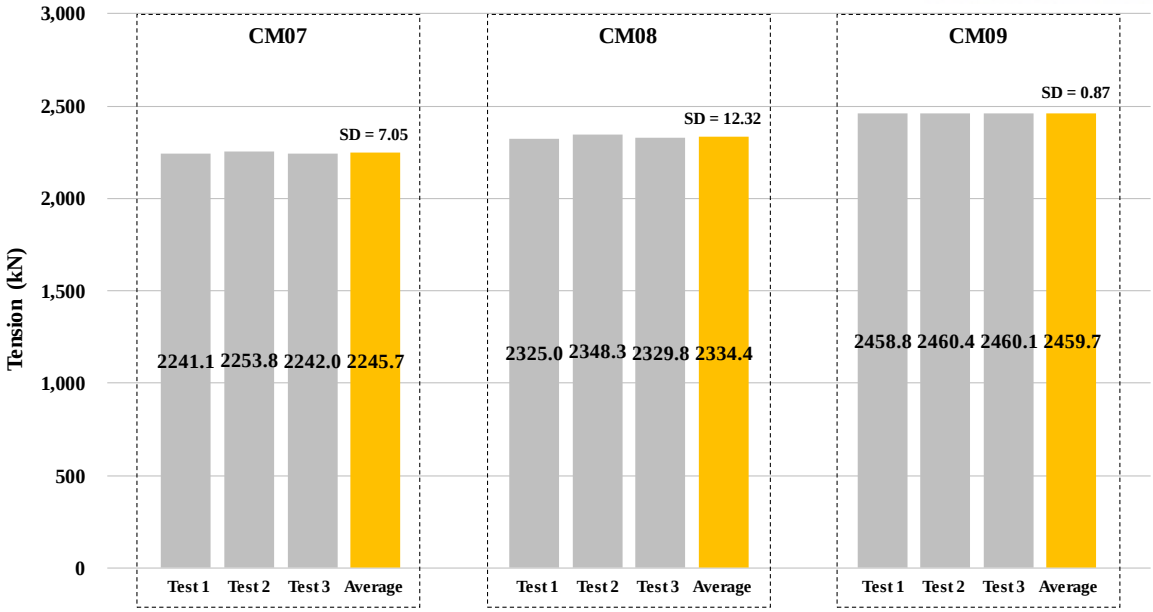

Figure 5-14. Estimated tension forces of the three cables

5.5. Summary

The aim of the present study was to develop the automated cable tension monitoring system using deep learning and wireless smart sensors. The developed system consisted of the gateway node and sensor nodes which were connected to each other by Bluetooth module. Different hardware platforms were used to construct two types of nodes: Bluetooth device for the gateway node and Raspberry Pi for the sensor nodes. Each node was designed to perform different functions for automated cable tension monitoring. The gateway node commanded sensor nodes to perform tension estimation and received tension forces through wireless communication. Sensor nodes featured embedded processing on the Raspberry Pi platform, including cable response acquisition, PSD calculation, automated peak-picking, peak-selection for natural modes, and tension estimation using the vibration-based indirect method. This study realized fully automated cable tension estimation by extracting modal properties using a peak-picking method. Faster R-CNN was adopted to automate the peak-picking process. Especially, the peak detector was trained only using numerically generated peak data tailored to stay-cable responses through the desktop environment. To embed an automated peak-picking algorithm into sensor nodes, the size of the trained detector was reduced by quantizing weights. This study conducted a series of experiments on a laboratory-scale cable and in-service stay-cables to verify the performance of the developed system. The experimental results confirmed that the developed system can estimate cable tension forces automatically under different tension conditions without human intervention.

This is the first study reporting the possibility of automated cable tension monitoring using deep learning and smart sensors. This work contributes to existing knowledge of structural health monitoring

of stay-cables. First, this study increases the potential of automated cable tension monitoring system applied to real-world stay-cables. Especially, the results of this work improve the applicability of the smart sensor-based systems to structural health monitoring. As a cost-effective measure, the developed monitoring system meets the increasing demand for maintenance of aging structures. Second, this work shows the potential of deep learning technique to be applied to cable monitoring by developing an automated peak detector using the Faster R-CNN. In conclusion, the automated cable tension monitoring system is expected to broaden current knowledge on structural health monitoring of stay-cables by showing significant implications for automating cable tension estimation and applying deep learning to civil engineering problems.

6. CONCLUDING REMARKS

This study aimed to improve current SHM research of a stay-cable, one of the critical members constituting cable-stayed bridges, by utilizing smart sensors and deep learning. To achieve this purpose, SHM-related issues of stay-cables were addressed, which includes serviceability problems, vibration control, and structural condition assessment. Three research topics were investigated to develop SHM systems for stay-cables, as follows:

Topic 1. Serviceability Assessment and Monitoring

Topic 2. Integrated Cable Vibration Control System

Topic 3. Automated Tension Force Monitoring using Deep Learning

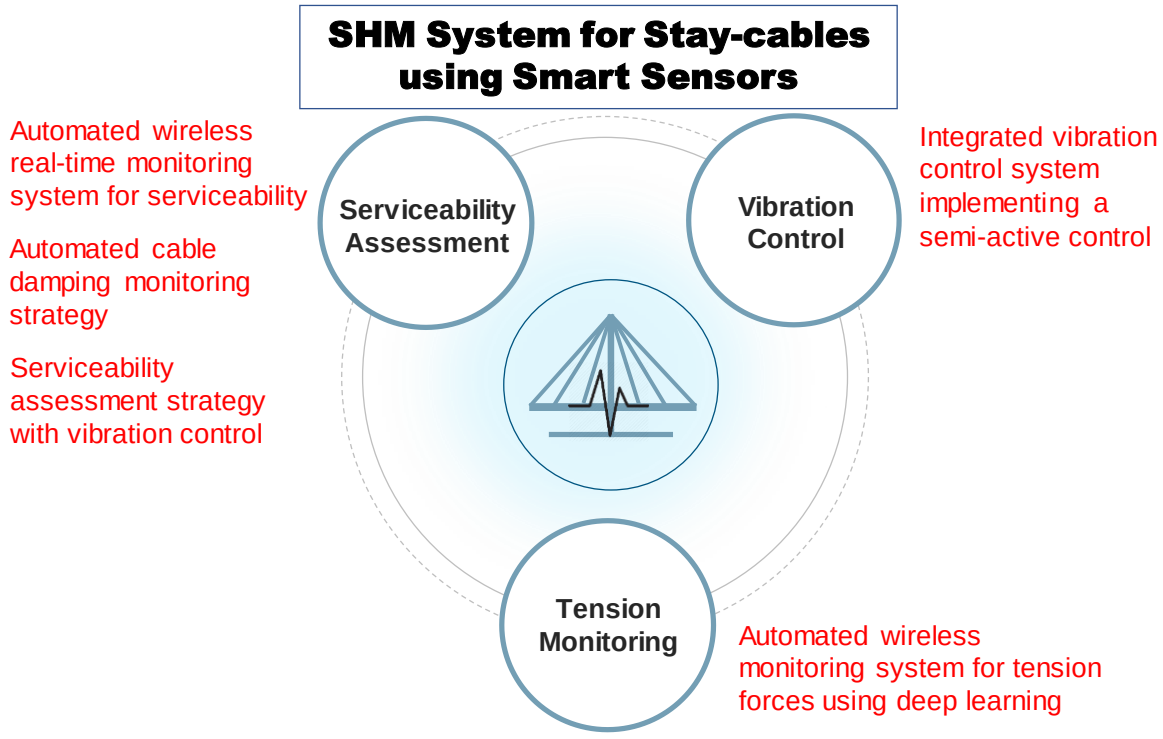

Figure 6-1. SHM system for stay-cables using smart sensors

The purpose of the first topic is to assess and monitor the serviceability level of stay-cables. Three research subjects were conducted to achieve the first objective, which includes 1) development of the automated real-time serviceability monitoring system using smart sensors, 2), present of the automated damping monitoring strategy and 3) propose the serviceability assessment method for stay-cables equipped with vibration control. Based on the guideline for allowable level of serviceability, the automated system for serviceability monitoring was designed to detect a serviceability failure in real-

time when the displacement of the cable in the mid-span exceeds the allowable serviceability level defined in design specifications. The automated damping monitoring strategy provides inspectors with the potential of serviceability failure under different external input conditions, such as wind. In addition, the proposed method can evaluate the performance of the damper in terms of reducing vibration by monitoring the damping ratio before and after the damper installation. Furthermore, the proposed serviceability assessment method can be used to provide a guideline to determine the possibility of using a cable-stayed bridge and the appropriate damping system given the wind environment. The second topic is related to the development of an integrated cable vibration control system based on the Arduino platform into which has been embedded a semi-active control algorithm. The performance of the developed integrated control system was verified by a series of laboratory-scale experiments. The third topic focuses on developing the automated cable tension monitoring system using wireless smart sensors and the Faster R-CNN algorithm, making it possible to measure the tension under the different tension conditions. The system embedded on the Raspberry Pi performs cable tension monitoring by applying an automated peak-picking method developed by the Faster R-CNN method. The embedded processing includes acceleration acquisition, PSD calculation, automated peak-picking, post-processing for peak-selection, and tension force estimation.

The results of this study are expected to have important implications in research on SHM of stay-cables. As a new pioneering study implementing wireless smart sensors for the maintenance of stay-cables, this study improves the possibility of using smart sensors in SHM research for stay-cables, such as for serviceability assessment, vibration control, and cable condition monitoring. As the number of cable-stayed bridges is increasing worldwide, maintenance costs are expected to increase, which means low-cost equipment will be required to ensure the structural integrity of stay-cables. The application of deep learning techniques to SHM of stay-cables can broaden our knowledge on the importance of interdisciplinary research to address complicated SHM-related issues. The outcomes of this study can facilitate the wider adoption of smart sensors in not only cable-stayed bridges but also the civil engineering field. In conclusion, the results of this study are expected to expand present knowledge on the application of smart sensors to monitor the structural health of the stay-cable.

7. PATH FORWARD

Although this study has successfully suggested the SHM system for stay-cables using smart sensors, further research can be performed to improve current knowledge on SHM of cables in cable-stayed bridges. Future works to be done are suggested as follows:

1) An automated damping monitoring system

The automated damping monitoring system can be developed using smart sensors for future work. As this study proposes the strategy of automating damping estimation, the presented method can be implemented to smart sensors, such as the Raspberry Pi, to monitor the damping ratio automatically. The future system for damping monitoring can be tested and verified in terms of performance by applying the system to in-service cables.

2) A prototype system for SHM of cables

Future studies can be headed to develop a wireless-based prototype system integrating all proposed systems by this study, possible to perform the serviceability monitoring, vibration control, damping monitoring, and tension force monitoring automatically. While this study took less attention to energy optimization to operate the developed system, the future prototype is expected to concentrate on energy management with less power consumption and energy harvesting. Other single board platforms can be used instead of Raspberry pi by considering energy optimization problem.

3) Data anomaly detection

As cable-stayed bridges are exposed to the harsh environment, a sensor fault could be a critical problem to operate the SHM system for cables. Checking the data anomaly is one of the prerequisites to provide reliable and valuable response data for the purpose of SHM of stay-cables. Contaminated data by sensor faults can cause a severe effect on data analysis for SHM. Therefore, data anomaly detection is required to conduct cable condition monitoring, especially with a long-term period. The previous study suggested types of data anomaly as ‘missing values’, ‘minor values’, ‘outliers’, ‘square’, ‘trend with minor values’, and ‘drift with minor values’ from data measured by sensors on deck and towers of a cable-stayed bridge [79]. However, these classification criteria can be subjective, which are dependent on the experiences of researchers. Accordingly, future work is necessary to derive the definition and types of data anomaly tailored to a stay-cable response. Furthermore, it is required to develop a cable data anomaly detection method using real-time measured cable data collected from in-service cable-stayed bridges. One of the tentative methods is to apply deep learning to detect data anomaly.

REFERENCES

1. Kim, S. W., Jeon, B. G., Kim, N. S., & Park, J. C. (2013). Vision-based monitoring system for evaluating cable tensile forces on a cable-stayed bridge. *Structural Health Monitoring*, *12*(5-6), 440-456.
2. Cho, S., Yim, J., Shin, S. W., Jung, H. J., Yun, C. B., & Wang, M. L. (2012). Comparative field study of cable tension measurement for a cable-stayed bridge. *Journal of Bridge Engineering*, *18*(8), 748-757.
3. Podolny, W., & Fleming, J. F. (1972). Historical development of cable-stayed bridges. *Journal of the Structural Division*, *98*(st9).
4. Jeong, S., Lee, Y. J., & Sim, S. H. (2019). Serviceability Assessment Method of Stay Cables with Vibration Control Using First-Passage Probability. *Mathematical Problems in Engineering*, *2019*.
5. Chen, Z. Q., Wang, X. Y., Ko, J. M., Ni, Y. Q., Spencer, B. F., Yang, G., & Hu, J. H. (2004). MR damping system for mitigating wind-rain induced vibration on Dongting Lake Cable-Stayed Bridge. *Wind & structures*, *7*(5), 293-304.
6. Maślanka, M., Sapiński, B., & Snamina, J. (2007). Experimental study of vibration control of a cable with an attached MR damper. *Journal of Theoretical and Applied Mechanics*, *45*, 893-917.
7. Fujino, Y., Kimura, K., & Tanaka, H. (2012). Cable vibrations and control methods. In *Wind resistant design of bridges in Japan* (pp. 197-229). Springer, Tokyo.
8. Jeong, S., Lee, J., Cho, S., & Sim, S. H. (2019). Integrated cable vibration control system using Arduino. *Smart Structures and Syst*ems, *23*, 695-702.
9. Kim, J. T., Nguyen, K. D., & Huynh, T. C. (2013). Wireless health monitoring of stay cable using piezoelectric strain response and smart skin technique. *Smart Structures and Syst*ems, *12*(3-4), 381-397.
10. Watson, S.C. and D. Stafford, *Cables in trouble.* Civil Engineering, 1988. **58**(4): p. 38.
11. Johnson, E. A., Christenson, R. E., & Spencer Jr, B. F. (2003). Semiactive damping of cables with sag. *Computer-Aided Civil and Infrastructure Engineering*, *18*(2), 132-146.
12. Li, H., Liu, M., Li, J., Guan, X., & Ou, J. (2007). Vibration control of stay cables of the shandong binzhou yellow river highway bridge using magnetorheological fluid dampers. *Journal of Bridge Engineering*, *12*(4), 401-409.
13. Nakamura, T., Kaneko, S., Inada, F., Kato, M., Ishihara, K., Nishihara, T., & Langthjem, M. A. (Eds.). (2013). *Flow-induced vibrations: classifications and lessons from practical experiences*. Butterworth-Heinemann.
14. Diamantoulaki, I., & Angelides, D. C. (2013). Risk-based maintenance scheduling using monitoring data for moored floating breakwaters. *Structural Safety*, *41*, 107-118.
15. Živanović, S., Pavic, A. L. E. K. S. A. N. D. A. R., & Reynolds, P. (2005). Vibration serviceability of footbridges under human-induced excitation: a literature review. *Journal of*

sound and vibration, *279*(1-2), 1-74.

16. Jenelius, E., Petersen, T., & Mattsson, L. G. (2006). Importance and exposure in road network vulnerability analysis. *Transportation Research Part A: Policy and Practice*, *40*(7), 537-560.
17. Estes, A. C., & Frangopol, D. M. (2001). Bridge lifetime system reliability under multiple limit states. *Journal of bridge engineering*, *6*(6), 523-528.
18. Minervino, C., Sivakumar, B., Moses, F., Mertz, D., & Edberg, W. (2004). New AASHTO guide manual for load and resistance factor rating of highway bridges. *Journal of Bridge Engineering*, *9*(1), 43-54.
19. Jeong, Y., Kim, W., Lee, I., & Lee, J. (2018). Bridge inspection practices and bridge management programs in China, Japan, Korea, and US. *Journal of Structural Integrity and Maintenance*, *3*(2), 126-135.
20. Hu, W. H., Moutinho, C., Caetano, E., Magalhães, F., & Cunha, A. (2012). Continuous dynamic monitoring of a lively footbridge for serviceability assessment and damage detection. *Mechanical Systems and Signal Processing*, *33*, 38-55.
21. Chen, C. C., Wu, W. H., Yu, S. T., & Lai, G. (2019). Investigation of modal damping ratios for stay cables based on stochastic subspace identification with ambient vibration measurements. *Advances in Structural Engineering*, 1369433219855900.
22. Mao, J. X., Wang, H., Fu, Y. G., & Spencer Jr, B. F. (2019). Automated modal identification using principal component and cluster analysis: Application to a long-span cable-stayed bridge. *Structural Control and Health Monitoring*, *26*(10), e2430.
23. Kim, S., J. Park, and H.-K. Kim, Damping identification and serviceability assessment of a cable-stayed bridge based on operational monitoring data. *Journal of Bridge Engineering*, 2016. **22**(3): p. 04016123.
24. Wu, W. J., & Cai, C. S. (2006). Experimental study of magnetorheological dampers and application to cable vibration control. *Journal of Vibration and Control*, *12*(1), 67-82.
25. Duan, Y. F., Ni, Y. Q., & Ko, J. M. (2005). Cable vibration control using magneto-rheological (MR) dampers. In *Electrorheological Fluids and Magnetorheological Suspensions (ERMR 2004)* (pp. 829-835).
26. Wu, Z. H., Lou, W. J., Chen, Y., Chen, Y. Y., Tang, J. C., & Sun, B. N. (2004). Simplified model of MR damper and its application. *Journal of Disaster Prevention and Mitigation Engineering*, *24*(2), 210-213.
27. Weber, F., Distl, H., Feltrin, G., & Motavalli, M. (2005, September). Simplified approach of velocity feedback for MR dampers on real cable-stayed bridges. In *Proceedings of the 6th International Symposium on Cable Dynamics* (pp. 19-22).
28. Zhou, H. J., & Sun, L. M. (2013). Damping of stay cable with passive-on magnetorheological dampers: a full-scale test. *International Journal of Civil Engineering*, 2013. **11**(3): p. 154-159.
29. Sun, Z., Dyke, S. J., Pena, F., & Wilbee, A. (2015, March). Development of Arduino based wireless control system. In *Sensors and Smart Structures Technologies for Civil, Mechanical, and Aerospace Systems 2015* (Vol. 9435, p. 94351D). International Society for Optics and Photonics.
30. Cho, S., Lynch, J. P., Lee, J. J., & Yun, C. B. (2010). Development of an automated wireless

tension force estimation system for cable-stayed bridges. *Journal of Intelligent Material Systems and Structures*, *21*(3), 361-376.

31. Sim, S. H., Li, J., Jo, H., Park, J. W., Cho, S., Spencer Jr, B. F., & Jung, H. J. (2013). A wireless smart sensor network for automated monitoring of cable tension. *Smart Materials and Structures*, *23*(2), 025006.
32. Li, H., Zhang, F., & Jin, Y. (2014). Real-time identification of time-varying tension in stay cables by monitoring cable transversal acceleration. *Structural Control and Health Monitoring*, *21*(7), 1100-1117.
33. Bao, Y., Shi, Z., Beck, J. L., Li, H., & Hou, T. Y. (2017). Identification of time-varying cable tension forces based on adaptive sparse time-frequency analysis of cable vibrations. *Structural Control and Health Monitoring*, *24*(3), e1889.
34. Yang, Y., Li, S., Nagarajaiah, S., Li, H., & Zhou, P. (2015). Real-time output-only identification of time-varying cable tension from accelerations via complexity pursuit. *Journal of Structural Engineering*, *142*(1), 04015083.
35. Kim, B. H., & Park, T. (2007). Estimation of cable tension force using the frequency-based system identification method. *Journal of Sound and Vibration*, *304*(3-5), 660-676.
36. Casas, J. R. (1994). A combined method for measuring cable forces: The cable-stayed Alamillo Bridge, Spain. *Structural Engineering International*, *4*(4), 235-240.
37. Kim, H., & Sim, S. H. (2019). Automated peak picking using region-based convolutional neural network for operational modal analysis. *Structural Control and Health Monitoring*, e2436.
38. Rainieri, C., & Fabbrocino, G. (2014). Operational modal analysis of civil engineering structures. *Springer, New York*, *142*, 143.
39. Jeong, S., Lee, Y. J., Shin, D. H., & Sim, S. H. (2019). Automated Real-Time Assessment of Stay-Cable Serviceability Using Smart Sensors. *Applied Sciences*, *9*(20), 4469.
40. Jeong, S., Kim, H., Lee, J., & Sim, S. H. Automated wireless monitoring system for cable tension forces using deep learning*, Structural Health Monitoring,* Under Review.
41. Kumarasena, S., Jones, N. P., Irwin, P., & Taylor, P. (2005). *Wind induced vibration of stay cables* (No. RI-98-034). Missouri. Dept. of Transportation. Research, Development and Technology Division.
42. Samim, F., & Nakamura, S. (2015, September). Static and seismic characteristics of cable-stayed bridges with new stay systems. In *IABSE Symposium Report* (Vol. 105, No. 8, pp. 1-8). International Association for Bridge and Structural Engineering.
43. Cheng, J., & Xiao, R. C. (2005). Serviceability reliability analysis of cable-stayed bridges. *Structural Engineering and Mechanics*, *20*(6), 609-630.
44. Park, J. W., Sim, S. H., & Jung, H. J. (2013). Development of a wireless displacement measurement system using acceleration responses. *Sensors*, *13*(7), 8377-8392.
45. Lee, H. S., Hong, Y. H., & Park, H. W. (2010). Design of an FIR filter for the displacement reconstruction using measured acceleration in low-frequency dominant structures. *International Journal for Numerical Methods in Engineering*, *82*(4), 403-434.
46. Moreu, F., Jo, H., Li, J., Kim, R. E., Scola, S., Spencer Jr, B. F., & LaFave, J. M. (2015). Reference-free displacement estimation and assessment for railroad bridges using wireless

smart sensors. *Journal of Bridge Engineering*, *21*(2).

47. Huang, F. L., Wang, X. M., Chen, Z. Q., He, X. H., & Ni, Y. Q. (2007). A new approach to identification of structural damping ratios. *Journal of sound and vibration*, *303*(1-2), 144-153.
48. Yi, J. H., & Yun, C. B. (2003). A comparative Study on modal parameter identification methods without input excitation information. *Journal of the Korean society of civil engineers*, *23*(2A), 187-201.
49. 진승섭, 추계론적 부공간 규명법: Part 2. 추계론적 프로세스와 추계론적 부공간 규명법. *한국소음진동공학회 소음·진동*, 2017. **27**(5): p. 24-30.
50. Juang, J. N., & Pappa, R. S. (1985). An eigensystem realization algorithm for modal parameter identification and model reduction. *Journal of guidance, control, and dynamics*, *8*(5), 620-627.
51. Bishop, R. E. D., & Gladwell, G. M. L. (1963). An investigation into the theory of resonance testing. *Philosophical Transactions of the Royal Society of London. Series A, Mathematical and Physical Sciences*, *255*(1055), 241-280.
52. Brincker, R., Zhang, L., & Andersen, P. (2000, September). Output-only modal analysis by frequency domain decomposition. In *Proceedings of the ISMA25 noise and vibration engineering* (Vol. 11, pp. 717-723).
53. Irvine, H. (1981). Cable Structures. *Cambridge.* The MIT Press.
54. Pacheco, B. M., Fujino, Y., & Sulekh, A. (1993). Estimation curve for modal damping in stay cables with viscous damper. *Journal of Structural Engineering*, *119*(6), 1961-1979.
55. Johnson, E. A., Baker, G. A., Spencer Jr, B. F., & Fujino, Y. (2007). Semiactive damping of stay cables. *Journal of Engineering Mechanics*, *133*(1), 1-11.
56. Johnson, E. A., Baker, G. A., Spencer Jr, B. F., & Fujino, Y. (2000, April). Mitigating stay cable oscillation using semiactive damping. In *Smart structures and materials 2000: smart systems for bridges, structures, and highways* (Vol. 3988, pp. 207-216). International Society for Optics and Photonics.
57. Huang, H., Sun, L., & Jiang, X. (2012). Vibration mitigation of stay cable using optimally tuned MR damper. *Smart Structures and Systems*, *9*(1), 35-53.
58. Duan, Y. F., Ni, Y. Q., & Ko, J. M. (2005). State-derivative feedback control of cable vibration using semiactive magnetorheological dampers. *Computer-Aided Civil and Infrastructure Engineering*, *20*(6), 431-449.
59. Sun, Z., Ou, G., Dyke, S. J., & Lu, C. (2017). A state estimation method for wireless structural control systems. *Structural Control and Health Monitoring*, *24*(6), e1929.
60. Liu, M., Li, H., Li, J., Guan, X., & Ou, J. (2006, April). Experimental investigation on vibration control of one stay cable using one magnetorheological fluid damper. In *Smart Structures and Materials 2006: Sensors and Smart Structures Technologies for Civil, Mechanical, and Aerospace Systems* (Vol. 6174, p. 61740R). International Society for Optics and Photonics.
61. Aly, A. M. (2013). Vibration control of buildings using magnetorheological damper: a new control algorithm. *Journal of Engineering*, *2013*.
62. Dyke, S. J., Spencer Jr, B. F., Sain, M. K., & Carlson, J. D. (1996). Modeling and control of magnetorheological dampers for seismic response reduction. *Smart materials and*

structures, *5*(5), 565.

63. Shimada, T. (1994). Estimating method of cable tension from natural frequency of high mode. *Doboku Gakkai Ronbunshu*, *1994*(501), 163-171.
64. Spencer Jr, B. F., Hoskere, V., & Narazaki, Y. (2019). Advances in computer vision-based civil infrastructure inspection and monitoring. *Engineering*.
65. Kim, H., Kim, H., Hong, Y. W., & Byun, H. (2017). Detecting construction equipment using a region-based fully convolutional network and transfer learning. *Journal of Computing in Civil Engineering*, *32*(2), 04017082.
66. Cha, Y. J., Choi, W., Suh, G., Mahmoudkhani, S., & Büyüköztürk, O. (2018). Autonomous structural visual inspection using region-based deep learning for detecting multiple damage types. *Computer-Aided Civil and Infrastructure Engineering*, *33*(9), 731-747.
67. Ren, S., He, K., Girshick, R., & Sun, J. (2015). Faster r-cnn: Towards real-time object detection with region proposal networks. In *Advances in neural information processing systems* (pp. 91-99).
68. Lutes, L. D., & Sarkani, S. (2004). *Random vibrations: analysis of structural and mechanical systems*. Butterworth-Heinemann.
69. Vanmarcke, E. H. (1975). On the distribution of the first-passage time for normal stationary random processes. *Journal of applied Mechanics*, 215-220.
70. Cramér, H., & Leadbetter, M. R. (2013). *Stationary and related stochastic processes: Sample function properties and their applications*. Courier Corporation.
71. Park, Y. S., Choi, S. M., Yang, W. Y., Hong, H. J., & Kim, W. H. (2008). A study on tension for cables of a cable-stayed bridge damper is attached. *Journal of Korean Society of Steel Construction*, *20*(5), 609-616.
72. Gu, M., Du, X. Q., & Li, S. Y. (2009). Experimental and theoretical simulations on wind–rain-induced vibration of 3-D rigid stay cables. *Journal of Sound and Vibration*, *320*(1-2), 184-200.
73. Kwon, D., & Kareem, A. (2006). NatHaz on-line wind simulator (NOWS): simulation of Gaussian multivariate wind fields. NatHaz Modeling Laboratory Report Univ. of Notre Dame.
74. Fischler, M. A., & Bolles, R. C. (1981). Random sample consensus: a paradigm for model fitting with applications to image analysis and automated cartography. *Communications of the ACM*, *24*(6), 381-395.
75. Kim, R. E., Moreu, F., & Spencer, B. F. (2015). System identification of an in-service railroad bridge using wireless smart sensors. *Smart Structures and Systems*, *15*(3), 683-698.
76. Spencer Jr, B., Cho, S., & Sim, S. H. (2011). Wireless monitoring of civil infrastructure comes of age. *Structure*, *13*, 12-16.
77. Basford, P. J., Johnston, S. J., Perkins, C. S., Garnock-Jones, T., Tso, F. P., Pezaros, D., ... & Cox, S. J. (2020). Performance analysis of single board computer clusters. *Future Generation Computer Systems*, *102*, 278-291.
78. BT CHAT, *https://play.google.com/store/apps/details?id=com.hardcopy.btchat&hl=ko.* 2018.
79. Bao, Y., Tang, Z., Li, H., & Zhang, Y. (2019). Computer vision and deep learning–based data anomaly detection method for structural health monitoring. *Structural Health Monitoring*, *18*(2), 401-421.

ACKNOWLEDGEMENT

It has been ten years since I first come to the Ulsan National Institute of Science and Technology (UNIST) in 2009. As UNIST has started to receive applications for admission from 2009, I was one of the undergraduate students who were willing to spend time studying in the newly opened university. The enrollment in the campus was a kind of adventure not only for me but also for others. When I arrived at the campus on March 1st, 2009, the campus was still under the construction even the starting of the new semester. In those days, the environment of the campus used to be not good for studying.

During my undergraduate course, however, I received lots of things, including financial support and opportunities to study state-of-the-art knowledge by experts. One of the memorable experiences was that I had visited the United States for the first time for the purpose of lab tours. Supported by UNIST and Prof. Myoungsu Shin at UEE, I had experienced a lot of materials and visited schools and offices in charge of architecture and construction engineering. This great experience had given me a broad eye to see the world and opportunities to study construction engineering. After that, I luckily participated in an internship program at Lotte Engineering & Construction for about 1 month. I really want to express my gratitude to Prof. Chung-Bang Yun (now at Zhejiang University, China) and Prof. Myoungsu Shin for helping me experience the construction field. These practices gave me fruitful insights and knowledge during my undergraduate period.

In 2012, summer vacation was one of the significant periods for the future. In those days, I hesitated about applying to the graduate program because I didn't find what I really wanted to study further. When I was in trouble in thinking of my career, Prof. Chung-Bang Yun recommended me to enter a graduate program, especially Disaster Management Engineering in UNIST which was newly opened in 2013. From the fall semester in 2012, Prof. Dong Keun (D.K.) Yoon (now at Yonsei University), who are experts in disaster management, started to teach related knowledge at UNIST. I finally entered the graduate program and started to learn disaster management under the supervision of Prof. D.K. Yoon from 2013. I would like to express my appreciation to Prof. D.K. Yoon for giving me opportunities to learn disaster management and extra knowledge. I learned lots of things and left one SCIE paper and one book chapter under his guidance.

The year 2016 was one of my turning points that I have faced ever. The advisor changed his position to a different university, and two choices were left to me whether to move to another school or stay on the current campus. In that time, Dr. Soojin Cho (now at the University of Seoul as a Professor) recommended me to study different field, structural health monitoring, under the Prof. Sung-Han Sim. Thanks for his recommendation, I could meet with my advisor, Prof. Sung-Han Sim, and start to learn a new research field. I am really thankful to Prof. Soojin Cho who let me know the current research

field. Although the new research topic was absolutely different from the previous one, learning new knowledge has been interesting and helpful to improve my skill and career. I am grateful for the benefits and opportunities to continue the study that I receive from Prof. Sung-Han Sim. Without their supervision and advice for the research, I couldn't be here.

As my advisor, Prof. Sung-Han Sim, has an open mind about doing research, he encouraged me to study my previous research topic further as well, and I could conduct my research about disaster vulnerability and submit the paper with guidance by Prof. Ji-Bum Chung and my teacher. Because of this relationship with Prof. Ji-Bum Chung, I could participate in the research project related to the vulnerability framework used in the world. I would like to appreciate help by Prof. Ji-Bum Chung who gave me wonderful chances to study vulnerability research further. During my last semester, Prof. Young-Joo Lee provided me with considerable support to finish my dissertation under the confusing situation after Prof. Sung-Han Sim moved to Sungkyunkwan University. He has been always diligent for teaching and research advising and left fruitful comments required to keep in mind as a researcher. With his support, I managed to finish my doctor courses, and thus I am really thankful to Prof. Young-Joo Lee for his consideration. In addition, it's an honor to invite outstanding experts to my committee members, who are Prof. Sung-Han Sim, Prof. Young-Joo Lee, Prof. Myoungsu Shin, Prof. Marco Torbol, Prof. Robin Eunju Kim (at Hanyang University), and Dr. Seung-Seop Jin (at KICT).

In 2019, UNIST held a ceremony to celebrate the 10th year anniversary. I am really proud of my school and myself to be here. Without help from many people whom I have met, I might not have finished doctoral courses. I would like to express my deep gratitude to the people whom I mentioned. Furthermore, I am a lucky guy because I have had a relationship with many friends and colleagues who helped each other. First of all, I am really happy to meet and do research with my previous lab members from 2013 to 2016, Junsung Park (now, working at Korea Land and Housing Corporation), Byeong Je Kim, Youngjun Kim, Juhyeon Park, and Soyeon Yoon (now at Yonsei University as a Ph. D student). Especially, I am working on papers with Byeong Je Kim, and hope we can publish our paper successfully. Also, I am thankful to the current lab members, Junhwa Lee, Hyunjun Kim, Jinyoung Yoon, Eun-Jin Kim (now at Ulsan Metropolitan City), Jaebeom Lee and Sangmok Lee. Furthermore, I would like to thank all of my friends, especially UEE friends, Eunkyo Seo, Seongwoo Kwon, Daehyun Kang, and Seonyoung Park, who supported each other during the graduate program. Also, I am really happy to conduct research with my one of friends, Jae-Seon Yeom, regarding changes in research topics of structural health monitoring study, which is inter-disciplinary research.

Lastly, I would like to express my sincere gratitude to my family, Mr. Cheulho Jung (father), Mrs. Jeongsuk Ha (mother), and Dongwoo Jeong (younger brother). Without their supports, I couldn't finish my doctoral dissertation. Furthermore, I am really thankful to my girlfriend, Sunyoung Son for her support during my doctor courses.